



**Casa abierta al tiempo**

**UNIVERSIDAD AUTÓNOMA METROPOLITANA**  
**UNIDAD IZTAPALAPA**

**“OPERACIÓN Y ANÁLISIS DE UN REACTOR INTEGRADO ANAEROBIO-  
AEROBIO-ANÓXICO PARA EL TRATAMIENTO DE AGUAS RESIDUALES”**

**TESIS**

QUE PARA OBTENER EL GRADO DE

DOCTOR EN BIOTECNOLOGÍA

PRESENTA:

**M. C. I. Rigoberto Plascencia Jatomea**

**Director de tesis:**

Dr. Oscar Armando Monroy Hermsillo

**Asesores:**

Dr. Jorge Gómez Hernández

Dra. Margarita M. González Brambila

Ciudad de México a 12 de Febrero de 2016

Ciudad de México, a 12 de Febrero de 2016

El H. Jurado designado por la División de Ciencias Biológicas y de la Salud de la Universidad Autónoma Metropolitana Unidad Iztapalapa aprobó la tesis:

**“OPRACIÓN Y ANÁLISIS DE UN REACTOR INTEGRADO ANEROBIO-AEROBIO-ANÓXICO PARA EL TRATAMIENTO DE AGUAS RESIDUALES”**

Que presenta:

**M. C. I. Rigoberto Plascencia Jatomea**

**Comité tutorial:**

**Director de tesis:**

Dr. Oscar Monroy Hermosillo

Universidad Autónoma Metropolitana-Iztapalapa, Departamento de Biotecnología.

**Asesores de tesis:**

**Dr. Jorge Gómez Hernández**

Universidad Autónoma Metropolitana-Iztapalapa, Departamento de Biotecnología.

**Dra. Margarita M. González Brambila**

Universidad Autónoma Metropolitana-Azcapotzalco, Departamento de Energía.

**H. Jurado:**

Presidente: Dr. Jorge Gómez Hernández



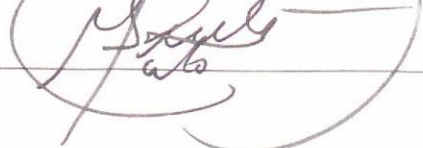
Secretario: Dra. Margarita M. González Brambila



Vocal: Dr. Ignacio González Martínez



Vocal: Dr. Pablo Gortáres Moroyoqui





Casa abierta al tiempo

UNIVERSIDAD AUTÓNOMA METROPOLITANA

# ACTA DE DISERTACIÓN PÚBLICA

No. 00162

Matrícula: 2111800225

OPERACION Y ANALISIS DE UN REACTOR INTEGRADO ANAEROBIO-AEROBIO-ANOXICO PARA EL TRATAMIENTO DE AGUAS RESIDUALES

En México, D.F., se presentaron a las 12:00 horas del día 12 del mes de febrero del año 2016 en la Unidad Iztapalapa de la Universidad Autónoma Metropolitana, los suscritos miembros del jurado:

- DR. GREGORIO JORGE GOMEZ HERNANDEZ
- DR. IGNACIO GONZALEZ MARTINEZ
- DR. PABLO GORTARES MOROYOQUI
- DRA. MARGARITA MERCEDES GONZALEZ BRAMBILA

Bajo la Presidencia del primero y con carácter de Secretaria la última, se reunieron a la presentación de la Disertación Pública cuya denominación aparece al margen, para la obtención del grado de:

DOCTOR EN BIOTECNOLOGIA

DE: RIGOBERTO PLASCENCIA JATOMEA

y de acuerdo con el artículo 78 fracción IV del Reglamento de Estudios Superiores de la Universidad Autónoma Metropolitana, los miembros del jurado resolvieron:

APROBAR

Acto continuo, el presidente del jurado comunicó al interesado el resultado de la evaluación y, en caso aprobatorio, le fue tomada la protesta.



RIGOBERTO PLASCENCIA JATOMEA  
ALUMNO

REVISÓ

LIC. JULIO CESAR DE LARA ISASSI  
DIRECTOR DE SISTEMAS ESCOLARES

DIRECTORA DE LA DIVISIÓN DE CBS

DRA. EDITH PONCE ALQUICIRA

PRESIDENTE

DR. GREGORIO JORGE GOMEZ HERNANDEZ

VOCAL

DR. IGNACIO GONZALEZ MARTINEZ

VOCAL

DR. PABLO GORTARES MOROYOQUI

SECRETARIA

DRA. MARGARITA MERCEDES GONZALEZ  
BRAMBILA

Doctorate in Biotechnology of the Universidad Autónoma Metropolitana is included in the National Postgraduate Quality Program (PNPC) of CONACYT No.001466.

This thesis was conducted at the Wastewater Laboratory W-106, Biotechnology Department, Division of Biological and Health Sciences of the Universidad Autónoma Metropolitana-Iztapalapa, under the direction of Dr. Oscar Armando Monroy Hermosillo. Hydrodynamic studies were conducted with the assistance of Dr. Ignacio González Martínez at the Electrochemistry pilot-plant, Chemistry Department, Division of Basic Sciences and Engineering.

We are grateful to CONACYT for the graduate scholarship No. 208799 granted to Rigoberto Plascencia Jatomea, and to SECITI DF (Project No. PICS012-106) for the scholarship to write this thesis.

Ciudad de México, a 12 de Febrero de 2016

El H. Jurado designado por la División de Ciencias Biológicas y de la Salud de la Universidad Autónoma Metropolitana Unidad Iztapalapa aprobó la tesis:

**“OPRACIÓN Y ANÁLISIS DE UN REACTOR INTEGRADO ANEROBIO-AEROBIO-ANÓXICO PARA EL TRATAMIENTO DE AGUAS RESIDUALES”**

Que presenta:

**M. C. I. Rigoberto Plascencia Jatomea**

**Comité tutorial:**

**Director de tesis:**

Dr. Oscar Monroy Hermosillo

Universidad Autónoma Metropolitana-Iztapalapa, Departamento de Biotecnología.

**Asesores de tesis:**

**Dr. Jorge Gómez Hernández**

Universidad Autónoma Metropolitana-Iztapalapa, Departamento de Biotecnología.

**Dra. Margarita M. González Brambila**

Universidad Autónoma Metropolitana-Azcapotzalco, Departamento de Energía.

**H. Jurado:**

Presidente: Dr. Jorge Gómez Hernández \_\_\_\_\_

Secretario: Dra. Margarita M. González Brambila \_\_\_\_\_

Vocal: Dr. Ignacio González Martínez \_\_\_\_\_

Vocal: Dr. Pablo Gortáres Moroyoqui \_\_\_\_\_

## **DEDICATORIAS**

A mis padres, Lupita y Rigoberto, porque siempre se esforzaron a inclinarme hacia el buen camino, por el ejemplo de trabajo y esfuerzo que toda la vida he visto en ustedes, por el apoyo, confianza y todo ese amor que siempre me han brindado a manos llenas.

A mis hermanas Nydia, Maribel y Xóchitl, que son parte fundamental en mi vida, por sus consejos y apoyo.

A mi esposa porque me ha impulsado a alcanzar mis metas. Porque en estos momentos comenzamos una hermosa etapa en nuestras vidas y porque los dos somos la fuerza que necesitamos para salir adelante. Gracias por todo tu apoyo y por creer en mí.

A mis sobrinas y sobrinos; Shepis, Vivi, Maya, Regis, Kia, Ika, Porthos y Pablito, por hacerme el tío más feliz y recordarme mis momentos de niñez con sus ocurrencias.

## AGRADECIMIENTOS

A Dios, por darme la vida y prestarme la oportunidad para vivir esta etapa de mi desarrollo profesional, por ponerme en el lugar y con las personas apropiadas.

Al Dr. Oscar Monroy, por la confianza otorgada al dejarme formar parte de su grupo de trabajo y abrirme las puertas de su laboratorio, por ser un excelente director de tesis, y por los consejos y el apoyo tanto profesional como personal.

Al Dr. Jorge Gómez y la Dra. Margarita González, mis asesores, los cuales considero un gran ejemplo, agradezco su disponibilidad y orientación durante la realización de este trabajo.

Al Dr. Nacho González por todo su apoyo, atención y dedicación a este trabajo. Gracias por haber aceptado colaborar con nosotros.

A mis compañeros y ex compañeros de laboratorio W-106: Lalo, Carlos, Adri, Gabiruchis, Coni, Reinita, Doc caireles, Liz; gracias por su agradable compañía durante los momentos de trabajo agobiante, porque de cada uno de ustedes logre aprender.

Agradezco también a mis compañeros de laboratorio de electroquímica aplicada: FF, Huizache, Amigo, Luneta y Pacorro, gracias por esos ratos agradables de distracción en los momentos de estrés.

Pancho Almazán, gracias Pacorro por tu amistad y apoyo en todos los momentos de frustración con la hidrodinámica, y en especial el que me hayas introducido al uso del famosísimo Comsol. Recuerda que el dibujo y el mallado controlado por la física es la clave. No al uso de la jiribilla.

## Index

Figure Captions .....	XI
Table Captions .....	XV
ABSTRACT .....	XVI
RESUMEN .....	XIX
CHAPTER 1: General Introduction .....	1
1.1 Justification .....	2
1.2 Thesis description .....	2
1.3 Objectives .....	4
1.3.1 General objective.....	4
1.3.2 Specific objectives.....	4
1.4 Integrated bioreactors: An overview .....	4
1.4.1 Integrated bioreactors.....	4
1.4.2 Classification of the integrated anaerobic-aerobic bioreactors .....	5
1.4.3 Integrated bioreactors without physical separation of anaerobic and aerobic zones .....	6
1.4.4 Integrated bioreactors based on combined anaerobic-aerobic cultures .....	7
1.4.5 The use of integrated reactors in wastewater treatment.....	8
1.5 Hypothesis.....	10
References.....	11
CHAPTER 2: Operation and dynamic modeling of a novel integrated anaerobic-aerobic- anoxic reactor for sewage treatment.....	14
Abstract.....	16
2.1 Introduction.....	18

2.2 Materials and methods .....	20
2.2.1 ICR configuration .....	20
2.2.2 Inoculation .....	21
2.2.3 Feed composition .....	22
2.2.4 Reactor start-up and operation strategy .....	22
2.2.5 Analytical methods .....	23
2.2.6 The ICNRM .....	24
2.2.6.1 Bulk liquid: .....	25
2.2.6.2 Biofilm .....	28
2.2.7 Modeling .....	30
2.2.8 Model calibration, validation and simulation .....	32
2.3 Results and discussion .....	33
2.3.1 COD removal performance of the ICR .....	33
2.3.2 Nitrogen removal performance of the ICR .....	35
2.3.3 Calibration and validation of the ICNRM.....	38
2.3.4 Model simulation: effect of the $k_L a$ , $C_O$ and $\beta$ on the performance of the ICR ..	42
2.4 Conclusions.....	44
References.....	50
CHAPTER 3: Hydrodynamic study of a novel membrane aerated biofilm reactor (MABR): Tracer experiments and CFD simulation.....	
Abstract.....	57
3.1 Introduction.....	59
3.2 Methods.....	62
3.2.1 Experimental set-up .....	62

3.2.2 Tracer studies .....	64
3.3 Mathematical models used for RTD analysis .....	65
3.3.1 ADM .....	65
3.3.2 TIS.....	67
3.3.3 MCM.....	68
3.3.4 CFD.....	70
3.3.4.1 Hydrodynamic Model .....	72
3.3.4.1.1 Boundary conditions .....	73
3.3.4.2 Mass transfer Model (diffusion-convection equation).....	73
3.3.4.2.1 Boundary conditions .....	74
3.4 Results and discussion .....	75
3.4.1 Comparison of RTD curves and evaluation of the fluid dispersion with ADM, TIS and MCM models. ....	75
3.4.2 Validation of hydrodynamic and mass transport simulation using RTD experiments .....	80
3.4.3 Hydrodynamic profile and mass transport of tracer inside MABR obtained with Comsol Multiphysics 4.3b .....	80
3.5 Conclusions .....	86
References.....	89
CHAPTER 4: The effect of inlet flow distributors on the hydrodynamic and mass transfer on a MABR using CFD and experimental validation with residence time distribution (RTD)..	
Abstract.....	93
4.1 Introduction.....	95
4.2 Experimental .....	97
4.2.1 Reactor structure and flow distributors design.....	97

4.2.2 Residence time distribution (RTD) experiments.....	97
4.3 Inlet flow distribution distributor design and RTD curve description with mathematical models and Comsol Multiphysics.....	98
4.3.1 Mathematical model of tracer concentration in MABR.....	98
4.3.2 New geometry design of inlet flow distributors of MABR.....	98
4.3.3 Simulation of experimental RTD curve with hydrodynamic-mass transfer model for laminar flow .....	101
4.3.3.1 Hydrodynamic model .....	102
4.3.3.2 Mass transport model (convection-diffusion equation).....	103
4.3.3.3 RTD curves from step signal response .....	105
4.4 Results and discussion .....	107
4.4.1 Analysis and selection of the inlet flow distributor; comparison of hydrodynamic behavior.....	107
4.4.2 Comparison of RTD experimental curves and evaluation of the dispersion grade of MABR reactor with COMSOL Multiphysics 4.3b and mixing cell model (MCM) .....	114
4.4.2.1 Validation of hydrodynamic and mass transport simulation using RTD experiments.....	116
4.4.2.2 Validation of hydrodynamic and mass transport simulation using RTD experiments.....	117
4.4.3 Effect of the inlet flow distributors in the hydrodynamic and mass transfer inside the MABR.....	117
4.4.4 Hydrodynamic profile and mass transport of the tracer inside MABR with flow distributors obtained with Comsol Multiphysics 4.3b.....	119
4.5 Conclusions .....	121
References.....	122

CHAPTER 5: Epilog .....	123
5.1 General Conclusions .....	124
5.2 Perspectives .....	127
5.3 Recomendations .....	128
ATTACHMENTS .....	134
A1. Tubular hollow membranes (PCI Membranes).....	134
A2. Airtight distribution Chamber and support for the tubular membranes.....	134
A3. Integrated Column Reactor (ICR).....	135
A4. Residence Time Distribution. ....	136
A5. Works derivate from this thesis .....	137

## Figure Captions

Figure 1.1. Types of integrated anaerobic-aerobic bioreactors (Chan et al. 2009).....	6
Figure 1.2. Oxygen supply and biofilm stratification. a) bulk liquid oxygenation, b) support oxygenation and c) bulk liquid and support oxygenation.....	8
Figure 2.1. Integrated (anaerobic-aerobic-anoxic) column reactor.....	21
Figure 2.2. COD removal efficiency ( $\eta_C$ ) and COD at influent ( $C_{CI}$ ) and effluents ( $C_{CE}$ ) of the ICR. $\eta_{C-UASB}$ (—), $\eta_{C-Global}$ (—), $C_{CI-UASB}$ (□), $C_{CE-UASB}$ (○) and $C_{CE-MABR}$ (△); ICNRM predictions: $C_{CE-UASB}$ (—) and $C_{CE-MABR}$ (••••).....	34
Figure 2.3. TAN removal efficiency ( $\eta_N$ ) and nitrogen compounds concentrations at influent ( $C_{NI}$ ) and effluents ( $C_{NE}$ ) of the ICR. $\eta_{N-MABR}$ (—), $\eta_{N-DNB}$ (—); TAN concentration: $C_{NI-UASB}$ (□), $C_{NE-UASB}$ (○), $C_{NE-MABR}$ (△) and $C_{NE-DNB}$ (◇); $mgNO_2^- - N$ concentration: $C_{NE-DNB}$ (◇); ICNRM predictions: TAN at $C_{NE-DNB}$ (—) and $mgNO_2^- - N$ at $C_{NE-DNB}$ (••••).....	36
Figure 2.4. Oxygen concentration ( $C_O$ ) profile and model predictions during run IV to VI: $C_{O-MABR}$ (■) and ICNRM prediction; $C_{O-MABR}$ (—).....	40
Figure 2.5. ICNRM predicted reaction rate profile within the biofilm. Reaction rate (—).....	41
Figure 2.6. $k_L a$ , $C_O$ and $\beta$ effect on the $\eta_C$ and $R_{a/n}$ . A) $\eta_{N-MABR}$ at $\beta = 0.85$ (■), $\beta = 0.9$ (●) and $\beta = 0.95$ (▲); $C_O$ at $\beta = 0.85$ (□), $\beta = 0.9$ (○) and $\beta = 0.95$ (△). B) $R_{a/n}$ at $\beta = 0.85$ (—), $\beta = 0.9$ (••••) and $\beta = 0.95$ (-•-)......	43
Figure 3.1. Schematic of the membrane aerated biofilm reactor (MABR) and liquid flow circuit used for RTD experiments: a) MABR, b) Type-Y connector, c) UV-Vis spectrophotometer, d) Peristaltic pump and e) Container.....	62

Figure 3.2. Membrane distribution at the MABR reactor (cross-section view): a) Inner wall of the reactor, b) Tubular membranes, c) Lateral inlet, d) Airtight distribution chamber and e) central inlet.....64

Figure 3.3. Geometry of the MABR and computational mesh established in *Comsol Multiphysics 4.3b*: a) Geometry of MABR and b) The computational mesh.....72

Figure 3.4. RTD curves obtained in the MABR at different flow rates. a) 3.6 mL/min, b) 6 mL/min, c) 8 mL/min and d) 10 mL/min. Experimental data (open circle), constructed RTD curves, with the different models: i) ADM (red dashed line), ii) TIS (blue dots), iii) MCM (green continuous line) and iv) *Comsol Multiphysics 4.3b* (orange stars).....76

Figure 3.5. Velocity field obtained from the hydrodynamic study with *Comsol Multiphysics 4.3b* for the MABR (volumetric flow rate of 10 mL/min). The multicolor bars located beside image represent the magnitude of the velocity field, dark blue color represents the lowest velocities and red color represents the highest velocities.....81

Figure 3.6. Velocity field (m/s) in cross section at the inlet and outlet of the MABR (volumetric flow rate of 10 mL/min): a) inlet and b) outlet. The multicolor bars located beside images represent the magnitude of the velocity field, dark blue color represents the lowest velocities (minimal) and red color represents the highest velocities (maximum).....82

Figure 3.7. Scheme of cross-section of the MABR: a) Central perforation of the distribution chamber, b) Tubular membrane and c) Inner wall of the reactor.....83

Figure 3.8. Normalized velocity profile in cross-section of the MABR.....84

Figure 3.9. Particle tracer experiments inside the MABR in transient regime obtained with *Comsol Multiphysics 4.3b*. Different times passing after the fluid entrance are indicate in the figure (volumetric flow rate of 10 mL/min and 3000 planted particles).....85

Figure 4.1. Schematic of the membrane aerated biofilm reactor (MABR) and liquid flow circuit used for RTD experiments: a) MABR, b) Type-Y connector, c) UV-Vis

spectrophotometer, d) Peristaltic pump and e) Container (Plascencia-Jatomea et al. 2015).....99

Figure 4.2. Geometric configuration of the inlet flow distributors. a) plane distributor, b) concave distributor, c) coronary distributor, d) plane-convex distributor, e) plane-inverted cone distributor, f) convex distributor, g) plane wall distributor and h) conical wall distributor. The scheme of the flow distributors are presented in cross section view. The external diameter is represented by  $x$  and the high of the inlet flow distributors is represented by  $y$ .....100

Figure 4.3. Inlet flow distributors position at the MABR. a) tubular membranes, b) airtight distribution chamber and c) flow distributor.....101

Figure 4.4. Output response curves of the step-signal at the entrance of MABR. Without flow distributor (black line), convex (red circle), conical wall (green diamond) and straight wall flow distributor (blue triangle). Volumetric flow rate ( $Q$ ) of 10 mL/min.....106

Figure 4.5. Influence of the geometry of flow distributors on fluid velocity profiles (m/s) of the MABR obtained with Comsol Mutiphysics 4.3 b (volumetric flow rate ( $Q$ ) of 10 mL/min). a) without distributor, b) plane distributor, c) concave distributor, d) coronary distributor, e) plane-convex distributor, f) plane-inverted cone distributor, g) convex distributor, h) plane wall distributor and i) conical wall distributor. The images have shown the first 10 cm of the MABR from the inlet to the top.....108

Figure 4.6. Scheme of cross-section of the MABR: a) Central perforation of the distribution chamber, b) Tubular membrane and c) Inner wall of the reactor .....110

Figure 4.7. Comparison of normalized velocity profile in cross-section obtained with different geometries of inner flow distributors in steady state of the MABR. Without distributor (black square), plane distributor (red circle), concave distributor (green triangle), coronary distributor (blue inverted triangle), plane-convex distributor (ciani diamond), plane-inverted cone distributor (purple left triangle), convex distributor (yellow right triangle), plane wall

distributor (olive hexagon) and conical wall distributor (blue star). Volumetric flow rate ( $Q$ ) of 10 mL/min.....111

Figure 4.8. RTD curves obtained in the MABR with different geometric arrangements of inlet flow distributors at a volumetric flow rate ( $Q$ ) of 10 mL/min. a) without flow distributor (normal operation), b) straight wall flow distributor, c) conical wall flow distributor and d) convex flow distributor. Experimental data (black dots) and constructed RTD curves with different model: COMSOL Multiphysics 4.3b (continuous red line) and MCM (blue dashed line).....115

Figure 4.9. Mass transport distribution of tracer inside along the MABR in transient regimen obtained with Comsol Multiphysics 4.3b. Different times passing after the fluid entrance on the reactor are indicated in the figure. The figure corresponds to a volumetric flow rate of 10 mL/min.....120

Figure A1. Tubular hollow membranes.....134

Figure A2. Aithigt distribution chamber and support for the tubular membranes.....134

Figure A3. Integrated Column Reactor (ICR).....135

Figure A4. Residence time distribution.....136

## Table Captions

Table 1.1. Integrated bioreactors used for wastewater treatment.....	9
Table 2.1. Operation conditions of the ICR.....	23
Table 2.2. Parameter values used in the ICNRM.....	31
Table 2.3. The $k_{La}$ profile and adjusted $kl$ parameter for the MABR.....	39
Table 3.1. Experimental conditions of MAB reactor and parameters obtained from experimental data according to Eqs. (5) and (9), used to construct the RTD curves with ADM and TIS models.....	77
Table 3.2. Parameter values obtained for the best fit of RTD experimental curves with MCM model and diffusion-convection equations ( <i>Comsol Multiphysics 4.3b</i> ) at different inflow values.....	79
Table 4.1. Velocity ratio ( $R_{V_{maxcz}/V_{maxsz}}$ ) of maximum average fluid velocity in the channeling zone and the maximum average fluid velocity in the stagnant zone of the MABR, with and without inlet flow distributors.....	113
Table 4.2. RTD experimental conditions and parameter values obtained from experimental data, mixing cell model (MCM) and Comsol Multiphysics 4.3b.....	116
Table 4.3. Parameter values obtained for the best fit of experimental RTD curves with the mixing cell model (MCM).....	118

## ABSTRACT

Integrated reactors (IR) combining anaerobic, aerobic and nitrogen removal processes are a viable alternative to reduce operational costs and footprint compared to conventional wastewater treatment plants. An integrated bench scale (6.4 L) anaerobic-aerobic-anoxic column reactor (ICR) was developed to remove carbon and nitrogen compounds from sewage of Universidad Autónoma Metropolitana-Iztapalapa campus. The ICR is comprised of an up-flow anaerobic sludge blanket reactor (UASB), a membrane aerated biofilm reactor (MABR) and a denitrifying biofilm reactor (DNB). The global COD removal efficiency ( $\eta_{C-Global}$ ) is ~82% at hydraulic retention time (HRT) of 8.4 h. The partial nitrification (PN) process is obtained with an ammonia/nitrite ratio ( $R_{a/n}$ ) of 4. The experimental data was used to calibrate and validate an integrated carbon-nitrogen removal model (ICNRM), in order to determine operating conditions for the improvement of the ICR performance, considering the hydrodynamic profile and reaction kinetics. A good agreement between the measured and modeled results is obtained with a least square error function ( $S$ ) lower than 0.09. The model predicts that the COD removal efficiency at the MABR ( $\eta_{C-MABR}$ ) and nitrite accumulation at the DNB are influenced by the volumetric oxygen transfer coefficient ( $k_La$ ) and oxygen concentration, respectively. The optimal operation zone for  $\eta_{C-MABR} > 90\%$  and  $R_{a/n}$  of 1.32 were reached for  $k_La$  between 1.26 to 1.36 1/h, and an inlet DO concentration of 1.5 to 1.6 mg/L respectively, standing out the importance of calibrating hydrodynamic behavior and kinetics.

The central part of the integrated reactor, the membrane-aerated biofilm reactor (MABR) is a promising technology for wastewater treatment, especially for simultaneous organic and

nitrogen removal. The knowledge of mass transfer phenomena induced by flow velocity and flow pattern is required in order to improve the reactor design and the pollutants removal efficiency. Tracer experiments and residence time distribution (RTD) theory were used to characterize the flow in a special MABR oxygenating from the membrane side and from the liquid side. The liquid phase flow patterns were investigated by means of tracer pulse stimulus-response technique using dextran blue as model tracer. RTD curves were analyzed by cold-model tests (axial dispersion model ADM, tanks in series model TIS and mixing cell model MCM). The detailed flow pattern of the reactor was obtained from computational fluid dynamic (CFD) simulation. According to experimental results of RTD studies and CFD simulation, the flow patterns were demonstrated to be analogous to completely mixed flow with deviations of the ideal hydrodynamic behavior; stagnant zones (low fluid velocity) in 85% of its volume, being the remainder a channeling trouble (high fluid velocity). These deviations were quantitatively described (macromixing level-global mixing) with a minimum quadratic error function value of (S) 0.01. The local mixing flow pattern (micromixing level) obtained by CFD allowed determining the location of each zone; the stagnant zone is situated in the area where membranes are located; therefore it is possible to assume that degradation reactions of pollutants would take place in this area.

MABR are gradually adapted to water treatment trains so its hydraulic profile directly affects the pollutant removal performance. The goal of this work was to develop a geometry design of inlet flow distributors of the MABR using Computational Fluid Dynamics (CFD). The new distributor geometry was experimentally evaluated with RTD experimental curves using the stimulus-response technique and approximated with the mixing cell model (MCM) and by solving the hydrodynamic Navier–Stokes (NS) equation for laminar flow and mass transport

(convection–diffusion equation) equations using computational fluid dynamics (F-tracer RTD method). Two sets of RTD experiments (common and new inlet flow distributors) in MABR were carried out. The volumetric flows (Q) employed were from 03.6 to 10 mL/min. The new inlet flow distributor (conical wall flow distributor) had a more homogeneous velocity field in the entire reaction zone (membrane zone), as shown by MCM values lower than those obtained with the common MABR (without flow distributor). The RTD curves obtained with Comsol Multiphysics 4.3b are in agreement with RTD experimental curves reinforced the data obtained by the MCM.

The operation of the integrated column reactor allowed the acquisition of experimental data under different operational conditions, enabling the appropriate development and validation of an integrated mathematical model (hydrodynamic-mass transfer-reaction). This model could predict the behavior of the reactor with an error of <5%, demonstrating the feasibility of the use of this model to predict the reactor behavior. According to model simulations, this system can be improved in design aspects and experimental conditions in order to establish a nitrification process with nitrite accumulation to obtain a suitable stoichiometry ratio by manipulating the reaction time, dissolved oxygen and the improvement of hydrodynamic behavior (reduction of the channeling zone).

## RESUMEN

Los reactores biológicos integrados son sistemas que permiten llevar a cabo procesos anaerobios y aerobios en un mismo reactor. Sin embargo, poco se sabe sobre su desempeño en el tratamiento de aguas residuales (municipales o industriales). En virtud de lo anterior, en esta tesis se estudiaron diversos factores que afectan el desempeño de un reactor biológico, tales como, la hidrodinámica, la transferencia de masa en biopelículas, así como diversas condiciones de operación del sistema; permitiendo la formulación de un modelo matemático integrado para predecir el comportamiento del reactor bajo nuevas condiciones de operación.

El estudio de la hidrodinámica y la transferencia de masa del reactor integrado en columna permitieron el conocimiento del patrón de mezclado del reactor utilizando la técnica de la determinación de tiempos de residencia. Esta técnica logró la identificación de problemas de estancamiento y canalización dentro del reactor. Estas desviaciones del patrón de flujo ideal fueron descritas correctamente mediante la utilización del modelo de celdas mezcladas, el cual es un modelo matemático que combina reactores ideales para describir el comportamiento de reactores reales. De acuerdo a este modelo, el reactor integrado en columna se ajusta a un reactor CSTR con problemas de canalización y estancamiento.

Las desviaciones del patrón de flujo del reactor fueron identificadas y corroboradas mediante la utilización de la dinámica computacional de fluidos. Esta técnica computacional permitió conocer la localización de cada zona de flujo, pudiendo así darle un mayor peso al modelo de celdas mezcladas al poder diferenciar las características de cada zona en aspectos como; volumen de cada zona y el flujo que pasa a través de ellas.

Una vez establecido el conocimiento de la hidrodinámica y la transferencia de masa del reactor, se procedió a su operación. El reactor integrado fue alimentado con agua residual del drenaje general de la universidad autónoma metropolitana unidad Iztapalapa, obteniendo eficiencias de degradación de materia orgánica (DQO) mayores al 83%, y la nitrificación con acumulación de nitrito permitiendo tener un efluente que pudiera servir para el proceso anammox.

Una vez obtenida la información sobre la operación del reactor bajo diversas condiciones de operación (seis etapas), se procedió a la formulación del modelo matemático integrado (Integrated Carbon-Nitrogen Removal Model -ICNRM-). Este modelo considera el aspecto hidrodinámico, la transferencia de masa y reacción del reactor, permitiendo predecir el comportamiento del reactor con un error menor al 5% de acuerdo al proceso de validación del modelo.

El modelo ICNRM permitió la propuesta de nuevas condiciones de operación que podrían permitir aumentar la eficiencia de degradación de materia orgánica a un 93% y un proceso de nitrificación con acumulación de nitrito estable, produciendo un efluente equimolar de amonio/nitrito adecuado para el proceso anammox. Esas simulaciones se realizaron siguiendo dos aspectos importantes, como son; la concentración de oxígeno y la mejora hidrodinámica. De acuerdo a esto, se encontró que la eficiencia del reactor podría ser aumentada mediante una mejora hidrodinámica, es decir, disminuir la canalización del reactor.

En la búsqueda de estrategias para mejorar el patrón de mezclado del reactor, se hizo uso de la dinámica computacional de fluidos. Esta técnica permitió el diseño de dispositivos que

permiten distribuir el flujo en todo el reactor, disminuyendo así los problemas de canalización. Acorde a los resultados obtenidos, se implementó un distribuidor de flujo denominado “distribuidor de flujo de pared cónica”, el cual permitió homogenizar la velocidad del fluido dentro del reactor, disminuyendo la relación de velocidad de la zona canalizada y estancada de 9 a 2.6.

# **CHAPTER 1: General Introduction**

## **1.1 Justification**

In conurbations like México City, where the high population density and high land costs obstruct the installation of normal wastewater treatment plants there is a need for innovative designs that can reduce the footprint of the bioreactors providing a denitrified secondary effluent in a single tower of three linked reactors for the anaerobic, aerobic and denitrification steps. Separately, these systems have shown acceptable performance in the organic matter and nitrogen degradation, and the reactor designs and operating rules are well established. However, the proposed integrated prototype has not been studied from the kinetic, mass transfer-reaction and hydrodynamic aspects, which would allow a scale-up analysis.

This issue generates the need to study these integrated reactors more rigorously, using mathematical models that involve this phenomenology. These studies could provide a better overview of the operation and viability of applying this kind of biological wastewater treatment reactors amid highly populated areas.

## **1.2 Thesis description**

In order to fulfill the main goal of "Design and operation of an integrated anaerobic-aerobic-anoxic for wastewater treatment reactor", the results obtained during this research are presented in the following order:

The rest of chapter one states the objectives and summarizes some background of integrated bioreactors used in wastewater treatment. Also presents a literature review on the main characteristics of these type of reactors as well as their advantages and disadvantages

compared to conventional treatment systems. Finally, it presents some hypotheses on the subject under study.

Chapter two presents the analysis of the reactor operation during the treatment of wastewater. Presents and validates an integrated mathematical simulation model (hydrodynamic-mass transfer-reaction); the operating conditions that increase the efficiency of pollutant degradation and possible strategies to improve the reactor design were determined.

Chapter three analyzes the hydrodynamic profile of the integrated bioreactor using the residence time distribution technique. Several hydrodynamic models were tested as well as computational fluid dynamics to diagnose the reactor mixed profile. A comparison of different mathematical predictions and computational fluid dynamics models with the experimental data is performed and finally, a model that adequately describes the flow pattern or mixing is proposed.

Chapter four presents and analyzes some improvement alternatives for the reactor design. The use of computational fluid dynamics for the proposed reactor modifications is exposed. This technique permitted the visualization of comparative flow reactor profiles with each change of design.

Finally, chapter five presents a general conclusion based on the main results of this research, foresees the perspectives and proposes recommendations that can be helpful for future research on this topic.

## **1.3 Objectives**

### **1.3.1 General objective**

To design and operate an integrated anaerobic-aerobic-anoxic column reactor for simultaneous removal of carbon and nitrogen compounds contained in municipal wastewater.

### **1.3.2 Specific objectives**

- To design and build an integrated bioreactor.
- To assess the reactor operation with municipal wastewater.
- To develop an integrated mathematical model (hydrodynamic-mass transfer-reaction) to simulate the behavior of the integrated reactor.
- To propose an innovative integrated reactor design.

## **1.4 Integrated bioreactors: An overview**

### **1.4.1 Integrated bioreactors**

Conventional anaerobic-aerobic plants are usually equipped with different treatment units that have a variety of functions to achieve acceptable treatment performances (Li et al. 2010). The conventional systems, which utilize suspended biomass only, are well known, widely tested and generally considered reliable. However, there are many potential issues related to the management of these plants: first, they require onerous process controls due to the sensitivity of the biomass to organic and hydraulic load variability, and second, a large surface area is generally required, making limited area availability another critical issue (Antonella et al. 2012). These eventually decrease the attractiveness of conventional anaerobic-aerobic

treatments plants for reason of economy and location. Due to this, there is a tremendous need to develop reliable technologies for the treatment of domestic wastewater. Such treatment systems must fulfill many requirements, such as simple design, use of non-sophisticated equipment, high treatment efficiency, and low operating and capital costs. In addition, consonant with population growth and intensification in urbanization, the cost and availability of land is becoming a limiting factor, and “footprint size” is increasingly becoming important in the choice of a treatment system (Aiyuk et al. 2004). In recent years, substantial attention has been paid towards compact high-rate bioreactors for wastewater treatment to meet the strict constraints with respect to space, odor, view, and biosolids production. Thus, the integrated bioreactors which combine the aerobic and anaerobic process in a single reactor, are seen as a viable alternative. A combination of aerobic and anaerobic degradation pathways in a single reactor is capable of enhancing the overall degradation efficiency. The integrated bioreactors are cost effective, efficient and have smaller foot prints as compared to the conventional anaerobic-aerobic systems. Nonetheless, the design, operation and process development of integrated anaerobic-aerobic bioreactors need further studies (Chan et al. 2009).

#### **1.4.2 Classification of the integrated anaerobic-aerobic bioreactors**

The integrated bioreactors can be classified into four types of integrated anaerobic-aerobic bioreactors. These are (a) integrated bioreactors with physical separation of anaerobic-aerobic zone, (b) integrated bioreactors without physical separation of anaerobic-aerobic zone, (c) Sequencing Batch Reactors (SBR) based on temporal separation of the anaerobic and the aerobic phase, and (d) combined anaerobic-aerobic cultures system based on the principle of

limited oxygen diffusion in microbial biofilms. An overview of this classification is delineated in Figure 1.1.

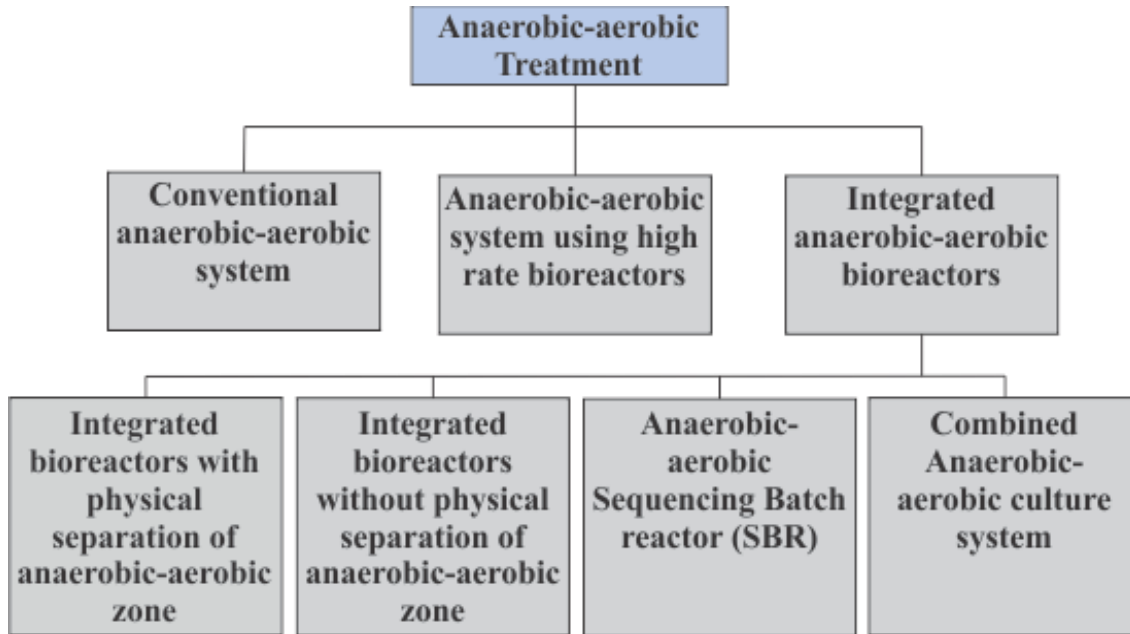


Figure 1.1. Types of integrated anaerobic-aerobic bioreactors (Chan et al. 2009).

Since this work is referred to the use of integrated bioreactors without physical separation of anaerobic-aerobic zones and the use of biofilm reactors, a better description of these types of bioreactors is discussed next.

### **1.4.3 Integrated bioreactors without physical separation of anaerobic and aerobic zones**

These types of bioreactors allow the coexistence of anaerobic and aerobic population inside the same reactor. This is done without physical separation using stacked configuration in which aerobic conditions are maintained in the upper part. This is achieved by introducing aeration at an intermediate height within the reactor.

#### **1.4.4 Integrated bioreactors based on combined anaerobic-aerobic cultures**

Combined culture is the mixture of anaerobic and aerobic cultures that could survive under alternating anaerobic-aerobic conditions in the same reactor. In biofilm reactors, the biomass can metabolize the substrate with short residence times, which results in compact reactors with smaller area requirements. In these systems, the oxygen delivery to the liquid phase, rather than the biomass concentration, is the limiting factor (Nicolella et al. 2000b; Tomaszek and Grabas, 1998). The low oxygen concentrations in the inner region of the biofilm (due to the limited diffusion of oxygen through the biofilm and consumption of oxygen by the aerobic reactions) stratify the biofilm into two zones: an aerated outer zone and an anaerobic deeper zone (see Figure 1.2). This stratification can lead to the removal of the nitrate by denitrification. “Simultaneous nitrification and denitrification” (SND) in a single reactor has been tested using different methods, such as using a flexible biofilm reactor with an adjustable aerobic buffer and anoxic zones (Zhang et al. 2007; Guo et al. 2005); a biofilm airlift suspension reactor operating with film-covered biodegradable carriers (Walters et al. 2009); a fixed-film reactor with different aerobic, transition and anoxic zones (Del Pozo and Diez, 2005); or other types of integrated bioreactors. If well operated, the SND process can reduce the reactor volume and the recirculation energy cost required by the more traditional systems that use separate aerobic and anoxic processes.

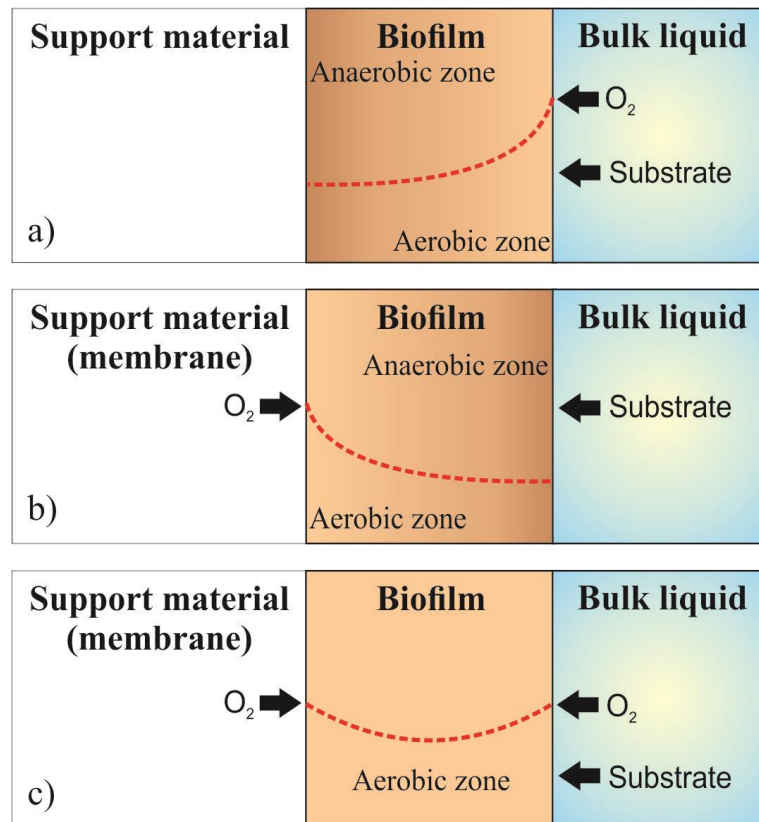


Figure 1.2. Oxygen supply and biofilm stratification. a) bulk liquid oxygenation, b) support oxygenation and c) bulk liquid and support oxygenation.

It is worth mentioning that the stratification of the biofilm will depend on the oxygenation pathway as is shown in Figure 1.2. Several research works has been done about the use of this oxygenation ways in the treatment of wastewater (Plascencia-Jatomea et al. 2015; Hu et al. 2008, González-Brambila et al. 2006).

#### 1.4.5 The use of integrated reactors in wastewater treatment

In recent years, the use of integrated reactors has been extending. These systems have shown a satisfactory performance in the removal of contaminants; reporting removal efficiencies of carbon and nitrogen above 90%. It is worth mentioning that in all mentioned works synthetic

wastewater was used. Different works about the use of integrated bioreactors in the treatment of wastewater are presented in Table 1.1.

Table 1.1. Integrated bioreactors used for wastewater treatment.

Reference	Reactor	COD ( $\text{gCOD} \cdot \text{m}^{-3} \cdot \text{d}^{-1}$ )	$\text{N-NH}_4^+$ ( $\text{gNH}_4^+ \cdot \text{m}^{-3} \cdot \text{d}^{-1}$ )	HRT (h)	COD-NT $\eta$ (%)	COD/NT
Hasar H., 2009	Sequencing batch reactor	2000	200	12	>90	10
Chae et al. 2006	With physical separation	900	116	8		8
Chang et al. 2002	Without physical separation	3300	288	7		12
Choi et al. 2008	Without physical separation	900	119	12		8
Fu et al. 2009	Without physical separation	1455	134	36		11

The integrated bioreactors might be a good alternative for the wastewater treatment with minimal footprint. However, the application of this kind of reactor is limited to lab scale and the use of synthetic wastewater. A better insight in the real capacity if these systems could be obtained with the operation of this integrated systems in the treatment of real wastewater where the pollutant concentrations present considerable variations. The operation under real conditions will help to establish some bases for the design and operation strategies in the treatment of real wastewater.

## **1.5 Hypothesis**

It is possible to achieve simultaneous removal of carbon and nitrogen compounds through anaerobic digestion, aerobic digestion, partial nitrification and anammox in a three zones integrated reactor.

The use of membranes will optimize oxygenation, both on the inside and outside of the biofilm, to achieve the oxidation of organic matter and partial nitrification.

By controlling OLR to the UASB reactor and oxygenation rate at the MABR, COD will be feasible to control at concentrations close to zero, dissolved oxygen concentration, flow and reaction times to achieve partial nitrification and anammox for complete nitrogen removal.

Proper hydrodynamics will allow a suitable reactor design for the simultaneous removal of carbon and nitrogen.

## References

1. Antonella Luciano, Paolo Viott, Giuseppe Mancini, Vincenzo Torretta (2012). An integrated wastewater treatment system using a BAS reactor with biomass attached to tubular supports. *Journal of Environmental Management* 113, 51-60.
2. Aiyuk Sunny, Amoako Joyce, Raskin Lutgarde, Haandel Adrianus van, Verstraete Willy (2004). Removal of carbon and nutrients from domestic wastewater using a low investment, integrated treatment concept. *Water Research* 38, 3031–3042
3. Chae S.R., Kang S.T., Watanabe Y. and Shin H.S. (2006). Development of an innovative vertical submerged membrane bioreactor (VSMBR) for simultaneous removal of organic matter and nutrients. *Water Research* 40, 2161-2167.
4. Chan Yi Jing, Chong Mei Fong, Law Chung Lim, Hassell D. G. (2009). A review on anaerobic-aerobic treatment of industrial and municipal wastewater. *Chemical Engineering Science* 155, 1-18.
5. Chang Won-Seok, Hong Seok-Won and Park Joonkyu (2002). Effect of zeolite media for the treatment of textile wastewater in a biological aerated filter. *Process Biochemistry* 37, 693-698.
6. Choi Changkyoo, Lee Jaekeun, Lee Kwangho and Kim Moonil (2008). The effects on operation conditions of sludge retention time and carbon/nitrogen ratio in an intermittently aerated membrane bioreactor (IAMBR). *Bioresource Technology*. 99, 5397-5401.
7. Del Pozo R., Diez V. (2005). Integrated anaerobic-aerobic fixed film reactor for slaughterhouse wastewater treatment. *Water Research*. 39, 1114-1122.

8. Fu Zhimin, Yang Fenglin, Zhou Feifei and Xue Yaun (2009). Control of DQO/N ratio for nutrient removal in a modified membrane bioreactor MBR treating high strength wastewater. *Bioresource Technology* 100, 136-141.
9. González-Brambila, M., Monroy, O., López-Isunza, F., 2006 Experimental and theoretical study of membrane-attached biofilm reactor behavior under different modes of oxygen supply for the treatment of synthetic wastewater. *Chemical Engineering Science* 61, 5268-5281.
10. Hu, S., Yang, F., Sun, C., Zhang, J., Wang, T., 2008. Simultaneous removal of COD and nitrogen using a novel carbon-membrane aerated biofilm reactor. *Journal of Environmental Sciences* 20, 142-148.
11. Guo H., Zhou J., Su J., Zhang Z. (2005). Integration of nitrification and denitrification in air lift bioreactor. *Biochemical Engineering Journal* 23, 57-62.
12. Hasar Halil (2009). Simultaneous removal of organic matter and nitrogen compounds by combining a membrane bioreactor and a membrane biofilm reactor. *Bioresource Technology* 100 (10), 2699-2705.
13. Li Z.H., Yang K., Yang X.J., Li L. (2010). Treatment of municipal wastewater using a contact oxidation filtration separation integrated bioreactor. *Journal of Environmental Management* 91, 1237–1242.
14. Nicolella C., Van Loosdrecht M.C.M., Heijnen S.J. (2000b). Particle-based biofilm reactor technology. *Tibtech* 18, 312-320.
15. Plascencia-Jatomea R., González I., Gómez J., Monroy O. (2015). Operation and dynamic modeling of a novel integrated anaerobic–aerobic–anoxic reactor for sewage treatment. *Chemical Engineering Science* 138, 31-40.

16. Tomaszek, J.A., Grabas, M. (1998). Biofilm reactors: a new form of wastewater treatment. In: Pawlowski, et al. (Eds.), Environmental Science Research Chemistry for the Protection of the Environment, vol. 55 (3). Plenum Press, p. 116.
17. Walters E., Hille A., He M., Ochmann C., Horn H. (2009). Simultaneous nitrification/denitrification in a biofilm airlift suspension (BAS) reactor with biodegradable carrier material. Water Research. 43, 4461-4468.
18. Zhang X., Zhou J., Guo H., Qu Y., Liu G., Zhao L. (2007). Nitrogen removal performance in a novel combined biofilm reactor. Process Biochemistry 42, 620-626.

**CHAPTER 2: Operation and dynamic modeling of a novel integrated anaerobic-aerobic-anoxic reactor for sewage treatment**

R. Plascencia-Jatomea • I. González • J. Gómez • O. Monroy

*Chemical Engineering Science (2015) 138, 31-40*



## Operation and dynamic modeling of a novel integrated anaerobic–aerobic–anoxic reactor for sewage treatment



R. Plascencia-Jatomea<sup>a</sup>, I. González<sup>b</sup>, J. Gómez<sup>a</sup>, O. Monroy<sup>a,\*</sup>

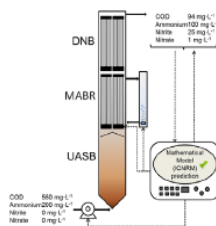
<sup>a</sup> Departamento de Biotecnología, Universidad Autónoma Metropolitana-Iztapalapa, Av. San Rafael Atlixco 186, C.P. 09340 Iztapalapa, México D. F., Mexico

<sup>b</sup> Departamento de Química, Universidad Autónoma Metropolitana-Iztapalapa, Av. San Rafael Atlixco 186, C.P. 09340 Iztapalapa, México D. F., Mexico

### HIGHLIGHTS

- A small footprint integrated column reactor for wastewater treatment was developed.
- High COD removal efficiency in short HRT was obtained.
- Stable nitrification process with nitrite accumulation was obtained.
- A validated dynamic model was used for the reactor operation and design.

### GRAPHICAL ABSTRACT



### ARTICLE INFO

#### Article history:

Received 5 March 2015

Received in revised form

9 June 2015

Accepted 26 July 2015

Available online 11 August 2015

#### Keywords:

Anaerobic digestion  
Partial nitrification  
Mathematical model  
Hydrodynamic profile  
Reaction kinetics

### ABSTRACT

Integrated reactors (IR) combining anaerobic, aerobic and nitrogen removal processes are a viable alternative to reduce operational costs and footprint compared to conventional wastewater treatment plants. An integrated bench scale (6.4 L) anaerobic–aerobic–anoxic column reactor (ICR) is developed to remove carbon and nitrogen compounds from sewage of our university campus. The ICR is comprised of an up-flow anaerobic sludge blanket reactor (UASB), a membrane aerated biofilm reactor (MABR) and a denitrifying biofilm reactor (DNB). The global COD removal efficiency ( $\eta_{C-Global}$ ) is  $\sim 82\%$  at hydraulic retention time (HRT) of 8.4 h. The partial nitrification (PN) process is obtained with an ammonia/nitrite ratio ( $R_{a/n}$ ) of 4. The experimental data were used to calibrate and validate an integrated carbon-nitrogen removal model (ICNRM), in order to determine operating conditions for the improvement of the ICR performance, considering the hydrodynamic profile and reaction kinetics. A good agreement between the measured and modeled results is obtained with a least square error function ( $S$ ) lower than 0.09. The model predicts that the COD removal efficiency at the MABR ( $\eta_{C-MABR}$ ) and nitrite accumulation at the DNB are influenced by the volumetric oxygen transfer coefficient ( $k_L a$ ) and oxygen concentration, respectively. The optimal operation zone for  $\eta_{C-MABR} > 90\%$  and  $R_{a/n}$  of 1.32 were reached for  $k_L a$  between 1.26 and 1.36 1/h, and an inlet DO concentration of 1.5 to 1.6 mg/L respectively, standing out the importance of calibrating hydrodynamic behavior and kinetics.

© 2015 Elsevier Ltd. All rights reserved.

### 1. Introduction

Wastewater treatment processes are typically equipped with different treatment units (up-flow anaerobic sludge bed reactors (UASB) followed by conventional activated sludge (CAS) systems) to achieve satisfactory water quality (Buntner et al., 2013; Chung

\* Corresponding author. Tel.: +52 55 58044816; fax: +52 58046407.  
E-mail address: [monroy@xanum.uam.mx](mailto:monroy@xanum.uam.mx) (O. Monroy).

# Operation and dynamic modeling of a novel integrated anaerobic-aerobic-anoxic reactor for sewage treatment

R. Plascencia-Jatomea • I. González • J. Gómez • O. Monroy

*Chemical Engineering Science (2015) 138, 31-40*

## Abstract

Integrated reactors (IR) combining anaerobic, aerobic and nitrogen removal processes are a viable alternative to reduce operational costs and footprint compared to conventional wastewater treatment plants. An integrated bench scale (6.4 L) anaerobic-aerobic-anoxic column reactor (ICR) is developed to remove carbon and nitrogen compounds from sewage of our university campus. The ICR is comprised of an up-flow anaerobic sludge blanket reactor (UASB), a membrane aerated biofilm reactor (MABR) and a denitrifying biofilm reactor (DNB). The global COD removal efficiency ( $\eta_{C-Global}$ ) is ~82% at hydraulic retention time (HRT) of 8.4 h. The partial nitrification (PN) process is obtained with an ammonia/nitrite ratio ( $R_{a/n}$ ) of 4. The experimental data were used to calibrate and validate an integrated carbon-nitrogen removal model (ICNRM), in order to determine operating conditions for the improvement of the ICR performance, considering the hydrodynamic profile and reaction kinetics. A good agreement between the measured and modeled results is obtained with a least square error function ( $S$ ) lower than 0.09. The model predicts that the COD removal efficiency at the MABR ( $\eta_{C-MABR}$ ) and nitrite accumulation at the DNB are influenced by the volumetric oxygen transfer coefficient ( $k_La$ ) and oxygen concentration, respectively. The optimal

operation zone for  $\eta_{C-MABR} > 90\%$  and  $R_{a/n}$  of 1.32 were reached for  $k_L a$  between 1.26 to 1.36 1/h, and an inlet DO concentration of 1.5 to 1.6 mg/L respectively, standing out the importance of calibrating hydrodynamic behavior and kinetics.

**Keywords**

anaerobic digestion; partial nitrification; mathematical model; hydrodynamic profile;  
reaction kinetics

## **2.1 Introduction**

Wastewater treatment processes are typically equipped with different treatment units (up-flow anaerobic sludge bed reactors (UASB) followed by conventional activated sludge (CAS) systems) to achieve satisfactory water quality (Buntner et al. 2013; Chung et al. 2007). Although UASB is compact and present low operational cost and sludge production, and substantial quantity of generated clean energy (methane), their combination with CAS systems still presents drawbacks, such as high operation costs (power for aeration and solids disposal) and extensive areas (Abbasi and Abbasi, 2012; Antonella et al. 2012).

Global standards in terms of water quality are becoming stricter and land cost is increasing (Verlicchi et al. 2011), which demands the development of more efficient treatment technologies with minimum foot-print and capital cost. An alternative to the use of conventional technologies could be the implementation of integrated reactors (IR) combining anaerobic, aerobic and anoxic processes, to improve the removal of pollutants and decreasing operation costs and land (Chan et al. 2009).

Recently, a membrane aerated biofilm reactor (MABR) with immobilization of biofilm on permeable membranes has been proposed as an alternative to integrate biological processes, this system can directly supply oxygen from the inner side to the biofilm (Semmens, 2008; Hibiya et al. 2003). Oxygen supplied into the membrane lumen passes through the membrane wall, and it is utilized by the biofilm bacteria (Liu et al. 2010). Therefore, the region near to the membrane shell side is a favorable condition for aerobic process because of sufficient oxygen (Wei et al. 2012), while at the apposite side, the region near to the biofilm-liquid interface is a suitable condition for anaerobic process due to the oxygen-depleted conditions

(Zhang et al. 1995). Hu et al. (2008) reported chemical oxygen demand (COD), ammonia and total nitrogen removal efficiencies of 86%, 94% and 84% respectively, at a hydraulic retention time (HRT) of 20 h using this configuration.

A different alternative for supplying oxygen to the MABR arises from both sides of the biofilm; through the permeable membranes wall and dissolved in the bulk liquid (Wu et al. 2008; González-Brambila et al. 2006). Accordingly, the oxygen and substrate concentration's profiles within the biofilm are quite different. The region near to the bulk liquid is favorable to oxidize the organic matter as it penetrates along with the oxygen into the biofilm. On the other hand, the region near to the membrane shell side is suitable conditions for nitrification as a result of sufficient oxygen and organic carbon-depleted conditions (Terada et al. 2006a; Satoh et al. 2004). However, in the above MABR reports synthetic wastewater was used and the effect on the pollutant removal performance due to the hydrodynamic phenomenology has not been analyzed. Therefore, a detailed investigation on the feasibility of COD and nitrogen removal aided by integrated mathematical (kinetic-hydrodynamic) models is needed to draw on the application range of this technology for sewage treatment.

Based on these concepts, a novel integrated anaerobic-aerobic-anoxic column reactor (ICR) is designed and developed for wastewater treatment with a small footprint. As a first stage, the ICR performs an anaerobic treatment at the UASB, in order to remove most of the inlet COD. Subsequently, the almost complete oxidation of the COD and partial nitrification (PN) of the ammonium based on immobilization of biofilm on permeable membranes is carried out on the MABR, and finally a third stage based on an anoxic denitrifying reactor to convert the resulting mixture of  $\text{NO}_2^-$  and  $\text{NH}_4^+$  to  $\text{N}_2$  by the anammox process (Tsushima et al. 2007).

Therefore, the goal of this study is to investigate the feasibility of sewage treatment for the removal of COD and nitrogen in the ICR, aided by a mathematical model to characterize and predict COD and nitrogen removal kinetics, as well as mass transport and hydrodynamic performance.

## **2.2 Materials and methods**

### **2.2.1 ICR configuration**

A laboratory-scale ICR was made of three mm thick Plexiglas tube with an internal diameter of 0.082 m, an effective volume of 6.4 L and a total height of 1.42 m (Fig. 2.1). The reactor consisted of an UASB (3 L), a MABR (1.35 L), a denitrifying biofilm reactor (DNB) (1.95 L) and an external saturation column (ESC) (0.1L). The heights of each reactor were 0.55 (UASB), 0.4 (MABR) and 0.47 m (DNB). The ICR had several sample ports to evaluate its performance in different sections. The MABR has 24 tubular hollow membranes (32cm length, 5mm inner radius, 1mm thickness, superficial membrane area of  $0.17\text{m}^2$ ). Dissolved oxygen (DO) was provided by the ESC and through the membranes. The intermembrane pressure was maintained at two psi. The DNB had the same geometric configuration than the MABR, but no aeration was applied. The membranes were used only as a supporting material.

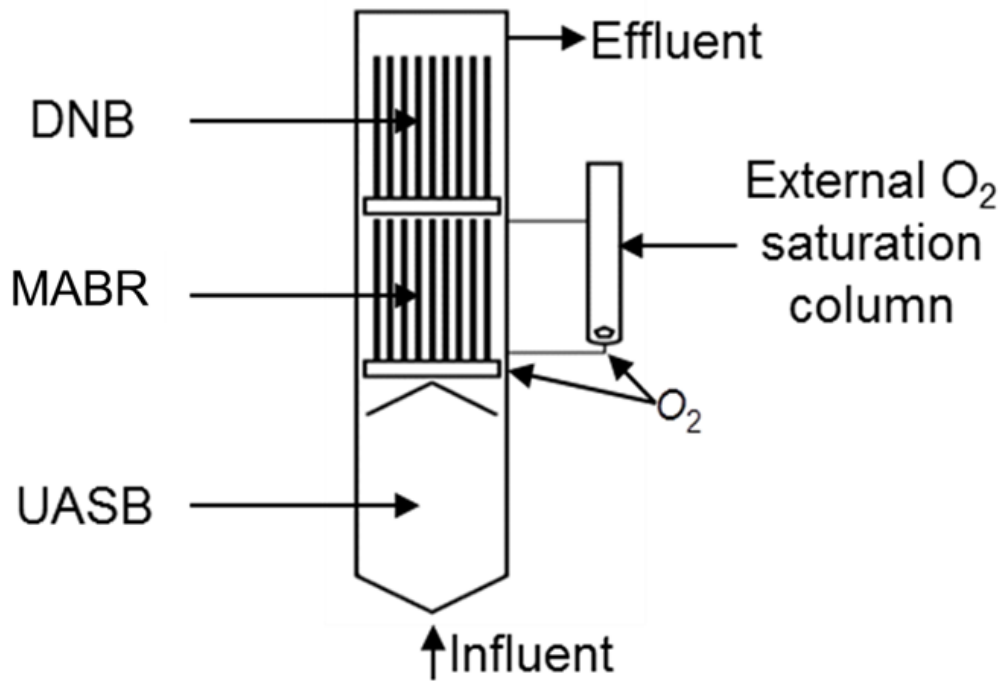


Figure 2.1. Integrated (anaerobic-aerobic-anoxic) column reactor.

The influent entered the ICR from the bottom of the UASB by a peristaltic pump, then through the three-phase separator to separate gas and liquid from solid and deviate out of the reactor the gas current to be quantified. The effluent of UASB flowed to the MABR and after that flowed to DNB. The operational temperature was maintained at  $29.6 \pm 0.8^\circ\text{C}$  without pH control.

### 2.2.2 Inoculation

The UASB and DNB were inoculated with 1 L and 0.2 L of anaerobic granular sludge (AGS) treating the university campus sewage. MABR was inoculated with 0.2 L of activated sludge (AS) from a domestic wastewater treatment plant in México, City. The initial volatile suspended solid (VSS) concentrations of sludge were approximately 52.5 gVSS/L (AGS) and 5.6 gVSS/L (AS).

### 2.2.3 Feed composition

The wastewater was collected from a general sewage of the university campus. Over our test period (200 days), it contained an average COD from 200 to 550 mg/L, an ammonium nitrogen concentration from 45 to 150 mg/L, an alkalinity from 650 to 870 mgCaCO<sub>3</sub>/L and pH 8.51±0.3.

### 2.2.4 Reactor start-up and operation strategy

The ICR was started at an inlet flow rate ( $F$ ) of 0.24 L/h. Initially; the UASB and MABR were operated with a HRT of more than 12 ( $HRT_{UASB}$ ) and 5 h ( $HRT_{MABR}$ ). The UASB influent concentration ( $I_{UASB}$ ) was about 200 mgCOD/L due to the rainy season. During this period (run I) the aerobic biofilm was formed in the external wall of the tubular membranes at the MABR. To induce the DNB biofilm formation the reactor was operated under batch conditions at a recycling flow rate ( $F_R$ ) of 2.4 L/h, using a synthetic medium (Gonzalez-Blanco et al. 2012). After 33 days of operation, a biofilm was formed and then was incorporated to the ICR on day 84 (run II). In order to calibrate and validated the integrated carbon-nitrogen removal model (ICNRM), experimental data were acquired at different HRT (Table 2.1) (stepwise decreased) in runs II to IV. The data were collected for analysis at steady-state conditions as COD removal efficiency reached 76% at the end of run IV. In runs V and VI, the  $HRT_{MABR}$  and HRT of the DNB ( $HRT_{DNB}$ ) were increased by splitting the UASB effluent ( $E_{UASB}$ ) and discharging a fraction of it. During all experimental runs the DO at the MABR was maintained around 0.7 to 0.9 mgDO/L by changing the  $F_R$  between the MABR and ESC.

Table 2.1. Operation conditions of the ICR.

Run	HRT <sub>UASB</sub> (h)	HRT <sub>MABR</sub> (h)	HRT <sub>DNB</sub> (h)
I	12.5	5.6	-
II	8.3	3.8	5.4
III	6.7	3	4.3
IV	5.9	2.6	3.8
V		4.5	6.5
VI		6.4	9.3

### 2.2.5 Analytical methods

COD, VSS and alkalinity were determined according to standard methods (APHA/AWWA/WEF, 2005). Ammonium was determined using a selective ammonium electrode (Orion Electrode Co.). DO was continuously monitored by WTW (oxi3410) meter with an optical probe. Nitrate and nitrite were determined by capillary electrophoresis (CIA) (Beckman Coulter, proteomeLab PA 800) according to González-Blanco et al. (2012). All liquid samples were filtered through a 0.45  $\mu\text{m}$  nylon membrane before analysis. The gas production was measured by displacement of a NaCl solution (30%) at pH 2 and its composition was determined by thermal conductivity gas chromatography (TCD) according to Durán et al. (2011).

### 2.2.6 The ICNRM

This model is based on two coupled models: a) COD removal at the UASB and MABR based on the AD1 and on a homogeneous model (González-Brambila et al. 2006), and b) ammonia nitrogen removal at the DNB based on a multiple species model (Huiliñir et al. 2010). The model's assumptions are:

- The UASB is a continuous stirred tank reactor (CSTR), and the MABR consists of two parallel CSTR: ESC and MABR.
- According to residence time distribution (RTD) studies (data not shown) the MABR presents flow pattern deviations; channeling in the central region and a low-velocity flow zone (stagnant zone) where the membranes are located and reactions take place.
- The MABR and DNB attained the same hydrodynamic profile.
- The biofilm is a homogeneous solid phase, exchanging with the liquid phase all substrates by convection.
- Constant biofilm thickness is considered.
- Oxygen is transferred through the membrane wall to the biofilm.
- The anaerobic ( $A_n$ ) and aerobic ( $A_e$ ) bacteria are represented by a single species.
- The nitrifying bacteria ( $X_3$ ) are represented by two species; ammonium-oxidizing bacteria ( $A_o$ ) and nitrite-oxidizing bacteria ( $N_o$ ).
- The microbial activity remains constant at the biofilm, and it is negligible at the bulk liquid.
- Mass transfer in biofilm follows Fick's law.

- The interfacial mass transfer coefficient ( $kl$ ) remains constant at the MABR and DNB.

Based on these assumptions the mass balances equations of the ICR are:

### 2.2.6.1 Bulk liquid:

➤ **UASB:**

• COD:

$$\frac{dC_{Cl}}{dt} = \frac{F}{V_l} \cdot (C_{Cl_0} - C_{Cl}) - \left( \frac{\mu_{An}}{Y_{An/COD}} \right) \cdot X_{An} \quad (1)$$

• The specific growth rate of  $An$  ( $\mu_{An}$ ) is:

$$\mu_{An} = \mu_{maxAn} \cdot \left( \frac{C_{Cl}}{k_{S,An} + C_{Cl}} \right) \quad (2)$$

• The maximum specific substrate consumption of  $An$  ( $q_{max}$ ) is:

$$q_{max} = \frac{\mu_{maxAn}}{Y_{An/COD}} \quad (3)$$

By substituting Eq. 3 and Eq. 2 in and Eq. 1; the mass balance at the UASB is:

$$\frac{dC_{Cl}}{dt} = \frac{F}{V_l} \cdot (C_{Cl_0} - C_{Cl}) - q_{max} \cdot \left( \frac{C_{Cl}}{k_{S,An} + C_{Cl}} \right) \cdot X_{An} \quad (4)$$

• The methane production rate ( $Q_{CH_4}$ ) is:

$$\frac{dQ_{CH_4}}{dt} = \frac{F}{V_l} \cdot (C_{Cl_0} - C_{Cl}) \cdot (Y_{CH_4/COD}) \quad (5)$$

➤ **MABR:**

The COD and oxygen mass balance at the inlet (Eqs. 6 and 7), outlet (Eqs. 8 and 9) and ESC (Eqs. 10 and 11) are:

$$C_{C2_0} = \frac{F}{F + F_R} \cdot C_{C1} + \frac{F_R}{F + F_R} \cdot C_{C,column} \quad (6)$$

$$C_{O2_0} = \frac{F_R}{F + F_R} \cdot C_{O,column} \quad (7)$$

$$C_{C2} = \alpha \cdot C_{C2_{sz}} + (1 - \alpha) \cdot C_{C2_{cz}} \quad (8)$$

$$C_{O2} = \alpha \cdot C_{O2_{sz}} + (1 - \alpha) \cdot C_{O2_{cz}} \quad (9)$$

$$C_{C,column} = C_{C2} \quad (10)$$

$$\frac{dC_{O,column}}{dt} = \frac{F_R}{V_{column}} \cdot (C_{O2} - C_{O,column}) + k_L a \cdot (C_O^* - C_{O,column}) \quad (11)$$

According to RDT, flow pattern deviations were identified (channeling (cz) and stagnant (sz) zones), so the COD (Eqs.12 and 14) and oxygen (Eqs. 13 and 14) mass balances at the bulk liquid are:

$$\frac{dC_{C2_{cz}}}{dt} = \frac{(1 - \alpha)(F + F_R)}{V_{2_{cz}}} \cdot (C_{C2_0} - C_{C2_{cz}}) \quad (12)$$

$$\frac{dC_{O2_{cz}}}{dt} = \frac{(1 - \alpha)(F + F_R)}{V_{2_{cz}}} \cdot (C_{O2_0} - C_{O2_{cz}}) \quad (13)$$

$$\frac{\partial C_{C2_{sz}}}{\partial t} = \frac{\alpha \cdot (F + F_R)}{V_{2_{sz}}} \cdot (C_{C2_0} - C_{C2_{sz}}) - a_{P2} \cdot D_{COD} \cdot \frac{\partial C_C}{\partial z} \Big|_{z=L_{BL}} \quad (14)$$

$$\frac{\partial C_{O2_{sz}}}{\partial t} = \frac{\alpha \cdot (F + F_R)}{V_{2_{sz}}} \cdot (C_{O2_0} - C_{O2_{sz}}) - a_{P2} \cdot D_O \cdot \left. \frac{\partial C_O}{\partial z} \right|_{z=L_{BL}} \quad (15)$$

➤ **DNB:**

The nitrogen compounds and oxygen mass balances at the inlet (Eqs. 16 and 17) and outlet (Eqs. 18 and 19) are:

$$C_{i3_0} = C_{i2} \quad (16)$$

$$C_{O3_0} = C_{O2} \quad (17)$$

$$C_{i3} = \alpha \cdot C_{i3_{sz}} + (1 - \alpha) \cdot C_{i3_{cz}} \quad (18)$$

$$C_{O3} = \alpha \cdot C_{O3_{sz}} + (1 - \alpha) \cdot C_{O3_{cz}} \quad (19)$$

By considering the same hydrodynamic profile ( $cz$  and  $sz$ ) as in case of the MABR, the mass balance equations for nitrogen compounds (Eqs. 20 and 22) and oxygen (Eqs. 21 and 23) in the bulk liquid are:

$$\frac{dC_{i3_{cz}}}{dt} = \frac{(1 - \alpha) \cdot F}{V_{3_{cz}}} \cdot (C_{i3_0} - C_{i3_{cz}}) \quad (20)$$

$$\frac{dC_{O3_{cz}}}{dt} = \frac{(1 - \alpha) \cdot F}{V_{3_{cz}}} \cdot (C_{O3_0} - C_{O3_{cz}}) \quad (21)$$

$$\frac{\partial C_{i3_{sz}}}{\partial t} = \frac{\alpha \cdot F}{V_{3_{sz}}} \cdot (C_{i3_0} - C_{i3_{sz}}) - a_{P3} \cdot D_i \cdot \left. \frac{\partial C_i}{\partial z} \right|_{z=L_{BL}} \quad (22)$$

$$\frac{\partial C_{O3_{sz}}}{\partial t} = \frac{\alpha \cdot F}{V_{3_{sz}}} \cdot (C_{O3_0} - C_{O3_{sz}}) - a_{P3} \cdot D_O \cdot \left. \frac{\partial C_O}{\partial z} \right|_{z=L_{BL}} \quad (23)$$

### 2.2.6.2 Biofilm

Equations 24, 25, 33, 34, 35 and 36 denote the mass balances inside the biofilm considering diffusion and reaction by aerobic oxidation of organic matter (MABR) and nitrification (DNM).

➤ **MABR:**

$$\frac{\partial C_{C2_{sz}}}{\partial t} = D_{eff-C} \cdot \frac{\partial^2 C_{C2_{sz}}}{\partial z^2} - \left( \frac{\mu_{Ae}}{Y_{Ae/COD}} \right) \cdot X_{Ae} \quad (24)$$

$$\frac{\partial C_{O2_{sz}}}{\partial t} = D_{eff-O} \cdot \frac{\partial^2 C_{O2_{sz}}}{\partial z^2} - \left( \frac{\mu_{Ae}}{Y_{Ae/O}} \right) \cdot X_{Ae} \quad (25)$$

• The specific growth rate of *Ae* ( $\mu_{Ae}$ ) is:

$$\mu_{Ae} = \mu_{max_{Ae}} \cdot \left( \frac{C_{C2_{sz}}}{k_{S,Ae} + C_{C2_{sz}}} \right) \left( \frac{C_{O2_{sz}}}{k_{O,Ae} + C_{O2_{sz}}} \right) \quad (26)$$

• Oxygen balance at the permeable membrane is given by:

$$\frac{\partial C_{O_m}}{\partial t} = D_{eff-O_m} \cdot \frac{\partial^2 C_{O_m}}{\partial z^2} \quad (27)$$

Initial and boundary conditions are given by Eqs. 28 to 32, which represent the mass transfer of COD and oxygen at the interfaces between membrane-biofilm interface ( $Z=L_{MB}$ ), biofilm-liquid interface ( $Z=L_{BL}$ ) and gas-membrane interface ( $Z=L_{GM}$ ).

$$D_{eff-O_m} \cdot \frac{\partial C_{O_m}}{\partial z} = D_{eff-O} \cdot \frac{\partial C_O}{\partial z} \quad \text{for } Z=L_{MB} \quad (28)$$

$$\frac{\partial C_C}{\partial z} = 0 \quad \text{for } Z=L_{MB} \quad (29)$$

$$-D_{eff-C} \cdot \frac{\partial C_C}{\partial z} = kl \cdot (C_{C,liquid} - C_C) \quad \text{for } Z=L_{BL} \quad (30)$$

$$-D_{eff-O} \cdot \frac{\partial C_O}{\partial z} = kl \cdot (C_{O,liquid} - C_O) \quad \text{for } Z=L_{BL} \quad (31)$$

$$-D_{eff-O_m} \cdot \frac{\partial C_{O_m}}{\partial z} = kg \cdot (C_{O,gas} - C_{O_m}) \quad \text{for } Z=L_{GM} \quad (32)$$

➤ **DNB:**

$$\frac{\partial C_{TAN_{3sz}}}{\partial t} = D_{eff-TAN} \cdot \frac{\partial^2 C_{TAN_{3sz}}}{\partial z^2} - \left( \frac{\mu_{Ao}}{Y_{Ao/TAN}} \right) \cdot X_{Ao} \quad (33)$$

$$\frac{\partial C_{NO_2^-_{3sz}}}{\partial t} = D_{eff-NO_2^-} \cdot \frac{\partial^2 C_{NO_2^-_{3sz}}}{\partial z^2} + \left( \frac{\mu_{Ao}}{Y_{Ao/TAN}} \cdot Y_{NO_2^-/TAN} \right) \cdot X_{Ao} - \left( \frac{\mu_{No}}{Y_{No/NO_2^-}} \right) \cdot X_{No} \quad (34)$$

$$\frac{\partial C_{NO_3^-_{3sz}}}{\partial t} = D_{eff-NO_3^-} \cdot \frac{\partial^2 C_{NO_3^-_{3sz}}}{\partial z^2} + \left( \frac{\mu_{No}}{Y_{No/NO_2^-}} \cdot Y_{NO_3^-/NO_2^-} \right) \cdot X_{No} \quad (35)$$

$$\frac{\partial C_{O_{3sz}}}{\partial t} = D_{eff-O} \cdot \frac{\partial^2 C_{O_{3sz}}}{\partial z^2} - \left( \frac{\mu_{Ao}}{Y_{Ao/O}} \right) \cdot X_{Ao} - \left( \frac{\mu_{No}}{Y_{No/O}} \right) \cdot X_{No} \quad (36)$$

The  $Ao$  ( $\mu_{Ao}$ ) and  $No$  ( $\mu_{No}$ ) specific growth rates may be expressed as Huiliñir et al. (2010):

$$\mu_{Ao} = \mu_{max_{Ao}} \left( \frac{C_{NH_3}}{k_{S,Ao} \left( 1 + \left( \frac{C_{HNO_2}}{k_{I,Ao}} \right) \right) + C_{NH_3} + \left( \frac{C_{NH_3}^2}{k_{IS,Ao}} \right)} \right) \left( \frac{C_O}{(k_{O,Ao} + C_O)} \right) \quad (37)$$

$$\mu_{No} = \mu_{max_{No}} \left( \frac{C_{HNO_2}}{k_{S,No} \left( 1 + \left( \frac{C_{NH_3}}{k_{I,No}} \right) \right) + C_{HNO_2} + \left( \frac{C_{HNO_2}^2}{k_{IS,No}} \right)} \right) \left( \frac{C_O}{(k_{O,No} + C_O)} \right) \quad (38)$$

Equations 36 and 37 show that only non-ionized species are used as bacterial substrates (van Hulle et al. 2007). Thus,  $NH_4^+/NH_3$  and  $NO_2^-/HNO_2$  equilibriums as a function of pH in the

dynamic modeling were included.

$$C_{NH_3} = \frac{C_{TAN}}{1 + k_{d(NH_3)} \cdot 10^{-pH}} \quad (39)$$

$$C_{HNO_2} = \frac{C_{NO_2^-}}{1 + k_{d(HNO_2)} \cdot 10^{pH}} \quad (40)$$

The initial and boundary conditions are given by Eqs. 42 and 43 which represent the mass transfer of nitrogen compounds and oxygen at the interfaces.

$$\frac{\partial C_i}{\partial z} = 0 \quad \text{for } Z=L_{MB} \quad (41)$$

$$-D_{eff-i} \cdot \frac{\partial C_i}{\partial z} = kl \cdot (C_{i,liquid} - C_{i,biofilm}) \quad \text{for } Z=L_{BL} \quad (42)$$

The bacterial concentration of *Ao* ( $X_{Ao}$ ) and *No* ( $X_{No}$ ) were defined as:

$$X_{Ao} = f \cdot X_3 \quad (43)$$

### 2.2.7 Modeling

The partial differential equations of the model were numerically solved and discretized through the line method. The numerical method used to solve the system of ordinary differential equations was by stiff-type equations (included in Berkeley Madonna software). The parameter values used in the model are those published in the literature (Table 2.2).

Table 2.2. Parameter values used in the ICNRM.

Parameter	Unit	Value	Reference	
$\mu_{\max_{Ae}}$	1/h	0.1	Montalvo, 2003	
$\mu_{\max_{Ao}}$		0.078	Sorensen, 1993	
$\mu_{\max_{No}}$		0.045	Weismann, 1994	
$K_{S,Ai}$	mgCOD/L	226	Bhunia and Ghangrekar, 2008	
$K_{S,Ao}$	mgNH <sub>3</sub> -N/L	0.028	Weismann, 1994	
$K_{I,Ao}$	mgHNO <sub>2</sub> -N/L	0.003		
$K_{IS,Ao}$	mgNH <sub>3</sub> -N/L	540		
$K_{O,Ao}$	mgO <sub>2</sub> /L	0.3		
$K_{S,No}$	mgHNO <sub>2</sub> -N/L	3.2x10 <sup>-5</sup>		
$K_{I,No}$	mgNH <sub>3</sub> -N/L	0.01		
$K_{IS,No}$	mgHNO <sub>2</sub> -N/L	0.26		
$K_{O,No}$	mgO <sub>2</sub> /L	1		
$K_{O,Ae}$	mgO <sub>2</sub> /L	5		Montalvo, 2003
$K_{S,Ae}$	mgCOD/L	50		
$Y_{CH_4/COD}$	LCH <sub>4</sub> /mgCOD	3.4x10 <sup>-4</sup>		
$Y_{Ae/COD}$	mgSSV/mgCOD	0.5		
$Y_{Ae/O}$	mgVSS/mgO <sub>2</sub>	0.7		
$Y_{Ao/TAN}$	mgVSS/mgTAN	0.03	Sorensen, 1993	
$Y_{No/NO_2^-}$	mgVSS/mgNO <sub>2</sub> <sup>-</sup>	0.02		
$Y_{Ao/O}$	mgVSS/mgO <sub>2</sub>	0.051	Weismann, 1994	
$Y_{No/O}$	mgVSS/mgO <sub>2</sub>	0.042		
$Y_{NO_2/TAN}$	mgNO <sub>2</sub> /mgTAN	0.98		
$Y_{NO_3/NO_2}$	mgNO <sub>3</sub> /mgNO <sub>2</sub>	1		
$k_d(NH_3)$	-	3.89818x10 <sup>-4</sup>		

$k_{d(HNO_2)}$	-	$3.95 \times 10^{-9}$	
$X_{Ae}$	mgVSS/L	30000	González-Brambila et al. 2006
$D_{eff-O_m}$	m <sup>2</sup> /h	$4.36 \times 10^{-2}$	Atwater and Aske, 2007
$D_{eff-C}$		$1.8 \times 10^{-6}$	Sorensen, 1993
$D_{eff-O}$		$4.99 \times 10^{-6}$ (MABR)	
		$9.156 \times 10^{-6}$ (DNB)	
$D_{eff-TAN}$		$1.96 \times 10^{-7}$	This study
$D_{eff-NO_2}$		$4 \times 10^{-7}$	
$D_{eff-NO_2}$		$4 \times 10^{-7}$	
$L_{biofilm}$		m	
	$1 \times 10^{-3}$ (DNB)		
$T$	°C	30	
$\alpha$	-	0.85	
$X_{An}$	mgVSS/L	8330	
$X_{R3}$		35000	
$a_p$	m <sup>2</sup> /m <sup>3</sup>	126 (MABR)	
		87 (DNB)	
$f$	-	0.77	

### 2.2.8 Model calibration, validation and simulation

Calibration consisted to adjust two parameters which were determined as the ones that most affect COD removal and nitrite accumulation according to the methodology of Huiliñir et al. (2009):  $q_{max}$  and  $kl$ , using the experimental data from the continuous ICR operation. The adjustment was performed via a minimization of the least square error function ( $S$ ) presented in Eq. (44).

$$S = \sqrt{\frac{\sum_i^n \left( \frac{C_{i,exp} - C_{i,calc}}{C_{i,calc}} \right)^2}{n}} \quad (44)$$

where  $C_{i,exp}$  is the concentration of the species measured experimentally,  $C_{i,calc}$  is model's result calculated and  $n$  is the amount of data. For validation procedures, the experimental data was compared to those calculated by the ICNRM. The parameters compared were: COD, total ammonia nitrogen (TAN), nitrite, nitrate and DO concentrations. Experimental concentrations with errors lower than 5% with respect to the mean value were considered acceptable for calibration and validation procedures. From this, the effect of the oxygen concentration ( $C_O$ ) and the stagnant zone volume/reactor volume ratio ( $\beta = V_{isz} / V_i$ ) was simulated. The temperature and simulation time were 30°C and 30000 h.

## 2.3 Results and discussion

### 2.3.1 COD removal performance of the ICR

After 125 days, the global COD removal efficiency ( $\eta_{C-Global}$ ) of the ICR was stabilized around 76% (Fig. 2.2). As the  $HRT_{MABR}$  was increased (run V and VI),  $\eta_{C-Global}$  only augments to  $81 \pm 1.27\%$ . Since the ICR is an integrated reactor, the COD removal and conversion of organic matter were investigated in the UASB and MABR. The effluent of UASB was assumed as the influent of MABR ( $I_{MABR}$ ).

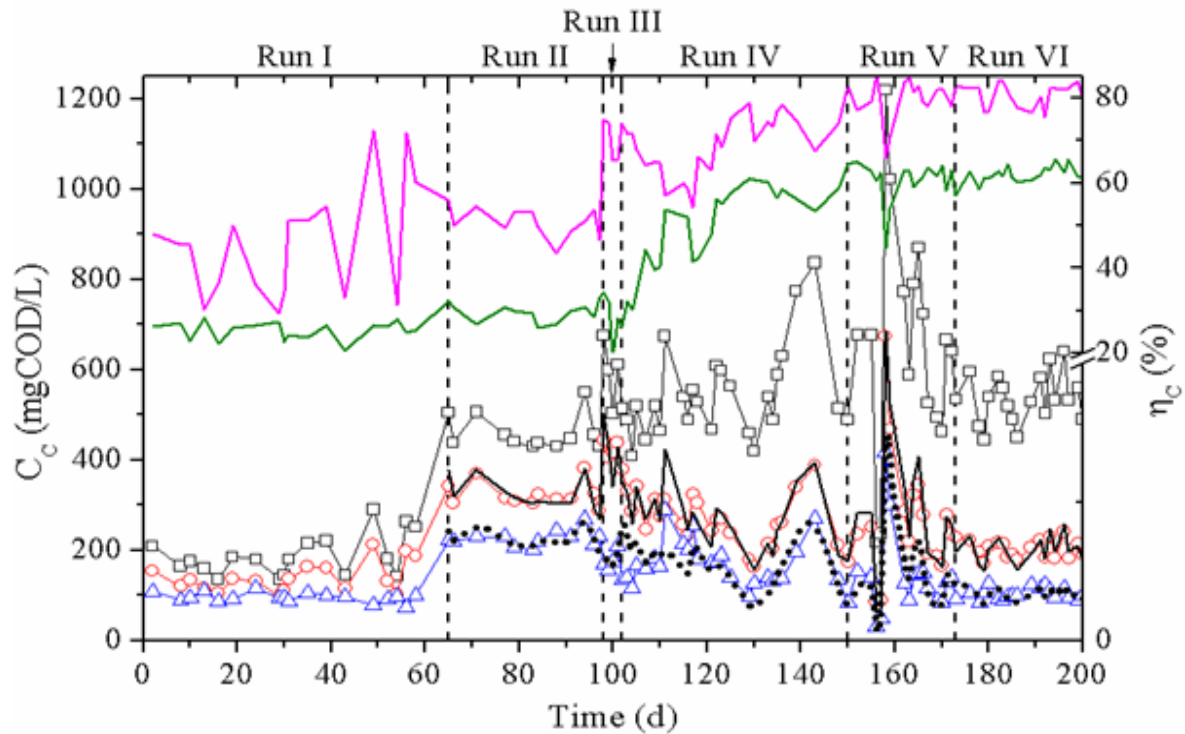


Figure 2.2. COD removal efficiency ( $\eta_c$ ) and COD at influent ( $C_{CI}$ ) and effluents ( $C_{CE}$ ) of the ICR.  $\eta_{C-UASB}$  (—),  $\eta_{C-Global}$  (—),  $C_{CI-UASB}$  ( $\square$ ),  $C_{CE-UASB}$  ( $\circ$ ) and  $C_{CE-MABR}$  ( $\triangle$ ); ICNRM predictions:  $C_{CE-UASB}$  (—) and  $C_{CE-MABR}$  (.....).

For UASB, the organic loading rate (OLR) affected the COD removal efficiency ( $\eta_{C-UASB}$ ). By decreasing the HRT (run II to III) the  $OLR_{UASB}$  was increased up to  $2.26 \pm 0.2$  gCOD/(L·d) and maintained at this value to the end of the experiment. During this period, the UASB showed a stable performance reaching an average  $\eta_{C-UASB}$  of  $61.2 \pm 2.4\%$  and a biogas production of  $0.37 \pm 0.03$  L<sub>biogas</sub>/(L<sub>reactor</sub>·d), while an average COD ( $C_{CE-MABR}$ ) of  $\sim 95$  mg/L was obtained at the effluent of MABR ( $E_{MABR}$ ). The organic removal using integrated reactors has been investigated in many studies (Chan et al. 2009). The  $\eta_{C-UASB}$  of 62% obtained was similar to that obtained in the treatment of municipal wastewater in a pilot-scale UASB at HRT of 6 h

and an OLR of 2.4 gCOD/(L·d) (Tandukar et al. 2007). On the other hand, the  $\eta_{C-Global}$  obtained (~80%) in 8.4 h of treatment is comparable to that reported operating an integrated anaerobic-aerobic system (UASB+AS) treating municipal wastewater with a  $\eta_{C-Global}$  of 85-93 % and HRT of 7.2 h (Sperling et al. 2001). The average pH value of the system (UASB-MABR) was  $8.25 \pm 0.2$ . The pH did not show high variations due to the UASB alkalinity ( $745 \pm 48$  mg/L  $\text{CaCO}_3$ ); this value is well within the range where each process works adequately. Therefore, under these operational conditions, it can be suggested that the ICR is a viable alternative for sewage treatment.

### **2.3.2 Nitrogen removal performance of the ICR**

From run II to IV, the TAN removal efficiency at the MABR ( $\eta_{N-MABR}$ ) was about  $14.3 \pm 3.5\%$ , while in the DNB ( $\eta_{N-DNB}$ ) was  $31.6 \pm 3.1\%$  (run IV) (Fig. 2.3). However, no ammonium oxidation occurred as indicated by the low nitrate and nitrite concentrations detected in the  $E_{MABR}$  and DNB effluent ( $E_{DNB}$ ) ( $< 3$  mg $\text{NO}_3^- - \text{N}/\text{L}$  and  $1$  mg $\text{NO}_2^- - \text{N}/\text{L}$ ). The low ammonia removal observed during this operation period might be associated to nitrogen assimilation for microbial growth. Thus, the HRT of both reactors was increased by splitting a fraction of the effluent coming from the UASB (run V and VI).

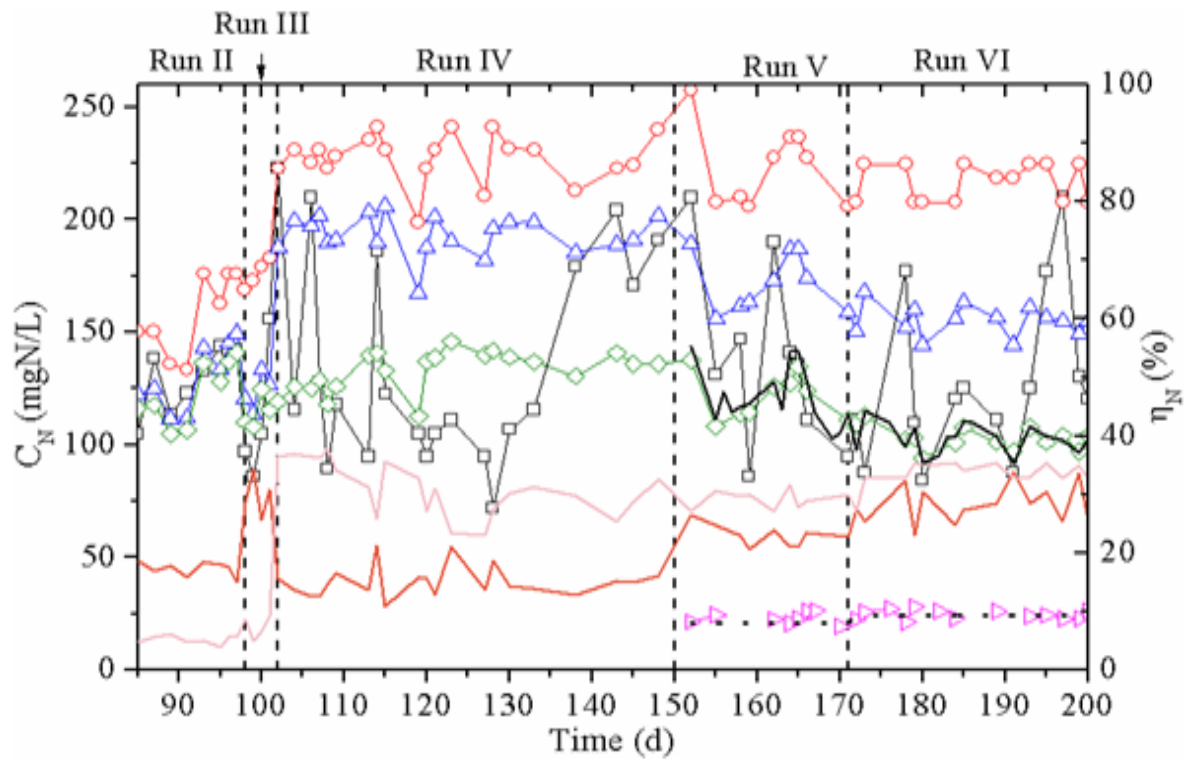


Figure 2.3. TAN removal efficiency ( $\eta_N$ ) and nitrogen compounds concentrations at influent ( $C_{NI}$ ) and effluents ( $C_{NE}$ ) of the ICR.  $\eta_{N-MABR}$  (—),  $\eta_{N-DNB}$  (—); TAN concentration:  $C_{NI-UASB}$  ( $\square$ ),  $C_{NE-UASB}$  ( $\circ$ ),  $C_{NE-MABR}$  ( $\triangle$ ) and  $C_{NE-DNB}$  ( $\diamond$ );  $mgNO_2^- - N$  concentration:  $C_{NE-DNB}$  ( $\triangleright$ ); ICNRM predictions: TAN at  $C_{NE-DNB}$  (—) and  $mgNO_2^- - N$  at  $C_{NE-DNB}$  (.....).

During this operation period (runs V and VI), TAN oxidation was observed at the MABR and DNB (Fig. 2.3). The nitrogen loading rates (NLR) in the MABR were  $1.18 \pm 0.1$  and  $0.81 \pm 0.03$  gTAN/(L·d) while the nitrite production rate (NPR) was 93% lower than the expected ( $0.032 \pm 0.01$  and  $0.021 \pm 0.01$  g $NO_2^- - N$ /(L·d)). Since alkalinity is high adequately for PN, this low oxidation might be related to insufficient oxygen for *Ao* due to its competition with heterotrophic bacteria (Wu et al. 2008). On the other hand, at the DNB nitrification activity with accumulation to nitrite was observed related to the presence of residual  $C_O$  coming from

the MABR ( $0.79 \pm 0.08$  mgDO/L) due to its characteristic flow pattern behavior. The residual TAN arrived to the DNB at NLR of  $0.62 \pm 0.06$  and  $0.4 \pm 0.01$  gTAN/(L·d), originated a NPR equivalent to 66% of the partial TAN oxidation ( $0.079 \pm 0.009$  and  $0.063 \pm 0.005$  gNO<sub>2</sub><sup>-</sup> - N/(L·d)).

The channeling zone at the MABR produced a deficient TAN and DO transfer to microorganisms causing gradient concentrations, which passed up to the DNB (Chen et al. 2010). The presence of oxygen in the DNB might have favored the nitrifiers activity and inhibited the anammox activity since these microorganisms are obligatory anaerobes and reversibly inhibited by low DO concentrations (Cho et al. 2011). The DNB produced an effluent with an ammonium/nitrite ratio ( $R_{a/n}$ ) of 5.3 and 4.17. These values are high for the anammox process since the stoichiometric ratio recommended for an efficient process is 1.32 (Jin and Zhen, 2009). On the other hand, the pH at the  $E_{DNB}$  was  $7.9 \pm 0.09$ ; this value showed quite variations with respect to the pH obtained in the UASB-MABR system ( $8.25 \pm 0.2$ ). These low changes might be associated to the elevated alkalinity (~780 mg/L) of the sewage.

Several reports have suggested that a key step in the implementation of the PN is to establish the pertinent environmental conditions for  $A_o$  and adverse conditions for  $N_o$ . Different strategies have been used to suppress the  $N_o$  activity, including inhibition by free ammonium (FA), temperature elevation (30°C), alkalinity/ammonium ratio (4.8) as well as control of DO concentration (0.7-1.4 mgDO/L) (Khin and Annachhatre, 2004; Ruiz et al. 2003). While the temperature ( $29.6 \pm 0.8^\circ\text{C}$ ), pH ( $7.9 \pm 0.09$ ) and alkalinity/ammonium ratio (4.8) were suitable for PN at the ICR,  $C_o$  was in the lower limit (0.7 - 0.9 mgDO/L). The high  $R_{a/n}$  obtained at the

DNB might be related to the insufficient DO concentration in the DNB influent ( $I_{\text{DNB}}$ ) as well as its characteristics hydrodynamic profile.

### 2.3.3 Calibration and validation of the ICNRM

In order to have a better insight on the performance of the ICR in kinetic and mass transfer phenomenology the ICNRM was used. The ICNRM predicted the COD ( $C_C$ ) at the  $E_{\text{UASB}}$  and  $E_{\text{MABR}}$  (Fig. 2.2). At all OLR values the experimental  $C_C$  were estimated by the model. The  $S$  value was lower than 0.092, confirming that the ICNRM adequately predicts the activity of the anaerobic sludge and aerobic biofilm of the ICR. A good agreement between the measured and modeled results was obtained despite the natural variability of the inlet  $C_C$ .

As is shown in Fig. 2.2, when the  $\text{OLR}_{\text{UASB}}$  increased from 1.3 to 2.6 gCOD/(L·d),  $\eta_{\text{C-UASB}}$  showed an increment from 24 to 61%, respectively. This trend agrees with the model's prediction and might be related by kinetic effects due to the adaptation of the anaerobic sludge over the time to the experimental conditions tasted.

The adjusted parameter used to calibrate the model was  $q_{\text{max}}$  in case of the UASB. The value of  $q_{\text{max}}$  was fitted to a sigmoidal profile over the time in order to predict the  $C_C$ . The equation used was:  $q_{\text{max}} = a + ((a-b)/(1-\text{EXP}((t-c)/d)))$ , where  $t$  is the time,  $a=0.7185$ ,  $b=0.35291$ ,  $c=113.84218$  and  $d=8.64203$ . It is worth mentioning that the maximum and stable value of  $q_{\text{max}}$  was 0.0145mgCOD/(mgVSS·h) (run V to VI). This value corresponds to values of maximum specific growth rate of *An* ( $\mu_{\text{maxAn}}$ ) and yield coefficient of *Ae* ( $Y_{\text{An/COD}}$ ) of  $2.62 \times 10^{-3}$  1/h and 0.18 mgVSS/mgCOD, respectively. The  $\mu_{\text{maxAn}}$  value is within the range ( $1.7 \times 10^{-3}$ -0.038 1/h) reported by Bhunia and Gangrekar (2008). The value of  $Y_{\text{An/COD}}$  resulted similar to

that reported by Montalvo (2003).

In case of MABR, the adjusted parameter used to calibrate the model was  $kl$  (Table 2.3) whose observed magnitude is within the wide range (0.003-0.42 m/h) reported for immobilized biofilms (Matsumoto et al. 2007; González-Brambila et al. 2006). This parameter seems to be affected by the up-flow velocity ( $V_{up}$ ) of the liquid. If the value of  $V_{up}$  is decreased results in a diminish value of  $kl$  and vice versa. This might be due to diminish the film of liquid, which offers maximum resistance to the transfer of substrate to the biofilm surface (Mudliar et al. 2008). The deduction of the  $V_{up}$  was done by considering the effective transversal area at the MABR and DNB of  $4.35 \times 10^{-3} \text{ m}^2$  and the flow rate at the MABR ( $F + F_R$ ) or DNB ( $F$ ).

Table 2.3. The  $k_{La}$  profile and adjusted  $kl$  parameter for the MABR.

Run	$F_R$ (L/h)	$k_{La}$ (1/h)	$V_{up}$ (m/h)	$kl$ (m/h)
II	2.87	0.61	0.74	$2.58 \times 10^{-2}$
III	5.07	1.44	1.27	$4.73 \times 10^{-2}$
IV	3.74	0.96	0.97	$3.09 \times 10^{-2}$
V	2.87	0.61	0.73	$2.46 \times 10^{-2}$
VI	1.56	0.53	0.4	$1.87 \times 10^{-2}$

The oxygen was supplied through the membrane and bubbled into the liquid at the ESC; therefore, there was an extra contribution to the total supply of oxygen. The oxygen dosage was related to the inlet COD during the whole experiment adjusting the oxygen transfer

coefficient of oxygen ( $k_L a$ ) at the ESC. This strategy was made by changing  $F_R$  between the MABR and the ESC (Table 2.3). The  $C_O$  estimate by the model corresponds to that obtained experimentally (Fig. 2.4) confirming a good prediction of the aerobic microorganisms's activity.

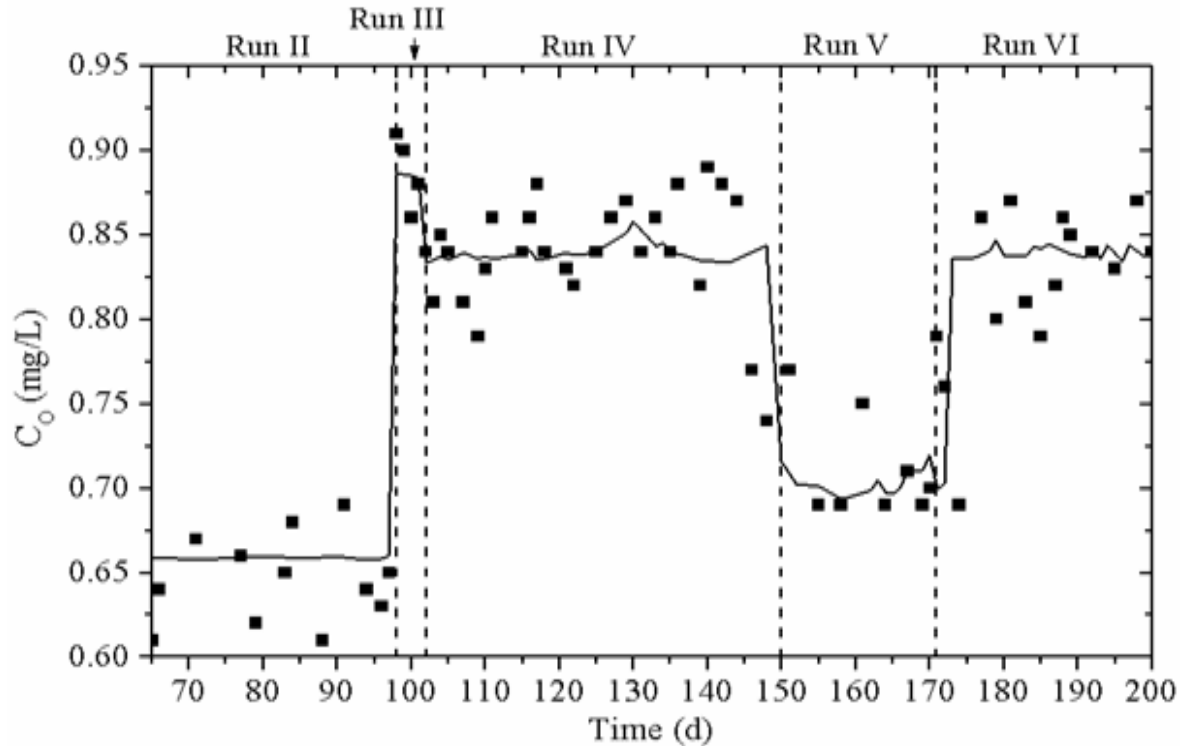


Figure 2.4. Oxygen concentration ( $C_O$ ) profile and model predictions during run IV to VI:  $C_{O-MABR}$  (■) and ICNRM prediction;  $C_{O-MABR}$  (—).

As the oxygen diffuses simultaneously from two opposite boundaries of the biofilm, whereas the substrate (COD) diffuses only from the biofilm-liquid interface, two regions of reaction rate with different magnitude and width were predicted (Fig. 2.5). The prediction corresponds to the operation of MABR during the run VI, assuming a constant biofilm thickness.

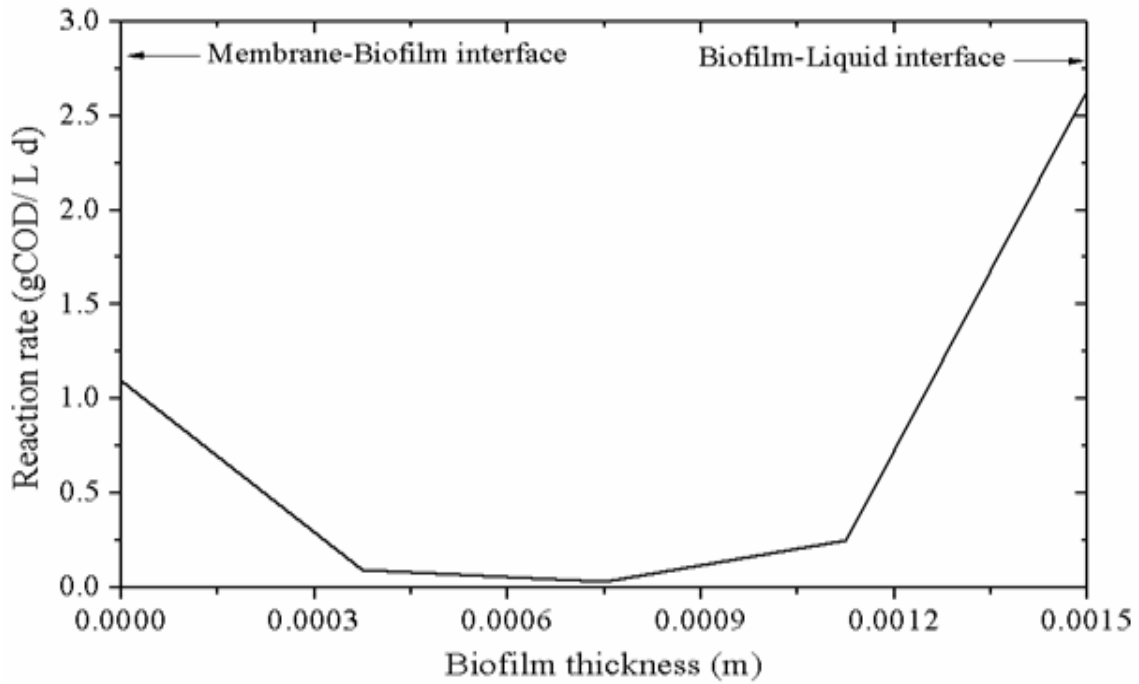


Figure 2.5. ICNRM predicted reaction rate profile within the biofilm. Reaction rate (—).

The reaction rate in the biofilm-liquid interface is 2.4 times higher than the one at the membrane-biofilm interface. This might be explained by the fact that substrate diffuses together with the dissolved oxygen from the bulk liquid, as the substrate diffuses to the nearest membrane wall region where oxygen is available, the reaction rate rises again.

In case of nitrogen compounds concentration ( $C_N$ ), the ICNRM could predict the ammonium and nitrite concentration at  $E_{DNB}$  in run V to VI (Fig. 2.3). As in case of carbon compounds, a good agreement between the measured and modeled results was obtained. The  $S$  value was lower than 0.07, confirming that the ICNRM adequately predicts the activity of the nitrifying biofilm under these experimental conditions. The adjusted parameter used to calibrate the model at the DNB was  $kl$ . The value of  $kl$  (0.013 m/h) was obtained by fitting the tendency of  $kl$  according to  $V_{up}$  (Table 2.3).

### 2.3.4 Model simulation: effect of the $k_La$ , $C_O$ and $\beta$ on the performance of the ICR

The performance of MABR was simulated using the following operating conditions: OLR at the MABR of 1.41 gCOD/(L·d) and  $HRT_{MABR}$  of 4.5 h. The  $F_R$ ,  $k_La$  and  $kl$  values were adjusted according to Table 2.3. The effect of the  $k_La$  on the steady-state performance of the MABR shows that a higher  $k_La$  value increases the COD removal efficiency ( $\eta_{C-MABR}$ ) besides the  $C_O$  at the  $E_{MABR}$  (Fig. 2.6A). This behavior shows that the  $\eta_{C-MABR}$  is found to be determined by the external transport of oxygen. A zone of optimal operation can be observed between  $k_La$  values of 1.26 and 1.36 1/h, where the  $\eta_{C-MABR}$  and  $C_O$  at the  $E_{MABR}$  are greater than 90% and 1.5 mgDO/L, according to the value of  $\beta$ . These operational conditions can produce a  $C_O$  at the  $E_{MABR}$  that allowed enhancing a favorable  $R_{a/n}$  for the partial nitrification process at the DNB (Fig. 2.6B).

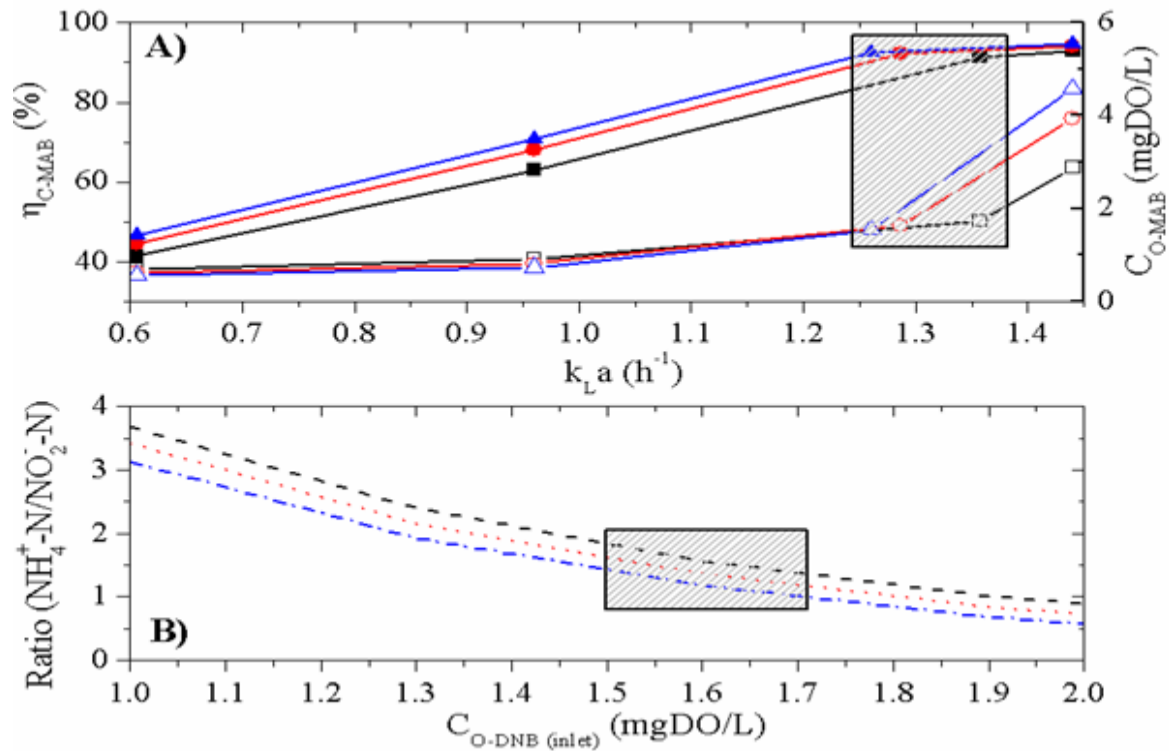


Figure 2.6.  $k_L a$ ,  $C_O$  and  $\beta$  effect on the  $\eta_C$  and  $R_{a/n}$ . A)  $\eta_{N-MABR}$  at  $\beta = 0.85$  (■),  $\beta = 0.9$  (●) and  $\beta = 0.95$  (▲);  $C_O$  at  $\beta = 0.85$  (□),  $\beta = 0.9$  (○) and  $\beta = 0.95$  (△). B)  $R_{a/n}$  at  $\beta = 0.85$  (—),  $\beta = 0.9$  (⋯) and  $\beta = 0.95$  (-.-).

The effect of the  $C_O$  on the steady-state performance at the  $I_{DNB}$  at pH of 7.9 and NLR of 0.61 gTAN/(L·d) was simulated (Fig. 3.6B). The main conclusion that can be drawn is the great influence of  $C_O$  on the  $R_{a/n}$  confirming that the nitrification process with accumulation of nitrite is limited by oxygen concentration. As shown in Fig. 2.6B, an ideal zone for operation can be observed between  $C_O$  values of 1.5 and 1.7 mgDO/L according to the value of  $\beta$ . Values out of this range can produce inadequate  $R_{a/n}$  limiting the anammox process. As in case of the MABR, the performance of the PN at the DNB is found to be controlled by the external transport of oxygen. It is worth mentioning that these results are the first for operation of ICR

and to be able to control the oxygen level and to operate different metabolic processes. On the other hand, the improvement of the hydrodynamic profile of the reactor in order to increase the volume of the homogeneous flow velocity zone ( $\beta > 0.85$ ) was seen to have an important effect too. The  $k_L a$  and  $C_O$  can be reduced in 7.4 and 11.8% with  $\beta$  of 0.95, respectively. This might be related to the reduction of the channeling zone allowing having a homogenous oxygen concentration in almost all the volume.

## 2.4 Conclusions

This work describes the operation of an ICR for the removal of carbon and nitrogen from sewage. Experiments were conducted upon different operational condition to assess the calibration and validation of the integrated model (ICNRM). The findings of this study can be concluded as follows:

- a) The ICR could produce an effluent with 95 mgCOD/L, suggesting that the proposed ICR configuration is a good alternative for the treatment of municipal wastewater reducing the footprint.
- b) Experimental measurements showed that the ICR could carry out a partial nitrification with an  $R_{a/n}$  of 4.7 and 3.99, which is still far from the recommended value (1.32). However, there is evidence showing that the carbon and nitrogen removal can be performed in the ICR.
- c) The anaerobic, aerobic and partial nitrification processes in the ICR operated over 200 days were represented using a dynamic model (ICNRM). The model adequately predicted ( $S < 0.09$ ) the continuous operation of ICR at different HRT and recirculation flow rates between the MABR and the ESC, providing a higher quality in the prediction of COD, ammonium nitrogen, nitrite, nitrate and DO concentrations.

d) The simulation studies and experimental assays used to study ICR indicated that COD oxidation and nitrification with nitrite accumulation presented a high sensitivity to the DO concentration.

e) It was possible to determine that the recommended  $R_{a/n}$  can be obtained at the DNB with DO concentration of 1.5 mg/L as well as the improvement of the flow pattern profile at the MABR and DNB. Future studies must be done in order to improve the ICR performance.

### **Acknowledgements**

Authors thank to the National Council for Science and Technology (CONACyT) México for scholarship (208977), México City's Science, Technology and Innovation Secretary (SECITI DF) and Mr. Ignacio Juarez for his invaluable support for the construction of the integrated column reactor.

## Nomenclature

$a_{pi}$	specific area for $i$ : 2)MABR and 3)DNB ( $m^2/m^3$ )
$C_{Ci}$	COD for $i$ : 1) UASB and 2)MABR (mgCOD/L)
$C_{C,column}$	COD at the ESC (mgCOD/L)
$C_{i3}$	total nitrogen concentration for $i$ at the DNB: total ammonia nitrogen (TAN) ( $NH_3 - N + NH_4^+ - N$ ); total nitrite concentration ( $HNO_2 - N + NO_2^- - N$ ) and total nitrate concentration ( $HNO_3 - N + NO_3^- - N$ ) (mgN/L)
$C_{Oi}$	DO concentration for $i$ : 2)MABR and 3)DNB ( $mgO_2/L$ )
$C_{O,column}$	DO concentration at the ESC ( $mgO_2/L$ )
$C_{O_m}$	oxygen concentration in the membrane ( $mgO_2/L$ )
$C_O^*$	equilibrium concentration of oxygen ( $mgO_2/L$ )
$D_i$	diffusion coefficient for $i$ : COD and $O_2$ ( $m^2/h$ )
$D_{eff-i}$	effective diffusion coefficient for $i$ : COD, TAN, $NO_2^- - N$ , $NO_3^- - N$ and $O_2$ ( $m^2/h$ )
$D_{eff-O_m}$	effective diffusion coefficient of $O_2$ in the membrane ( $m^2/h$ )
$F$	inlet flow rate (L/h)
$F_R$	recycling flow rate (L/h)
$V_i$	reactor volume for $i$ : 1)UASB, 2)MABR and 3)DNB (L)

$V_{column}$	volume of the ESC (L)
$\alpha$	liquid fraction passing through the stagnant zone
$\beta$	stagnant zone volume/reactor volume ratio
$kl$	mass transfer coefficient in the membrane-biofilm-liquid interface (m/h)
$kg$	mass transfer coefficient at the gas-membrane interface (m/h)
$k_L a$	volumetric oxygen mass transfer coefficient (1/h)
$V_{up}$	up-flow velocity (m/h)
$S$	least square error function
$X_i$	bacteria concentration for $i$ : $An$ , $Ae$ , $Ao$ and $No$ (mgVSS/L)
$X_3$	nitrifying bacteria (mgVSS/L)
$f$	volume fraction of ammonium-oxidizing bacteria
$\mu_i$	specific growth rate for $i$ : $An$ , $Ae$ , $Ao$ and $No$ (1/h)
$\mu_{max_i}$	maximum specific growth rate for $i$ : $An$ , $Ae$ , $Ao$ and $No$ (1/h)
$Q_{CH_4}$	methane production rate ( $L_{CH_4}/(L \cdot h)$ )
$q_{max}$	maximum specific substrate consumption of $An$ (mgCOD/(mgVSS·h))
$K_{S,i}$	saturation constant for $i$ : $An$ (mgCOD/L), $Ae$ (mgCOD/L), $Ao$ (mgNH <sub>3</sub> - N/L) and $No$ (mgHNO <sub>2</sub> - N/L)

$K_{O,i}$	saturation constant of oxygen concentration for $i$ : $Ae$ , $Ao$ and $No$ ( $\text{mgO}_2/\text{L}$ )
$K_{I,i}$	competitive inhibition for $i$ : nitrous acid for $Ao$ ( $\text{mgHNO}_2 - \text{N}/\text{L}$ ) and ammonia for $No$ ( $\text{mgNH}_3 - \text{N}/\text{L}$ )
$K_{IS,i}$	substrate inhibition for $i$ : $Ao$ ( $\text{mgNH}_3 - \text{N}/\text{L}$ ) and $No$ ( $\text{mgHNO}_2 - \text{N}/\text{L}$ )
$k_{d(i)}$	equilibrium constant for $i$ : $\text{NH}_3$ and $\text{HNO}_2$
$L_{\text{biofilm}(i)}$	biofilm thickness for $i$ : 1)MABR and 2)DNB (m)
$Y_{An/COD}$	yield coefficient of $An$ ( $\text{mgVSS}/\text{mgCOD}$ )
$Y_{CH_4/COD}$	yield coefficient of methane ( $L_{CH_4}/\text{mgCOD}$ )
$Y_{Ae/i}$	yield coefficient of $Ae$ over to $i$ : COD and DO ( $\text{mgVSS}/\text{mg}$ )
$Y_{Ao/i}$	yield coefficient of $Ao$ over to $i$ : TAN, $\text{NO}_2^-$ , $\text{NO}_3^-$ and DO ( $\text{mgVSS}/\text{mg}$ )
$Y_{No/i}$	yield coefficient of $No$ over to $i$ : TAN, $\text{NO}_2^-$ , $\text{NO}_3^-$ and DO ( $\text{mgVSS}/\text{mg}$ )
$Y_{\text{NO}_2^-/\text{TAN}}$	stoichiometric coefficient of component $\text{NO}_2^-$ over TAN ( $\text{mgN}/\text{mgN}$ )
$Y_{\text{NO}_3^-/\text{NO}_2^-}$	stoichiometric coefficient of component $\text{NO}_3^-$ over $\text{NO}_2^-$ ( $\text{mgN}/\text{mgN}$ )

### Subindex

$0$	inlet concentration
$cz$	channeling zone
$sz$	stagnant zone

*An* anaerobic bacteria

*Ae* aerobic bacteria

*Ao* ammonium-oxidizing bacteria

*No* nitrite-oxidizing bacteria

## References

1. Abbasi, T., Abassi, S., A., 2012. Formation and impact of granules in fostering clean energy production and wastewater treatment in up flow anaerobic sludge blanket (UASB) reactors. *Renewable and Sustainable Energy Reviews* 16, 1696-1708.
2. Antonella, L., Viotti, P., Mancini, G., Torretta, V., 2012. An integrated wastewater treatment system using a BAS reactor with biomass attached to tubular supports. *Journal of Environmental Management* 113, 51-60.
3. APHA/AWWA/WEF, 2005. *Standard Methods for the Examination of Water and Wastewater*, Washington DC, USA.
4. Atwater, J., E., Aske, J., R., 2007. Oxygen permeation through functionalized hydrophobic tubular ceramic membranes. *Journal of Membrane Science* 301, 76-84.
5. Bhunia, P., Ghangrekar, M., M., 2008. Analysis, evaluation and optimization of kinetic parameters for performance appraisal and desing of UASB reactors. *Bioresource Technology* 99, 2132-2140.
6. Buntner, D., Sánchez, A., Garrido, J. M., 2013. Feasibility of combined UASB and MBR system in dairy wastewater treatment at ambient temperatures. *Chemical Engineering Journal* 230, 475-481.
7. Chan, Y., J., Chong, M., F., Law, C., L., Hassel, D., G., 2009. A review on anaerobic-aerobic treatment of industrial and municipal wastewater. *Chemical Engineering Journal* 155 (1-2), 1-18.
8. Chen, X., Zheng, P., Guo, Y., Mahmood, Q., Tang, C., Ding, S., 2010. Flow patterns of super-high-rate anaerobic bioreactor. *Bioresource Technology* 101, 7731-7735.

9. Cho, S., Fujii, N., Lee, T., Okabe, S., 2011. Development of simultaneous partial nitrification and anaerobic ammonia oxidation process in a single reactor. *Bioresource Technology* 102, 652-659.
10. Chung, J., Bae, W., Lee, Y.W., Rittmann, B.E., 2007. Shortcut biological nitrogen removal in hybrid biofilm/suspended growth reactors. *Process Biochemistry* 42(3), 320–328.
11. Durán, U., Gómez, J., Monroy, O., Ramirez, F. 2011. The effect of vinyl acetate in acetoclastic methanogenesis. *Bioresource Technology* 102, 1644-1648.
12. González-Blanco, G., Beristain-Cardoso, R., Cuervo-Lopez, F., Cervantes, F., J., Gómez, J. 2012. Simultaneous oxidation of ammonium and p-cresol linked to nitrite reduction by denitrifying sludge. *Bioresource Technology* 103(1), 48-55.
13. González-Brambila, M., Monroy, O., López-Isunza, F., 2006 Experimental and theoretical study of membrane-attached biofilm reactor behavior under different modes of oxygen supply for the treatment of synthetic wastewater. *Chemical Engineering Science* 61, 5268-5281.
14. Halling-Sorensen, B., Jorgensen, J., 1993. Process chemistry and biochemistry of nitrification in: *Studies in Environmental Science 54/The Removal of Nitrogen Compounds from wastewater*, Elsevier, Amsterdam.
15. Hibiya, K., Terada, A., Tsuneda, S., Hirata, A., 2003. Simultaneous nitrification and denitrification by controlling vertical and horizontal microenvironment in a membrane-aerated biofilm reactor. *Journal of Biotechnology* 100, 23-32.
16. Hu, S., Yang, F., Sun, C., Zhang, J., Wang, T., 2008. Simultaneous removal of COD and nitrogen using a novel carbon-membrane aerated biofilm reactor. *Journal of Environmental Sciences* 20, 142-148.
17. Huiliñir, C., Aspe, E., Roeckel, M., 2009. Model of simultaneous denitrification and methanogenesis in an upflow packed-bed biofilm reactor: nitrogen compounds inhibition and

- pseudo two-dimensional biofilm model. *Journal of chemical technology and biotechnology* 84, 254-268.
18. Huiliñir, C., Romero, R., Munoz, C., Bornhardt, C., Roeckel, M., 2010. Dynamic modeling of partial nitrification in a rotating disk biofilm reactor: Calibration, validation and simulation. *Biochemical Engineering Journal* 52, 7-18.
  19. Jin, R., Zhen, P., 2009. Kinetics of nitrogen removal in high rate anammox upflow filter. *Journal of Hazardous Materials* 170(2-3), 652-656.
  20. Khin, T., Annachatre, A., P., 2004. Novel microbial nitrogen removal processes. *Biotechnol. Adv.* 22, 519-532.
  21. Liu, H., Yang, F., Shi, S., Liu, X., 2010. Effect of substrate COD/N ratio on performance and microbial community structure of a membrane aerated biofilm reactor. *Journal of Environmental Sciences* 22(4), 540-546.
  22. Matsumoto, S., Terada, A., Tsuneda, S., 2007. Modeling of membrane-aerated biofilm: Effect of C/N ratio, biofilm thickness and Surface loading of oxygen on feasibility of simultaneous nitrification and denitrification. *Biochemical Engineering Journal* 37, 98-107.
  23. Montalvo, M. S., Guerrero, S., L. 2003. Tratamiento Anaerobio de Residuos.
  24. Mudliar, S., Banerjee, S., Vaidya, A., Devotta, S., 2008. Steady state model for evaluation of external and internal mass transfer effects in an immobilized biofilm. *Bioresource Technology* 99, 3468-3474.
  25. Ruiz, G., Jeison, D., Chamy, R., 2003. Nitrification with high nitrite accumulation for the treatment of wastewater with high ammonia concentration. *Water Research* 37, 1371-1377.
  26. Satoh, H., Ono, H., Rulin, B., Kamo, J., Okabe, S., Fukushi, K., 2004. Macroscale and microscale analyses of nitrification and denitrification in biofilms attached on membrane aerated biofilm reactors. *Water Research* 38, 1633-1641.

27. Semmens, M., J., 2008. Alternative MBR configurations: using membranes for gas transfer. *Desalination* 231, 236-242.
28. Sperling, M, Freire, V.H., LemosChernicharo, C.A., 2001. Performance evaluation of a UASB-activated sludge system treating municipal wastewater. *Water Science and Technology* 43, 323–328.
29. Tandukar, M., Ohashi, A., Harada, H., 2007. Performance comparison of a pilot scale UASB and DHS system and activated sludge process for the treatment of municipal wastewater. *WaterResearch* 41, 2697-2705.
30. Terada, A., Yamamoto, T., Igarashi, R., Tsuneda, S., Hirata, A., 2006a. Feasibility of a membrane-aerated biofilm reactor to achieve controllable nitrification. *Biochemical Engineering Journal* 28, 123-130.
31. Tsushima, I., Ogasawara, Y., Kindaichi, T., Satoh, H., Okabe, S., 2007. Development of high rate anaerobic ammonium oxidizing (ANAMMOX) biofilm reactors. *Water Research* 41, 1623-1634.
32. Van Hulle, S., W., H., Volcke, E., I., P., Teruel, J., L., Donckels, B., van Loosdrecht, M., C., M., Vanrolleghem, P., A., 2007. Influence of temperature and pH on the kinetics of the SHARON nitrification process. *Journal of chemical technology and biotechnology* 82, 471-480.
33. Verlicchi, P., Massoti, L., Galletti, A., 2011. Wastewater polishing index: a tool for a rapid quality assessment of reclaimed wastewater. *Environ. Monit. Assess.* 173, 267-277.
34. Wei, X., Li, B., Zhao, S., Qiang, C., Zhang, H., Wang, S., 2012. COD and nitrogen removal in facilitated transfer membrane-aerated biofilm reactor (FT-MABR). *Journal of Membrane Science* 389, 257-264.
35. Wiesmann, U. 1994. Biological nitrogen removal from wastewater, in: A. Fiechter (Ed.), *Adv. Biochem. Eng./Biotechnol.*, vol. 51, Springer-Verlag, Berlin, pp. 113-154.

36. Wu, C., Ushiwaka, S., Horii, H., Yamagiwa, K. 2008. Membrane-attached biofilms as a mean to facilitate nitrification in activated sludge process and its effect on the microfaunal population. *Biochemical Engineering Journal* 40,430-436.
37. Zhang, T., C., Fu, Y., L., Bishop, P., L., 1995. Competition for substrate and space in biofilms. *Water Environment Research* 67, 992-1003.

**CHAPTER 3: Hydrodynamic study of a novel membrane aerated biofilm reactor (MABR): Tracer experiments and CFD simulation**

R. Plascencia-Jatomea • F. J. Almazán-Ruiz • J. Gómez • E. P. Rivero • O. Monroy • I. González

*Chemical Engineering Science (2015) 138, 324-332*



## Hydrodynamic study of a novel membrane aerated biofilm reactor (MABR): Tracer experiments and CFD simulation



R. Pascencia-Jatomea<sup>a</sup>, F.J. Almazán-Ruiz<sup>b</sup>, J. Gómez<sup>a</sup>, E.P. Rivero<sup>c</sup>, O. Monroy<sup>a</sup>,  
I. González<sup>b,\*</sup>

<sup>a</sup> Departamento de Biotecnología, Universidad Autónoma Metropolitana-Iztapalapa, San Rafael Atlixo 186, CP 09340 México, D.F., México

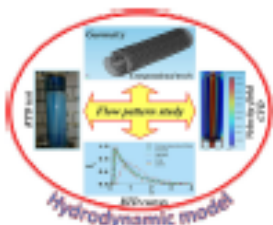
<sup>b</sup> Departamento de Química, Universidad Autónoma Metropolitana-Iztapalapa, San Rafael Atlixo 186, CP 09340 México, D.F., México

<sup>c</sup> Departamento de Ingeniería y Tecnología, Universidad Nacional Autónoma de México, Facultad de Estudios Superiores Cuautitlán, Av. Primero de Mayo, Cuautitlán Izcalli, Estado de México CP 54740, México

### HIGHLIGHTS

- The flow pattern inside an innovative aerated biofilm reactor was characterized.
- A methodology combining Residence Time Distribution models and CFD was developed.
- Mixing Cell Model match experimental Residence Time Distribution data.
- CFD Model describes experimental Residence Time Distribution data.
- Channeling (center) and stagnant (membranes) fluid zones were identified by CFD.

### GRAPHICAL ABSTRACT



### ARTICLE INFO

#### Article history:

Received 3 March 2015

Received in revised form

7 July 2015

Accepted 3 August 2015

Available online 24 August 2015

#### Keywords:

MABR

RTD

MCM

CFD

Navier–Stokes equations

Diffusion–convection equations

### ABSTRACT

The membrane-aerated biofilm reactor (MABR) is a promising technology for wastewater treatment, especially for simultaneous organic and nitrogen removal. The mass transfer phenomena induced by flow velocity and flow pattern is required in order to improve the reactor design and the removal pollutants efficiency. Tracer experiments and residence time distribution (RTD) theory were used to characterize the flow in a special MABR. The liquid phase flow patterns were investigated through tracer pulse stimulus-response technique using decton blue as model tracer. RTD curves were analyzed by mid-model tests (axial dispersion model ADM, tanks in series model TIS and mixing cell model MCM). The detailed flow pattern of the reactor was obtained from computational fluid dynamic (CFD) simulation. According to experimental results of RTD studies and CFD simulation, the flow patterns were demonstrated to be analogous to completely mixed flow with deviations of the ideal hydrodynamic behavior; stagnant zones (low fluid velocity) in 85% of its volume, being the remainder a channeling trouble (high fluid velocity). These deviations were quantitatively described (macro-mixing level-global mixing) with a minimum quadratic error function value of (5) 0.01. The local mixing flow pattern (micro-mixing level) obtained by CFD allowed determining the location of each zone; the stagnant zone is situated in the area where membranes are located; therefore it is possible to assume that degradation reactions of pollutants would take place in this area.

© 2015 Elsevier Ltd. All rights reserved.

\* Corresponding author. Tel./fax: +52 555804 4671x12.  
E-mail address: igm@unam.mx (I. González).

<http://dx.doi.org/10.1016/j.ces.2015.08.004>

0009-2509/© 2015 Elsevier Ltd. All rights reserved.

# **Hydrodynamic study of a novel membrane aerated biofilm reactor (MABR): Tracer experiments and CFD simulation**

R. Plascencia-Jatomea • F. J. Almazán-Ruiz • J. Gómez • E. P. Rivero • O. Monroy • I. González

*Chemical Engineering Science (2015) 138, 324-332*

## **Abstract**

The membrane-aerated biofilm reactor (MABR) is a promising technology for wastewater treatment, especially for simultaneous organic and nitrogen removal. The mass transfer phenomena induced by flow velocity and flow pattern is required in order to improve the reactor design and the removal pollutants efficiency. Tracer experiments and residence time distribution (RTD) theory were used to characterize the flow in a special MABR. The liquid phase flow patterns were investigated through tracer pulse stimulus-response technique using dextran blue as model tracer. RTD curves were analyzed by cold-model tests (axial dispersion model ADM, tanks in series model TIS and mixing cell model MCM). The detailed flow pattern of the reactor was obtained from computational fluid dynamic (CFD) simulation. According to experimental results of RTD studies and CFD simulation, the flow patterns were demonstrated to be analogous to completely mixed flow with deviations of the ideal hydrodynamic behavior; stagnant zones (low fluid velocity) in 85% of its volume, being the remainder a channeling trouble (high fluid velocity). These deviations were quantitatively described (macromixing level-global mixing) with a minimum quadratic error function value

of (S) 0.01. The local mixing flow pattern (micromixing level) obtained by CFD allowed determining the location of each zone; the stagnant zone is situated in the area where membranes are located; therefore it is possible to assume that degradation reactions of pollutants would take place in this area.

**Keywords:** MABR; RTD; MCM; CFD; Navier Stokes equations; Diffusion-convection equations.

### 3.1 Introduction

The MABR is a promising technology for wastewater treatment, especially for simultaneous organic and nitrogen removal. The main advantage of the MABR over conventional biofilm reactors is to enhance oxygen transfer into biofilms without any bubble formation, thus overcoming oxygen supply constraints. Moreover, membranes aeration allows changing the amount of oxygen supply by adjusting air pressure or flow rate, which reinforces rigorous control of the system (Hu et al. 2008; Matsumoto et al. 2007; Hibiya et al. 2003).

In MABR system, oxygen is supplied from membranes to biofilm, whereas pollutant is supplied from bulk to biofilm. (Liu et al. 2010). This counter-diffusive geometry creates a region close to the membrane-biofilm interface where concentration of oxygen is high and an anoxic zone close to the biofilm-liquid interface. Therefore, the MABR can achieve simultaneous aerobic and anaerobic processes in a single reactor (Matsumoto et al. 2007).

Based on the concept of dual oxygen supply (membranes and bulk), a special MABR with high large specific surface area for the sufficient living space for the biofilm was designed and constructed as a part of an anaerobic-aerobic-anoxic reactor (integrated column reactor, ICR) for sewage treatment with low footprint. This novel reactor has been operated in our laboratory obtaining similar removal efficiency of carbon and nitrogen compounds than conventional technologies. However, it is necessary to know the local oxygen flux through both the membrane and the liquid in order to find out reactor zones where the oxygen could be out of the appropriate limits (1-1.5 mg DO/L).

Notwithstanding these advantages of MABRs, a challenge emerges from engineering point of view: a better understanding on mass transfer phenomena induced by flow velocity and flow pattern is required in order to improve the reactor design and enhance the removal pollutants efficiency (Wei et al. 2012). It is well known that the reaction kinetic on immobilized biofilms is limited by substrate transport (Huiliñir et al. 2010; Mudliar et al. 2008), leading in the use of integrated mathematical models (kinetic and hydrodynamic) to have a better insight on the transport phenomena at the interfaces (membrane-biofilm-liquid) and to predict operation problems.

Currently, MABR modeling and designing is mainly based on the biokinetic. However, the hydrodynamics within a MABR system is critically important for the performance of the system since directly affects the pollutant removal (Qi et al. 2013; Brannock et al. 2010). Inadequate consideration of flow pattern inside a reactor can lead to misleading predictions regarding the mechanism, order and selectivity of the reaction and may cause problems during scale-up (Trinidad et al. 2006). Thus, an appropriate mathematical model to predict the hydrodynamic performance which relies on fluid mechanics to solve continuity and momentum of a bioreactor is likely to find wide practical application (Wang et al. 2010; Li et al. 2003; Vrana and Schuurmann, 2002).

The determination of experimental RTD is a very effective technique to study the flow pattern in a reactor (Rivera et al. 2010). Tracer studies are often conducted to estimate the RTD, which is the time distribution for particles entering and leaving the system (Chen et al. 2010). By analyzing the shape of RTD curve, some non-ideally mixed volume, such as dead zones and short-circuits, may be inferred (Holland et al. 2004). RTD technique had been used as an

efficient and simple approach of hydrodynamic study in trickling filters, sand filters, constructed wetlands, aerated biological filters, fluid bed bioreactors and compartmentalized anaerobic reactors (Qi et al 2013; Ji et al. 2012; Martinov et al. 2010; Montastruc et al. 2009). However, the visualization of the flow pattern is undefined due to the fact that RTD does not contain any information about the spatial distribution of the tracer, which is critical in describing the state of mixing (Qi et al. 2013).

The use of experimental techniques (tracer experiments) combined with modern tools as the computational fluid dynamic (CFD), which is a powerful approach that provides a detailed spatial distribution of flow fields providing two or three-dimensional visualization of the system (Klusener et al. 2007), might provide reliable quantitative results on hydrodynamics performance facilitating the development of integrated models (hydrodynamic-reaction kinetics) to optimize variables such as reactor design, nutrient removal and energy consumption (Glover et al. 2006; Essemiani, 2004).

In order to benefit the engineering design of MABR, (1) tracer experiments were conducted in special MABR to analyze the flow pattern profile; (2) several mathematical models (axial dispersion model (ADM), tanks in series model (TIS) and mixing cell model (MCM) were used for diagnostic purposes; (3) CFD software, *Comsol Multiphysics 4.3b*, was used to make a simulation and visualize the flow pattern; (4) the results of mathematical models and CFD results were analyzed and compared and finally (5) a hydrodynamic model was proposed.

## 3.2 Methods

### 3.2.1 Experimental set-up

The experimental study was performed in a special MABR. A schematic diagram of the liquid flow circuit for the MABR reactor used in the RTD experiments is shown in Fig. 3.1.

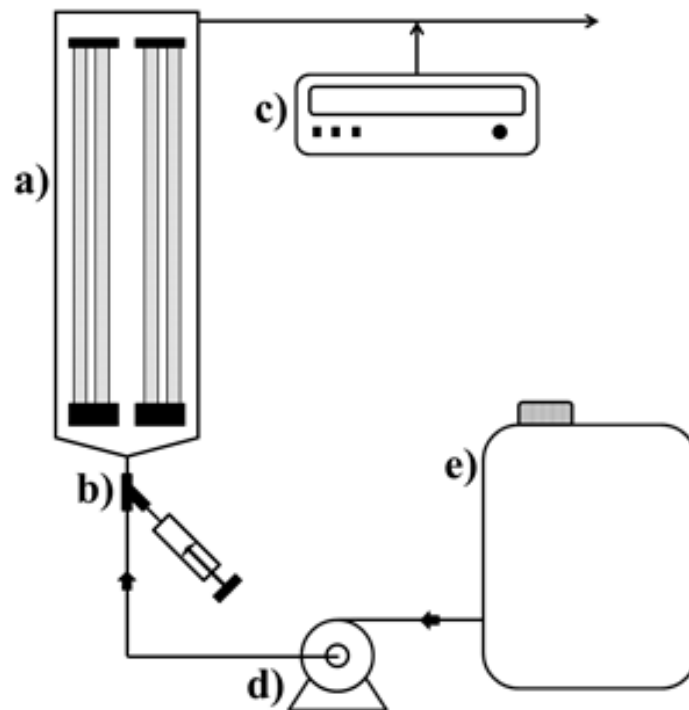


Figure 3.1. Schematic of the membrane aerated biofilm reactor (MABR) and liquid flow circuit used for RTD experiments: a) MABR, b) Type-Y connector, c) UV-Vis spectrophotometer, d) Peristaltic pump and e) Container.

The liquid phase was contained in a 20 L polycarbonate container (Figure 1-e), from which the liquid was fed to the bottom of the MABR (up-flow mode) (Figure 1-a) by means of a magnetic pump, Figure 1-d (MasterFlex L/S HV-07528-10 with a MasterFlex L/S Easy-Load II head for precision tubing HV-77200-60). In the inlet, a type-Y connector (Figure 1-b) for

the injection of a tracer pulse was installed. At the top of the outlet pipe, UV-Vis spectrophotometer equipment, Figure 1-c (Jaz Spectral Sensing Suit) with an optic fiber probe was installed to measure in-line the tracer liquid concentration. The liquid flow circuit was made of MasterFlex tubing (E3603 L/S 16).

The reactor has an operation volume of 1.95 L and is packed with 24 tubular hollow membranes 32 cm length, 5 mm inner side diameter, 1 mm thickness (superficial membranes area=0.17 m<sup>2</sup>). The membranes are distributed in almost all the cross-sectional area of the reactor (Fig. 2.2) whose internal diameter is 8.2 cm and height of 46 cm. The intermembrane pressure was maintained at 2 psi (*molecular oxygen*); the pressure was set to carry out the dissolution of oxygen preventing the formation of a steady stream of bubbles. Tubular hollow membranes (Figure 3.2-b) are connected to an airtight distribution chamber (Fig. 2.2-d) which has a series of perforations which allows the passage of liquid. In addition the chamber works as a flow distributor.

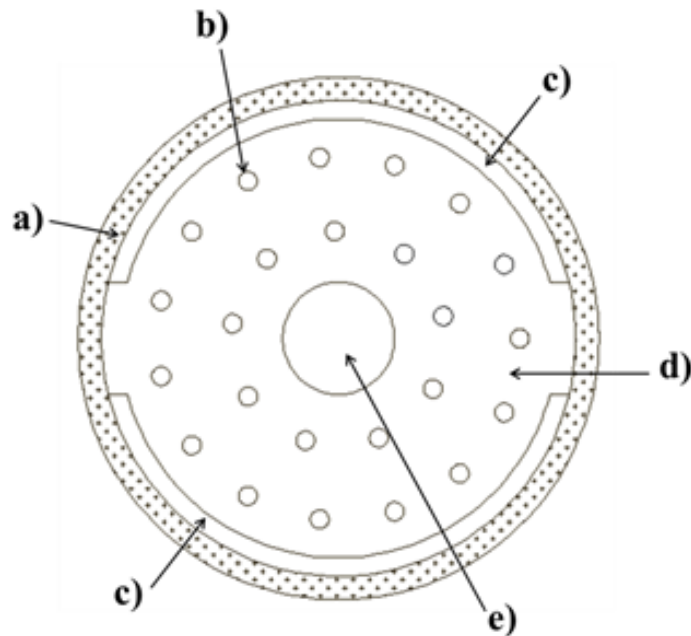


Figure 3.2. Membrane distribution at the MAB reactor (cross-section view): a) Inner wall of the reactor, b) Tubular membranes, c) Lateral inlet, d) Airtight distribution chamber and e) central inlet.

### 3.2.2 Tracer studies

In the RTD experiments dextran blue was used as model tracer in order to characterize the liquid phase flow pattern in MABR. This compound is well known to be unavailable to absorb or adsorb on plastic and membranes surfaces. Furthermore, due its high molecular weight, the diffusion coefficient is low enough ( $D_M=1.058 \times 10^{-11} \text{ m}^2/\text{s}$ , 25 °C, in water) to ensure that the tracer follows the liquid stream lines thus providing correct values of parameter (Rivera et al. 2010).

Four sets of experiments were carried out varying the volumetric flow rate and were planned to observe its effect on hydrodynamic parameters. The volumetric flows ( $Q$ ) employed were

3.6, 6, 8 and 10 mL/min. The experimental method applied is based on the one-point-injection/one-point-detection method (Fogler, 2008). To determine the mixing flow pattern in the liquid phase, the stimulus-response technique was employed as indicated by Rivera et al. 2010. The dextran blue concentration was 20,000 ppm and the volume of pulse injection was 5 mL; under such conditions the injection time (about 1 s) should be negligible with respect to the average residence time. The tracer was injected with a manual syringe of 5 mL connected to a plastic catheter (ID of 3 mm). The Lambert-Beer coefficients obtained during calibration of absorbance method were 0.00117 and correlation coefficient R of 0.998. The UV-Vis spectrophotometer has a Xenon lamp flashed only when acquiring a data point (1.2 ms). Response of tracer concentration during dye injection at cell inlet was measured and repeated 3 times in each experiment. Average degree of repeatability was 0.00135 u Abs for all dye injection experiments, indicating that all experiments have a good reproducibility.

### **3.3 Mathematical models used for RTD analysis**

The axial dispersion model ADM, tanks in series model TIS and mixing cell model MCM were used to describe the experimental RTD curves behavior and to determine the flow pattern deviations presented in the MABR. The experimental RTD data obtained was used for calculation of RTD functions;  $E(t)$  (residence time distribution function),  $\bar{t}$  (mean residence time) and  $\sigma_t^2$  (distribution variance), according to Fogler, 2008.

#### **3.3.1 ADM**

To characterize the spreading of the pulse within reaction area in MABR, diffusion like process imposed on plug flow is considered. This phenomenon is identified as longitudinal

dispersion ( $D_{ax}$ ) to distinguish it from molecular diffusion. ADM could be established by applying the Fick's law to the axial mixing (Rivera et al. 2010).

$$\frac{\partial c}{\partial \theta} = \frac{1}{Pe} \frac{\partial^2 c}{\partial z^2} - \frac{\partial c}{\partial z} \quad (1)$$

where  $c$  is the dimensionless tracer concentration,  $Pe$  is Peclet number,  $\theta$  is dimensionless time variable and  $z$  is the dimensionless variable in axial length. The tracer injection is a pulse and not a step; however the flow behaves closely to perfect plug-flow regime before the inlet ( $Z=0^-$ ) and immediately after the outlet ( $Z=L_Z^+$ ). In this way the dimensionless equation 2 considers the boundary condition at  $z=0$  and  $z=1$ , thus these boundary conditions account the dispersion and convection inside of reactor, these are the close-close vessel boundary condition described by Fogler, 2008:

$$z=0; \quad c = 1 + \frac{1}{Pe} \frac{\partial c(\theta^+, \theta)}{\partial z} \quad z=1; \quad \frac{\partial c(\theta^-, \theta)}{\partial z} = 0 \quad (2)$$

The initial condition before tracer inside MABR is:

$$\theta = 0; \quad c(Z, \theta) = 0 \quad (3)$$

The dimensionless variables in the above expressions are:

$$c = \frac{C}{C_0}; \quad z = \frac{Z}{L_Z}; \quad \theta = \frac{tu}{L_Z}; \quad Pe = \frac{uL_Z}{D_{ax}} \quad (4)$$

where  $C_0$  is the initial concentration of tracer and  $C$  is the concentration at different times,  $Z$  is the position in the axial direction and  $L_Z$  is the length of reactor,  $t$  is the discrete time,  $u$  is the superficial velocity and  $D_{ax}$  is the axial dispersion coefficient.

According to closed reactor boundary,  $Pe$  could be calculated by using Eq. (5):

$$\sigma^2 = 2\left(\frac{1}{Pe}\right) - 2\left(\frac{1}{Pe}\right)^2 (1 - e^{-Pe}) \quad (5)$$

where  $\sigma^2$  is the dimensionless variance of the experimental RTD,  $\sigma^2 = \sigma_t^2 / \bar{t}^2$ . Thus,  $(1/Pe)$  could be computed using Eqs. (1) and (5). If  $(1/Pe) \rightarrow 0$ , the reactor approximate to the ideal plug-flow reactor (PFR,  $(1/Pe)=0$ ), and if  $(1/Pe) \rightarrow 1$ , the reactor approximate to the ideal continuous-flow stirred-tank reactor (CSTR,  $(1/Pe)=1$ ). In case of non-ideal flow,  $0 < (1/Pe) < 1$ .

### 3.3.2 TIS

The tracer concentration in the effluent could be expressed as:

$$C_N(t) = 1 - e^{-t/\tau_s} \left[ 1 + \frac{t}{\tau_s} + \frac{1}{2!} \left(\frac{t}{\tau_s}\right)^2 + \frac{1}{3!} \left(\frac{t}{\tau_s}\right)^3 + \dots + \frac{1}{(N-1)!} \left(\frac{t}{\tau_s}\right)^{N-1} \right] \quad (6)$$

where  $\tau_s$  is the hydraulic retention time (HRT) of single tank and  $N$  is the number of tanks in series. The RTD function could be described as follows:

$$E(\theta) = \frac{N^N}{(N-1)!} \theta^{N-1} e^{-N\theta} \quad (7)$$

The dimensionless variance of TIS model could be calculated from Eq. (8) and  $N$  could be obtained:

$$\sigma^2 = \frac{\int_0^{\infty} (\theta-1)^2 E(\theta) d\theta}{\int_0^{\infty} E(\theta) d\theta} = \int_0^{\infty} \frac{N^N \theta^{N+1}}{(N-1)!} e^{-N\theta} d\theta - 1 = \frac{1}{N} \quad (8)$$

Rearranging Eq. (8), we obtained:

$$N = \frac{1}{\sigma^2} \quad (9)$$

Thus  $N$ , as a main parameter of tanks in series model, could be calculated by Eq. (9) using  $\sigma^2$  evaluated from experimental RTD. If  $N \rightarrow 1$ , the flow pattern of the reactor approach that of continuous stirred tank reactor (CSTR), and if  $N \rightarrow \infty$ , the flow pattern of the reactor approach that of plug-flow reactor (PFR).

### 3.3.3 MCM

The model (Van Swaaij et al. 1969) considers that a fraction of the inflow ( $\alpha$ ) passes to  $V_1$  (stagnant zone), where the flow velocity is low, and the rest of the inflow ( $1-\alpha$ ) passes to  $V_2$  (dynamic zone), where the flow velocity is high. Finally, both flows mix and produce an output with concentration  $C_3$ . To describe a pulse injection of tracer into the MAB, the following dimensionless first-order ordinary differential equations (10 to 14) are used.

The tracer dimensionless concentration at the stagnant zone is described by:

$$c_0 = c_1 + \frac{\tau_1}{\tau} \frac{dc_1}{d\theta} \quad (10)$$

where  $c_0$  is dimensionless inlet tracer concentration,  $c_1$  is dimensionless tracer concentration at the stagnant zone,  $\tau$  is the sum of the HRT of the stagnant zone and dynamic zone,  $\tau_1$  is the HRT of the stagnant zone and  $\theta$  is dimensionless time variable.

The tracer dimensionless concentration at dynamic zone is represented by:

$$c_0 = c_2 + \frac{\tau_2}{\tau} \frac{dc_2}{d\theta} \quad (11)$$

where  $c_2$  is dimensionless tracer concentration at the dynamic zone and  $\tau_2$  is the HRT of the dynamic zone.

The dimensionless tracer concentrations of the output current of both zone is described by:

$$\alpha c_1 + (1 - \alpha)c_2 = c_3 \quad (12)$$

where  $c_3$  is the sum of dimensionless tracer concentration at the stagnant and dynamic zones.

The initial condition before tracer inside MABR is:

$$\theta = 0; \quad c_{1,2,3} = 0 \quad (13)$$

The dimensionless variables in the above expressions are:

$$\theta = \frac{t}{\tau}; \quad \tau = \alpha\tau_1 + (1-\alpha)\tau_2; \quad \tau_1 = \frac{V_1}{\alpha Q}; \quad \tau_2 = \frac{V_2}{(1-\alpha)Q} \quad (14)$$

where,  $Q$  is inflow ( $\text{m}^3/\text{s}$ ).

The dimensionless mathematical models (ADM, TIS and MCM) were solved numerically using *FlexPDE* software, 6.06 academic version. To obtain numerical solution the response predicted by the models was compared with normalized experimental data by minimalizing  $S$  in Eq. (15):

$$S = \sqrt{\frac{\sum_i^n \left( \frac{C_{i,\text{exp}} - C_{i,\text{calc}}}{C_{i,\text{exp}}} \right)^2}{n}} \quad (15)$$

where  $C_{i,\text{exp}}$  is experimental concentration and  $C_{i,\text{calc}}$  is calculated concentration by means of the models. The tolerance of  $S$  value was  $S \leq 0.01$ .

### 3.3.4 CFD

CFD modeling formulates and solves the fundamental momentum and mass balance equations using numerical techniques. The fluid-flow equations, known as the Navier-Stokes (NS) equations, are non-linear and cannot be analytically solved in almost all cases. To solve the equations they must be linearized and solve over many small control volumes (the computational mesh). For determinations of the flow field these simulations require input of geometry, boundary conditions and fluid properties (Brannock et al. 2010). The geometry of the MABR was constructed in 3D using the software *Comsol Multiphysics 4.3b* (Fig. 3.3a)

(license number: 1038192). Despite of the experimental RTD curves were obtained with an intermembrane pressure of 2 psi, the model does not take in account this phenomenon, since similar RTD curves were obtained without pressuring the airtight distribution chamber (membrane module). This similarity could be explained by the fact that oxygen is transferred directly to the bulk liquid by diffusion from the membrane surface without any bubble formation that could disturb the flow pattern behavior (Semmens, 2008; Matsumoto et al. 2007). In order to obtain a good convergence and minimize the computing time, the geometric construction was elaborated avoiding small elements where the meshing is considerably increased (Fig. 3.3b). On the other hand, the computational mesh was chosen by user: a coarse mesh was used in the domain, but near solid walls the meshing was finer; in this case only three mesh layers were used in the walls. In order to obtain a first convergence, the simulation was initialized with a coarser mesh; later on it was refined till the response no longer depended on the size of the mesh.

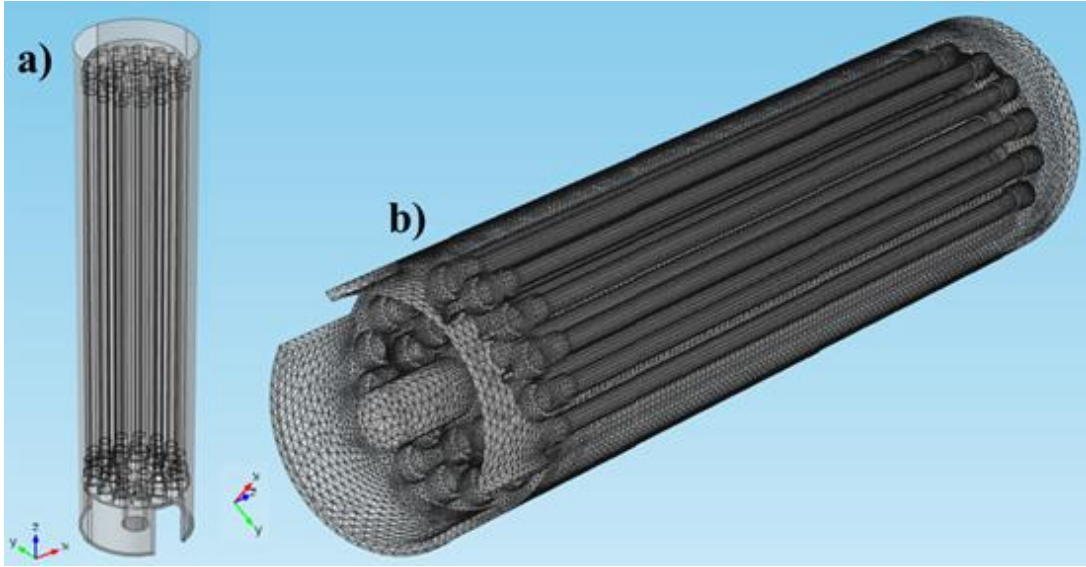


Figure 3.3. Geometry of the MABR and computational mesh established in *Comsol Multiphysics 4.3b*: a) Geometry of MABR and b) The computational mesh.

The computational domain meshing consisted of 2069049 tetrahedral elements, 6762 pyramid elements, 384934 prims elements, 200044 triangular elements and 264 quadrilateral elements. The solver used was PARDISO.

### 3.3.4.1 Hydrodynamic Model

The hydrodynamic of the MABR was simulated by solving the NS equations for laminar flow coupled to continuity equation for incompressible fluid. Assuming that liquid flow is in steady state, the solution of the hydrodynamic is not time dependent.

Assuming negligible variations in viscosity and density, NS model is:

$$\rho(\mathbf{u} \cdot \nabla)\mathbf{u} = \nabla \cdot \left[ -p\mathbf{I} + \mu(\nabla\mathbf{u} + (\nabla\mu)^T) \right] + \mathbf{F} \quad (16)$$

where  $\rho$  is the density of the fluid ( $\text{Kg/m}^3$ ),  $\mathbf{u}$  is the velocity vector (m/s),  $p$  is the pressure (Pa),  $\mu$  is the dynamic viscosity ( $\text{Pa}\cdot\text{s}$ ),  $\mathbf{F}$  is the volume force vector ( $\text{N/m}^3$ ) and  $T$  represent the absolute temperature (K).

### 3.3.4.1.1 *Boundary conditions*

The boundary conditions employed to solve the NS equations were:

- (1) At the inlet (constant velocity entry):

$$\mathbf{u} = -U_0 \mathbf{n} \quad (17)$$

Where  $U_0$  is the initial average velocity (m/s) at the inlet of the reactor which was calculated, taken into account the transversal area of the tube that fed the reactor and  $\mathbf{n}$  is the normal vector that points out of the fluid domain.

- (2) At the walls (no slip condition):

Since all velocities must disappear on the wall, therefore, the wall boundary conditions adjacent to a solid wall are:

$$\mathbf{u} = 0 \quad (18)$$

- (3) At the outlet of the reactor (no gradient forces):

$$\left[ \mu(\nabla u + (\nabla u)^T) \right] \cdot \mathbf{n} = 0 \quad P = 0 \quad (19)$$

### 3.3.4.2 **Mass transfer Model (diffusion-convection equation)**

The mass transport of tracer inside the MABR was simulated with diffusion-convection equation in transient and laminar regime using a “pulse-signal” at the inlet of the reactor. The

pulse-signal that represent the tracer pulse injection was defined using a mathematical function (Gaussian function) described in *Comsol Multhiphysics 4.3b* with a position  $t_0=10$  s and standard deviation ( $\sigma$ ) of 2.

In order to describe the mass transport of the tracer in water (binary mixture) for a dilute solution in transient regimen, the diffusion-convection equation in laminar regimen was used:

$$\frac{\partial C_i}{\partial t} = \nabla \cdot (D_i \nabla C_i) - \mathbf{u} \cdot \nabla C_i \quad (20)$$

where  $\mathbf{u}$  is the average velocity field (determined from Eq. 16 of hydrodynamic model),  $C$  is the averaged concentration field and  $D_i$  is the diffusion coefficient.

### 3.3.4.2.1 Boundary conditions

The boundary and initial conditions employed to solve the diffusion-convection equations were:

(1) Initial condition:

$$C_i = 0; \quad t \leq 0 \quad (21)$$

(2) At the reactor inlet (pulse-signal at entry):

$$C_i = C_o \frac{1}{\sigma \sqrt{2\pi}} \cdot e^{\left(\frac{-(t-t_0)^2}{2\sigma^2}\right)}; \quad t > 0; \quad -\mathbf{n} \cdot \mathbf{N}_o = U_o C_o \quad (22)$$

(3) At the walls (impermeable walls):

$$-\mathbf{n} \cdot N_i = 0 \quad (23)$$

(4) At the reactor outlet (only convective flux):

$$-\mathbf{n} \cdot D_i \nabla C_i = 0 \quad (24)$$

The equations of hydrodynamic (NS) for laminar flow and mass transfer (diffusion-convection equations) were solved in 3D in an *Alienware Aurora* computer equipped with a quad-core Intel® Core i7 processor, Windows® 7 Home Premium 64-bit, 16 GB, 1600 MHz RAM and NVIDIA® Ge Force® GTX 690 4GB video card.

### 3.4 Results and discussion

#### 3.4.1 Comparison of RTD curves and evaluation of the fluid dispersion with ADM, TIS and MCM models.

Figure 2.4 shows the experimental RTD curves at different flow rates and constructed curves with ADM, TIS and MCM models. The uncertainty of the RTD experiments was  $\pm 1.82\%$ , this value was determined by measuring the response of the tracer concentration three times in each experiment indicating that all experiments have a good reproducibility. The axis  $y$  represents the dimensionless age distributions,  $E_\theta$ , and the axis  $x$  represents dimensionless time,  $\theta$ .

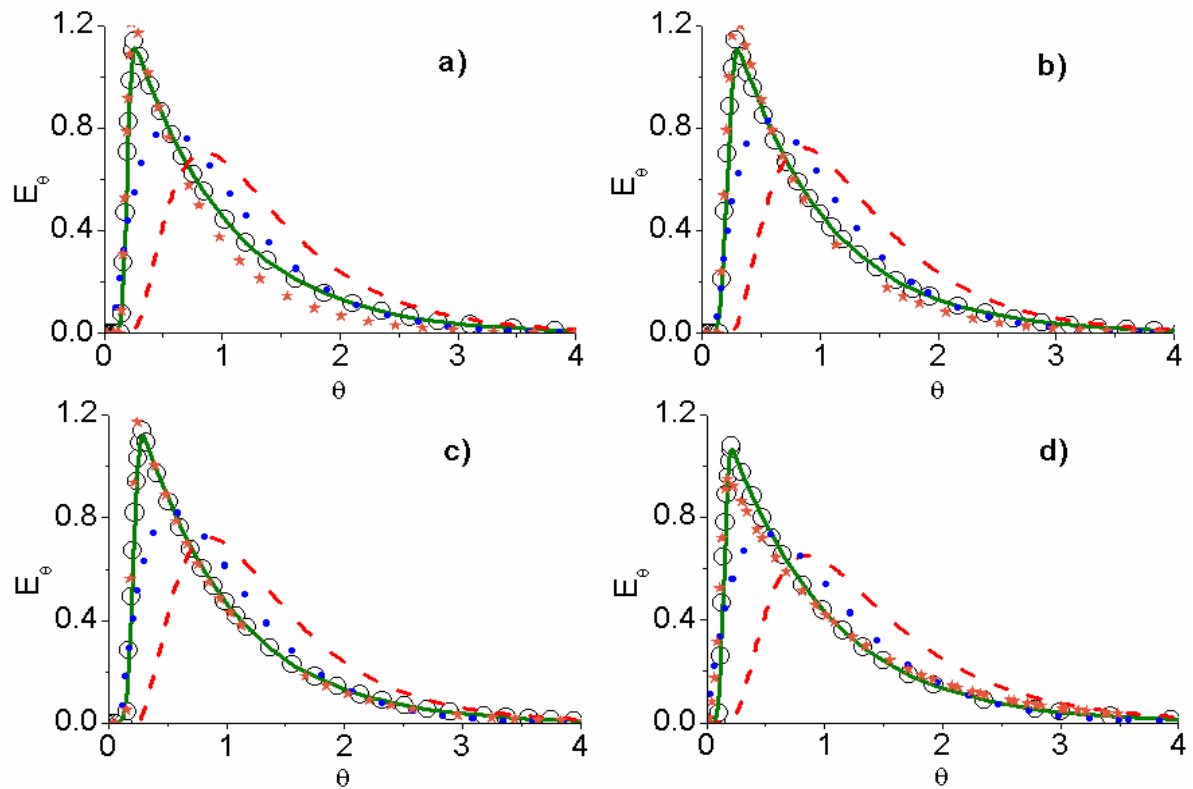


Figure 3.4. RTD curves obtained in the MABR at different flow rates. a) 3.6 mL/min, b) 6 mL/min, c) 8 mL/min and d) 10 mL/min. Experimental data (open circle), constructed RTD curves, with the different models: i) ADM (red dashed line), ii) TIS (blue dots), iii) MCM (green continuous line) and iv) *Comsol Multiphysics 4.3b* (orange stars).

After each RTD experiment the total tracer at the outlet was checked being most of the tracer recovered (~100%), in this way it is possible to have a good flow pattern estimation of the MAB. The experimental RTD curves show (Fig. 3.4, open circles) an overall mixing behavior close to complete mixing, however it is possible to identify the presence of flow pattern deviations; derivation (channeling or dynamic zones) and a significant tailing, which represent a stagnant phenomenon (stagnant zones) with less mass transfer of the tracer between them. In order to have a better description of the flow pattern in the liquid at the MABR, different

models were used to construct RTD curves. The characteristics parameters to identify the flow pattern were  $Pe$  (ADM) and  $N$  (TIS), these parameters were determined using the dimensionless variance obtained from experimental data according to Eqs. (5) and (9), and are reported in Table 3.1.

Table 3.1. Experimental conditions of MAB reactor and parameters obtained from experimental data according to Eqs. (5) and (9), used to construct the RTD curves with ADM and TIS models.

Run	$Q$ (mL/min)	$HRT$ (min)	$\bar{t}$ (min)	$\sigma^2$	$Pe$	$(1/Pe)$	$N$
1	3.6	541.7	663.6	0.64	1.52	0.66	1.56
2	6	325	420	0.62	1.64	0.61	1.61
3	8	243.8	314.3	0.62	1.64	0.61	1.61
4	10	195	233.4	0.71	1.13	0.88	1.4

Flow pattern deviation (non-ideal flow) is often described by the ADM and TIS model. In case of ADM, flow pattern deviation is characterized by  $Pe$ . The ADM curves constructed with  $Pe$  values of Table 1 (Figure 3.4, dashed line) do not describe correctly the RTD experimental curves (Fig. 4, open circle). The reciprocal of  $Pe$  value obtained for all runs was  $0.7 \pm 0.13$  (Table 1). This value is 3.5 bigger than the characteristic value for plug-flow reactors,  $(1/Pe) \leq 0.2$ , described in other papers (Fogler, 2008; Levenspiel, 1999; Tomlinson and Chambers, 1979), confirming that the MAB flow pattern deviates from these case.

On the other hand, the flow pattern deviation in TIS model is characterized by  $N$ . The number of reactors in series was obtained according to Eq. (9). The average number of tanks for all runs was  $1.55 \pm 0.1$  (Table 3.1). This value tends to 1, indicating that the flow pattern of the MABR approaches that of CSTR with non-ideal flow pattern (Qi et al. 2013). Moreover, the value of  $N$  obtained in this study is 52% smaller than the maximum limit of characteristic value for CSTR ( $N \leq 3$ ) previously described (Chen et al. 2010; Essemiani, 2004). It is important to mention by the fact that is not possible to have a fractional number of reactors this value was established as 2 reactors in series. The DRT curves constructed with TIS model (Fig. 3.4, dots), present a similar profile than those obtained experimentally; however it was unable to describe the zone where the maximum value of  $E_\theta$  (1.1) was obtained (Fig. 3.4, open circle). This behavior might be attributed to the fact that the model was not capable to completely describe the hydrodynamic phenomenology presented at the MABR.

Since the flow pattern in MABR cannot be described by ADM and TIS, the RTD experimental curves were fitted with a model combining ideal reactors (MCM). The parameters obtained for the best curve fit ( $S \leq 0.01$ ) of experimental RTD curves with MCM model are shown in Table 3.2. The RTD curves constructed with these parameters (Fig. 3.4, continuous line) described all the experimental RTD curves (Fig. 3.4, open circles).

Table 3.2. Parameter values obtained for the best fit of RTD experimental curves with MCM model and diffusion-convection equations (*Comsol Multiphysics 4.3b*) at different inflow values.

Run	$Q(mL/min)$	$V_1(L)$	$V_2(L)$	$V_1/V_2$	$\alpha$	$t_m(min)$	$t_{m-MCM}(min)$	$t_{m-COMSOL}(min)$
1	3.6	1.66	0.29	5.72	0.852	663.61	663.14	654.31
2	6	1.65	0.3	5.5	0.849	419.95	411.33	429.43
3	8	1.66	0.29	5.72	0.852	314.27	307.69	322.64
4	10	1.65	0.3	5.5	0.850	233.37	228.04	222.41

$t_m$  Average residence time of tracer calculated by the MCM and *Comsol Multiphysics 4.3b*.

The MCM model describes correctly the RTD curves in all cases using only one mixing cell. The value of  $t_{m-MCM}$  showed an error lower than 2% respecting to  $t_m$  value obtained experimentally indicating that good fitting results ( $S \leq 0.01$ ). In the other hand, the MABR presents a  $V_1$  of 1.66 L which correspond to a stagnant zone were the fluid present low velocity. It is noteworthy that the volume of the stagnant zone ( $V_1$ ) is unchanged when increasing feed flow maintaining a ratio ( $V_1/V_2$ ) of  $5.61 \pm 0.13$  in all cases (Table 3.2). This could be explained by the fact that the laminar flow pattern of the MABR does not change under the range of tested flow rates.

The MCM model allowed knowing the characteristics as volume and the fraction of the inlet volumetric flow rate crossing on the dynamic and stagnant zone of the MABR. Nonetheless, the model is unable to predict the location of each zone, because of this it was necessary to use

the computational fluid dynamic in order to visualize and identify the flow pattern presented in the MABR.

### **3.4.2 Validation of hydrodynamic and mass transport simulation using RTD experiments**

In order to verify if NS for laminar flow and diffusion-convection equations solved represent the actual hydrodynamic profile and mass transport of tracer inside the MABR, the experimental RTD curves were compared with those obtained by *Comsol Multiphysics 4.3b*. The RTD curves obtained are in agreement with experimental RTD curves (see Figure 2.4 and Table 2.2). The diffusion-convection equations describe correctly the RTD curves in all cases. The value of  $t_{m-COMSOL}$  showed an error lower than 5% respecting to  $t_m$  value obtained experimentally indicating that good fitting results.

### **3.4.3 Hydrodynamic profile and mass transport of tracer inside MABR obtained with Comsol Multiphysics 4.3b**

The flow velocity field of the MABR can be characterized using the velocity field extracted from the CFD model output. Fig. 3.5 shows the hydrodynamic (velocity field) behavior of the fluid in steady state inside the MABR at volumetric flow rate of 10 mL/min, it is important to mention that this flow pattern is similar at all volumetric flow rates tasted. The multicolor bars located beside image represent the magnitude of the velocity field, dark blue color represents the lowest velocities and red color represents the highest velocities.

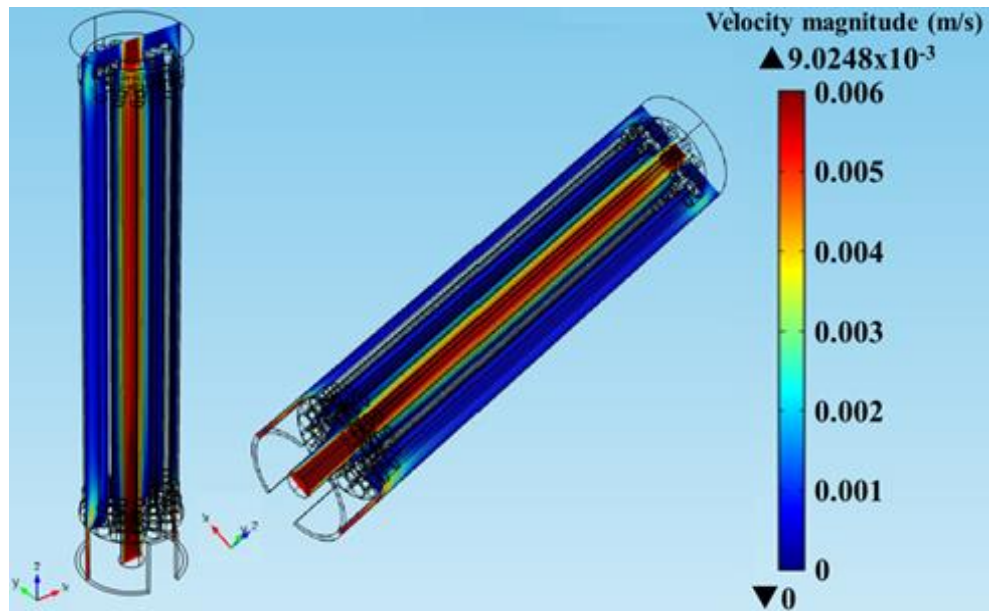


Figure 3.5. Velocity field obtained from the hydrodynamic study with *Comsol Multiphysics 4.3b* for the MABR (volumetric flow rate of 10 mL/min). The multicolor bars located beside image represent the magnitude of the velocity field, dark blue color represents the lowest velocities and red color represents the highest velocities.

Two flow velocity zones are identify; high velocity zone (channeling) identified by red color and located in the central region beginning from the central perforation of the distributor chamber to the outlet of the reactor, and low velocity zone (stagnant zone) identified by dark blue color presented in a high proportion of the reactor volume and it seems to be homogeneous. It is important to mention that CFD simulation detected similar flow pattern deviations than those observed in the experimental RTD curves and those assumed by the MCM.

Fig. 3.6 shows the velocity profile in cross section at the inlet and outlet of the reactor. The highest velocity flow is located in the center being a free region of membranes, while in the region where the membranes are located a uniform low velocity profile appears.

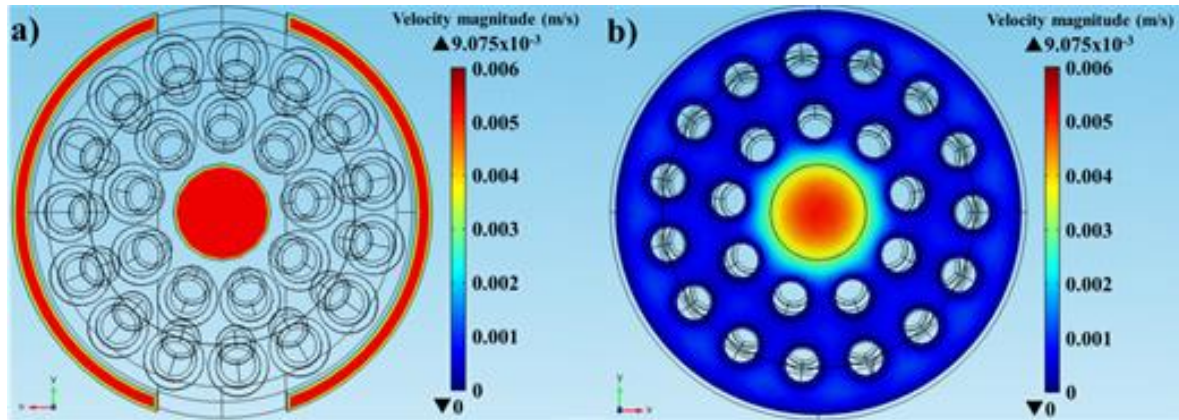


Figure 3.6. Velocity field (m/s) in cross section at the inlet and outlet of the MABR (volumetric flow rate of 10 mL/min): a) inlet and b) outlet. The multicolor bars located beside images represent the magnitude of the velocity field, dark blue color represents the lowest velocities (minimal) and red color represents the highest velocities (maximum).

In order to get a better understanding of the velocity profile of the liquid bulk inside the reactor a velocity study was done in a cross-section of the reactor from center to the inner wall passing through two membranes (Figure 3.7) and at different reactor heights (membranes zone).

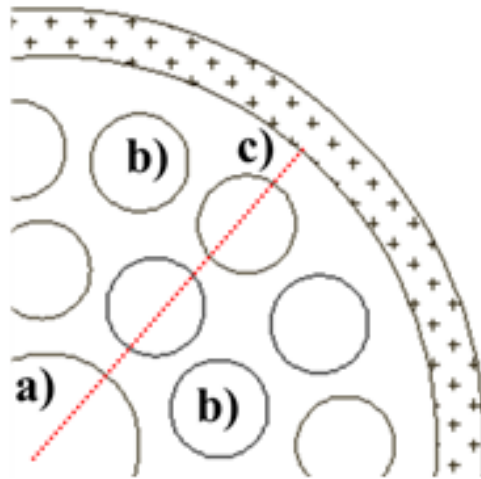


Figure 3.7. Scheme of cross-section of the MABR: a) Central perforation of the distribution chamber, b) Tubular membrane and c) Inner wall of the reactor.

Fig. 3.8 shows the normalized velocity profile between tubular membranes at different volumetric flow rates. The highest normalized velocity value (1) corresponds to the center of the reactor and diminishes almost to zero in the region nearest to the external wall of the membranes and in the inner wall of the reactor due to the shear stress. In the other hand the region between tubular membranes and tubular membrane-inner wall of the reactor maximum velocity is similar.

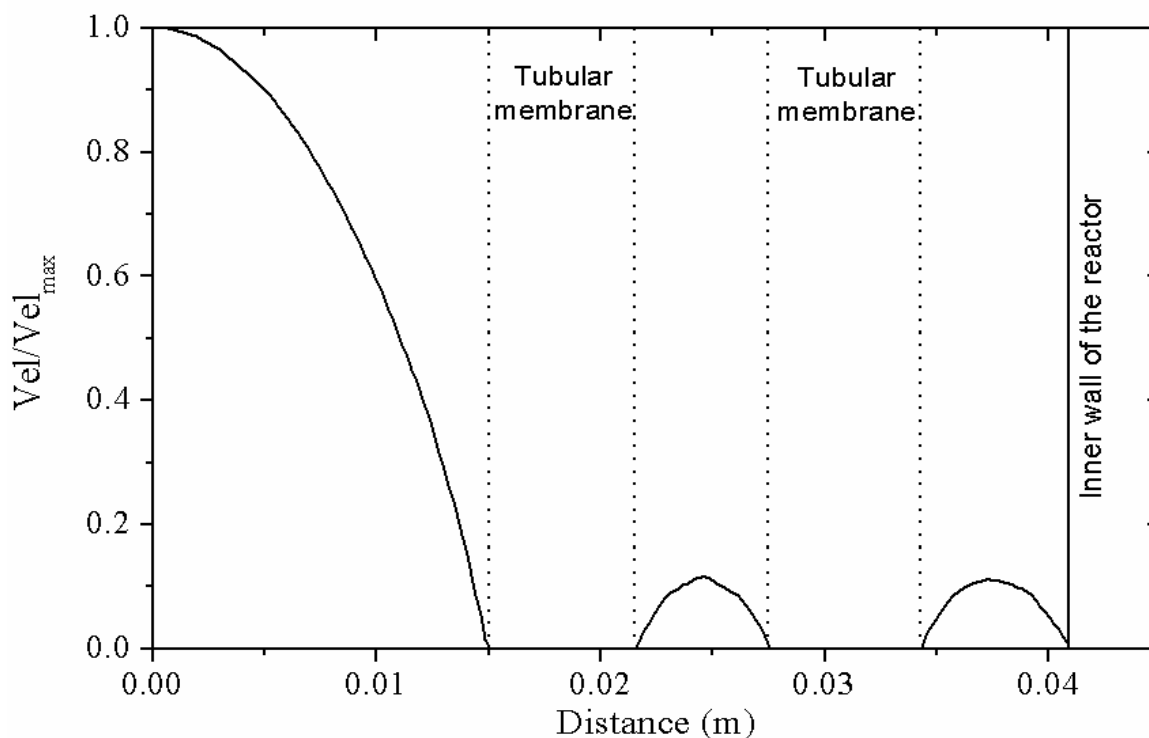


Figure 3.8. Normalized velocity profile in cross-section of the MABR.

The ratio of maximum value of the average fluid velocity in the channeling zone and the maximum value in the stagnant zone is around 9, and this profile is maintained at different reactor heights (membranes zone). It is worth to mention that the zone with stagnate troubles corresponds around the membranes are located. Due this, it can be assumed that this region is the zone reaction for the pollutants degradation.

Since a satisfactory validation of the hydrodynamic-mass transport model was obtained, a tracer computational experiment of particles inside the reactor was performed (Fig. 3.9). This experiment reinforced the arguments here presented, showing a channeling in the central region of the reactor and stagnant zone where membranes are located. A complete video in transient regime was obtained (see supplementary data).

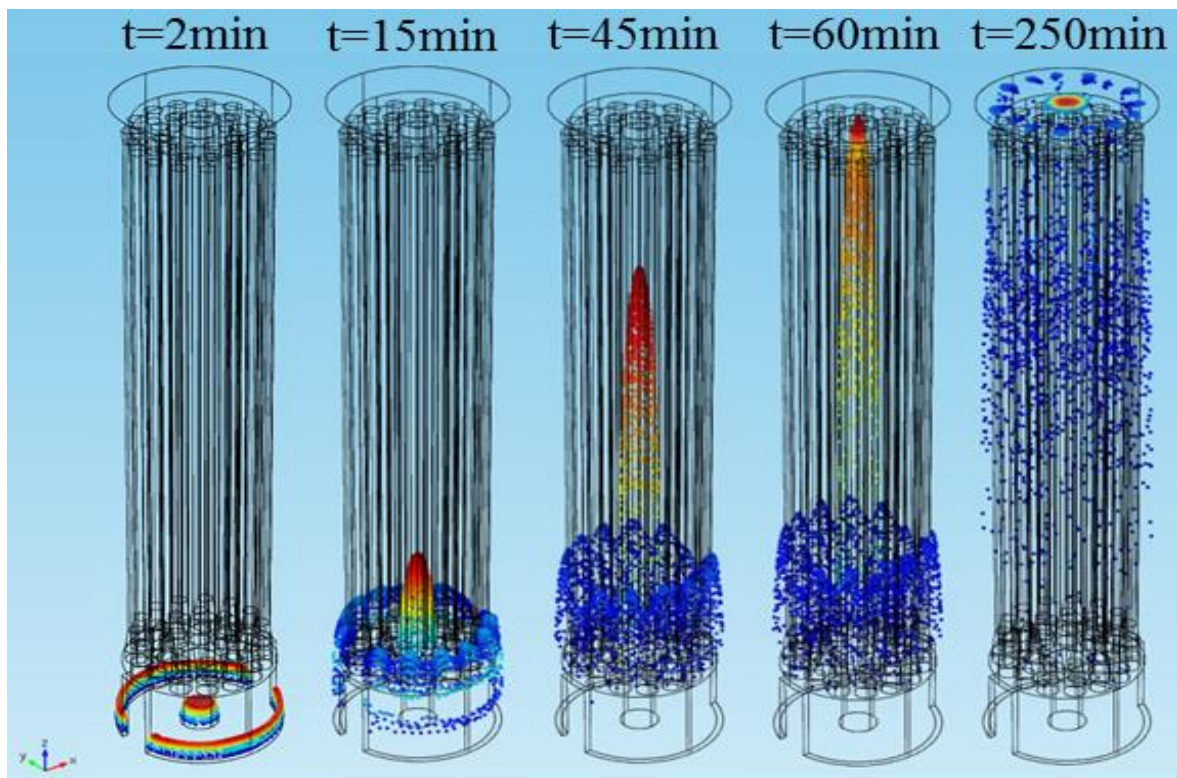


Figure 3.9. Particle tracer experiments inside the MABR in transient regime obtained with *Comsol Multiphysics 4.3b*. Different times passing after the fluid entrance are indicated in the figure (volumetric flow rate of 10 mL/min and 3000 planted particles).

According to these results, the geometry plays an important role of the MABR performance, in this way, the implementation of a device that serves as a flow distributor in the central perforation of the distributor chamber could diminish the ideality deviation of the flow pattern; this research is in progress in our research team.

### **3.5 Conclusions**

A novel membrane aerated biofilm reactor (MABR) packed with tubular hollow membranes was studied. Under tested operational conditions, strong deviations from ideal flow pattern were identified thus the ADM and TIS models failed to fit experimental RTD curves. On the other hand, the MCM model was able to adequately describe the flow pattern under these conditions showing a large stagnant zone in the reactor. According to MCM estimations and CFD simulation (hydrodynamic-mass transport equations), the central region of the MABR corresponds to the channeling zone and the membrane region to the stagnant zone (85% of the MABR volume), this zone can be designed as the region where reaction degradation of pollutants takes place.

The results obtained in this work show that the strategy of RTD modeling combined with CFD simulation is a useful methodology to identify ideal flow pattern deviations as well as to detect reactor design characteristics producing such flow behavior. The gained insight might be used to improve the reactor design, enhance the mass transport and increase the reactor space yield. The hydrodynamic-mass transport model here described has been the base for the development of an integrated model to find operation conditions and design control strategies for maintaining high removal pollutants rates at the ICR operated in our laboratory (results will be published soon).

### **Acknowledgments**

The authors thank to CONACyT México for scholarship (RPJ). We thank Mr. David Campos for his assistance in the reactor construction.

## Nomenclature

<i>Abbreviation</i>	<i>Description</i>
---------------------	--------------------

MABR	Membrane aerated biofilm reactor
CFD	Computational Fluid Dynamic
MCM	Mixing Cell Model
ADM	Axial Dispersion Model
TIS	Tanks in Series Model
RTD	Residence Time Distribution
NS-LF	Reynolds Average Navier-Stokes Equation for Lamina Flow

### *Symbols*

$V_1$	volume of the stagnant zone, L
$V_2$	volume of the dynamic zone, L
$c_i$	dimensionless tracer concentration of i: initial concentration of tracer (0), stagnant zone (1), dynamic zone (2), and sum of concentrations (3)
$Q$	volumetric flow rate, L/min
$\mathbf{u}$	Velocity vector, m/s
$\mathbf{F}$	volume force vector, N/m <sup>3</sup>
$T$	absolute temperature, K
$U_0$	Initial average velocity at the inlet of the reactor, m/s
$p$	pressure, Pa
$n$	normal vector

$t$	Time, s
$L$	Length of MABR, m
$D_i$	diffusion coefficient, m <sup>2</sup> /s

***Greek letters***

$\alpha$	liquid fraction passing through the stagnant zone
$\rho$	density, kg/m <sup>3</sup>
$\theta$	dimensionless time
$\mu$	dynamic viscosity, Pa/s
$\tau$	average residence time, s

## References

1. B. Vrana, G. Schuurmann, 2002. Calibrating the uptake kinetics of semipermeable membrane devices in water: impact of hydrodynamics. *Environmental Science and Technology* 36, 290-296.
2. C. Huiliñir, R. Romero, C. Muñoz, C. Bornhardt, M. Roeckel, C. Antileo, 2010. Dynamic modeling of partial nitrification in a rotating disk biofilm reactor: Calibration, validation and simulation. *Biochemical Engineering Journal* 52, 7-18.
3. E. J. Tomlinson, B. Chambers, B., 1979. The effect of longitudinal mixing on the settle ability of activated sludge. Technical Report TR 122, Stevenage, England.
4. F. F. Rivera, M. R. Cruz-Díaz, E. P. Rivero, I. González, 2010. Analysis and interpretation of residence time distribution experimental curves in FM01-LC reactor using axial dispersion and plug dispersion exchange models with closed-closed boundary conditions. *Electrochimica Acta* 56(1), 361-371.
5. G. C. Glover, C. Printemps, K. Essemiani, J. Meinhold, J., 2006. Modeling of wastewater treatment plants – how far shall we go with sophisticated modeling tools?. *Water Science and Technology* 53(3), 79-89.
6. H. Liu, F. Yang, S. Shi, X. Liu, 2010. Effect of substrate COD/N ratio on performance and microbial community structure of a membrane aerated biofilm reactor. *Journal Environmental Sciences* 22(4), 540-546.
7. H. S. Fogler, 2008. *Elements of Chemical Reactions Engineering*, fourth ed., Prentice-Hall, Mexico.
8. J. F. Holland, J. F. Martin, T. Granata, V. Bouchard, M. Quigley, L. Brown, 2004. Effects of wetlands depth and flow rate on residence time distribution characteristics. *Ecological Engineering* 23(3), 189-203.

9. J. Ji, K. Zheng, Y. Xing, P. Zheng, 2012. Hydraulic characteristics and their effects on working performance of compartmentalized anaerobic reactor. *Bioresource Technology* 116, 47-52.
10. K. Essemiani, S. Vermande, S. Marsal, L. Phan, J. Meinhold, J., 2004. Optimisation of WWTP units using CFD – A tool grown for real scale application, Prague.
11. K. Hibiya, A. Terada, S. Tsuneda, A. Hirata, 2003. Simultaneous nitrification and denitrification by controlling vertical and horizontal microenvironment in a membrane-aerated biofilm reactor. *Journal of Biotechnology* 100, 1127-1136.
12. L. Montastruc, J. P. Brienne, I. Nikov, 2009. Modeling of residence time distribution: Application to a three-phase inverse fluidized bed based on a Mellin transform. *Chemical Engineering Journal* 148(1), 139–144.
13. M. Brannock, Y. Wang, G. Leslie, 2010. Mixing characterization of full scale membrane bioreactors: CFD modeling with experimental validation. *Water Research* 44(10), 3181-3191.
14. M. J. Semmens, 2008. Alternative MBR configurations: using membranes for gas transfer. *Desalination* 231, 236-242.
15. M. Martinov, D. Hadjiev, S. Vlaev, 2010. Liquid flow residence time in a fibrous fixed bed reactor with recycle. *Bioresource Technology* 101(4), 1300–1304.
16. O. Levenspiel, 1999. *Chemical Reaction Engineering*, third ed., John Wiley and sons, New York.
17. P. A. A. Klusener, G. Jonkers, F. During, E. D. Hollander, C. J. Schellekens, I. H. J. Ploemen, A. Othman, A. N. R. Bos, 2007. Horizontal cross-flow bubble column reactors: CFD and validation by plant scale tracer experiments. *Chemical Engineering Science* 62 (18–20), 5495–5502.
18. P. Trinidad, C. Ponce de León, F. C. Walsh, 2006. The application of flow dispersion models to the FM01-LC laboratory filter-press reactor. *Electrochimica Acta* 52(2), 604-61.
19. S. Hu, F. Yang, C. Sun, J. Zhang, T. Wang, 2008. Simultaneous removal of COD and nitrogen using a novel carbon-membrane aerated biofilm reactor. *Journal of Environmental Sciences* 20, 142-148.

20. S. Matsumoto, A. Terada, S. Tsuneda, 2007. Modeling of membrane-aerated biofilm: Effects of C/N ratio, biofilm thickness and surface loading of oxygen on feasibility of simultaneous nitrification and denitrification. *Biochemical Engineering Journal* 37, 98-107.
21. S. Mudliar, S. Banerjee, A. Vaidya, S. Devotta, 2008. Steady state model evaluation of external and internal mass transfer effects in an immobilized biofilm. *Bioresource Technology* 99, 3468-3474.
22. W. P. M. Van Swaaij, J. C. Charpentier, J. Villermaux, J., 1969. Residence time distribution in the liquid phase of trickle flow packed columns. *Chemical Engineering Science* 24, 1083-1095.
23. W. Qi, T. Hojo, Y. Li, 2013. Hydraulic characteristics simulation of an innovative self-agitation anaerobic baffled reactor (SA-ABR). *Bioresource Technology* 136, 94-10.
24. W. Qi, Y. Guo, M. Xue, Y. Li, 2013. Hydraulic analysis of an upflow sand filter: Tracer experiments, mathematical model and CFD computation. *Chemical Engineering Science* 104, 460-472.
25. X. Chen, P. Zheng, Y. Guo, Q. Mahmood, C. Tang, S. Ding, 2010. Flow patterns of super-high-rate anaerobic bioreactor, *Bioresource Technology* 101(20), 7731-7735.
26. X. Li, Yuan, H. Wang, 2003. Hydrodynamics of biological aggregates of different sludge ages: an insight into the mass transport mechanisms of bioaggregates. *Environmental Science and Technology* 37(2), 292-299.
27. X. Wang, J. Ding, W. Guo. N. Ren, 2010. A hydrodynamics-reaction kinetics coupled model for evaluating bioreactors derived from CFD simulation. *Bioresource Technology* 101(24), 9749-9757.
28. X. Wei, B. Li, S. Zhao, C. Qiang, H. Zhang, S. Wang, 2012. COD and nitrogen removal in facilitated transfer membrane-aerated biofilm reactor (FT-MABR). *Journal of Membrane Science* 389, 257-264.

**CHAPTER 4: The effect of inlet flow distributors on the hydrodynamic and mass transfer on a MABR using CFD and experimental validation with residence time distribution (RTD)**

R. Plascencia-Jatomea • J. Gómez • J. Vázquez • I. González • O. Monroy

*“Under review”*

# **The effect of inlet flow distributors on the hydrodynamic and mass transfer on a MABR using CFD and experimental validation with residence time distribution (RTD)**

R. Plascencia-Jatomea • F. J. Almazán-Ruiz • M. González-Brambila • J. Gómez • J. Vázquez • I. González • O. Monroy

*“Under review”*

## **Abstract**

MABR are gradually being adapted for use in the water treatment and its hydraulic profile directly affects the pollutant removal performance. The goal of this work was to develop new geometry design of inlet flow distributors of the MABR previously designed and characterized using Computational Fluid Dynamics (CFD). Eight geometric configurations of inlet flow distributors were tested. The convex, straight wall and conical wall distributors were selected since they generated similar velocity ratios at the channeling and stagnant zones. The new distributor geometries were experimentally evaluated with RTD experimental curves using the stimulus-response technique and approximated with the mixing cell model (MCM) and by solving the hydrodynamic Navier–Stokes (NS) equation for laminar flow and mass transport (convection–diffusion equation) equations using computational fluid dynamics (F-tracer RTD method). Two sets of RTD experiments (common and new inlet flow distributors) in MABR

were carried out. The volumetric flows rate ( $Q$ ) employed were from 03.6 to 10 mL/min. The new inlet flow distributor (conical wall flow distributor) generates a more homogeneous velocity field in the entire reaction zone (membrane zone), as shown by Comsol Multiphysics 4.3b simulations, than those obtained with the common MABR (without inlet flow distributor). The RTD curves obtained with Comsol Multiphysics 4.3b and MCM are in agreement with RTD experimental curves indicating a good models validation.

**Keywords:** CFD, MABR, RTD, inlet flow distributor, mixing cell model

## 4.1 Introduction

Bioreactors have been investigated at laboratory and plant scales and optimized through a better knowledge of their hydrodynamic behavior (Plascencia-Jatomea et al. 2015). Moreover, it is well known that high cell density in bioreactors, in continuous mode, leads to high productivity. Bioreactor configuration is also important in optimizing the bioprocess (Gaida et al. 2012).

In biofilm reactors, complex mechanisms take place which are highly dependent on hydrodynamic. To improve and operate such MABR technology, it is necessary to understand the physical parameters which affect the hydraulics in order to take into account these effects through software modeling (Haoran et al. 2013). It is important for example, to assess the contact time between the polluted stream and the biofilm responsible for pollutant biodegradation; this contact time is directly dependent on liquid holdup and liquid film thickness. Therefore, the mixing process is a relevant factor to take into account in the optimization of a given design, for achieving a high performance of the biological process, along with a suitable energy efficiency of the anaerobic digester.

The hydrodynamic behavior of the reactor can be determined through the analysis of the Residence Time Distribution (RTD) allowing identify the presence of dead zones, channeling or short-circuiting. The experimental results can be compared with those obtained via mathematical models under ideal conditions (Levenspiel, 2009). The RTD can be obtained through experimental methods by the injection of chemical tracers at the inlet of the reactor and the measurement of the concentration evolution of the tracer at inlet and outlet of the

reactor (Fogler, 2009). However, these results do not yield information on the characteristics of the flow inside the digester (Plascencia-Jatomea et al. 2015).

The experimental methods are costly and time consuming, require internal placement of instrumentation and sometime may not be feasible in a full-scale plant. Computational Fluid Dynamics (CFD) modelling emerges as an effective method to design and optimize many applications in the wastewater treatment field. CFD provides a method for prediction of the effect design features have on the hydrodynamics from a fundamental level (Brannock et al. 2010). By means of the numerical modelling of the fluid flow inside a reactor is possible to analyze the mixing process and the distribution of residence times, to predict fluid velocity vectors, turbulence, streamlines and particle trajectories or the volume of dead zones (Hurtado et al. 2015). Moreover, the design of the bioreactor and the mixing process can be optimized by CFD modelling.

In the present work, a global hydrodynamic study was carried out with the MABR previously designed and characterized (Plascencia-Jatomea et al. 2015). CFD and RTD test which constitute efficient tools to give new insight into complex hydrodynamic phenomena occurring in bioreactor.

Our scientific objectives focus on the hydrodynamic investigation of MABR through CFD and RTD studies in order to (i) get new insights in hydrodynamic phenomena inside MABR with the improvement of the flow distribution at the inlet of the bioreactor and (ii) study and model RTD in order to validate the CFD simulation. An overall hydrodynamic characterization (under abiotic conditions) was carried out by using residence time (RTD) and internal age

(IAD) distribution studies, according to suitable methodology described by Plascencia-Jatomea et al. 2015. Firstly, CFD experiments with different geometric configuration were determined to improve the flow pattern at MABR in continuous mode. Secondly, a selection of the geometric configuration that works better was selected and used to identify its characteristic flow pattern through RTD test. Finally, results of CFD and RTD studies were analyzed and validated proposing a new geometry (inlet flow distributor) with an improved hydrodynamic performance.

## **4.2 Experimental**

### **4.2.1 Reactor structure and flow distributors design**

The experiments were carried out in a MABR with an effective volume of 1.95 L. A complete description of the reactor and the circulation system is described by Plascencia-Jatomea et al. 2015. The flow distributors were design using CFD (Comsol Multiphysics 4.3b) with a hydrodynamic- mass transfer model that had been completely described and validated in the mentioned work. Eight flow distributors were design and tested by CFD. By analyzing the hydrodynamic profile of each distributor, three devices were selected and constructed with Nylon. These devices were mounted at the central perforation of airtight distribution chamber of the MABR and the RTD test was carry on with each distributor.

### **4.2.2 Residence time distribution (RTD) experiments**

The reactor was fed with water as the carrying fluid, at different volumetric flow rates ( $Q$ ) (3.6 to 10 mL/min). The flow pattern experiment used tracer-response technology using dextran blue as a model tracer (20 g/L). This experiment adopted a pulse input method (Levenspiel,

2013). Data collection was initiated at the time of tracer injection. Water samples were analysis on line at the exit of the reactor every 5 s as is described by Plascencia-Jatomea et al. 2015. At least 9000 samples were used to describe the flow pattern. The experimental RTD data obtained was used for calculation of RTD functions;  $E(t)$  (residence time distribution function) and  $\bar{t}$  (mean residence time) according to Fogler, 2008.

### **4.3 Inlet flow distribution distributor design and RTD curve description with mathematical models and Comsol Multiphysics**

The computing strategies and mathematical models for the new geometry design of inlet distributors of MABR will be described in the following issues.

#### **4.3.1 Mathematical model of tracer concentration in MABR**

To approximate the experimental RTD curves behavior and determine the dispersion degree of previously designed and characterized and new MABR, the mixing cell model was used. This model has been completely described in the work reported by Plascencia-Jatomea et al. 2015.

#### **4.3.2 New geometry design of inlet flow distributors of MABR**

The new geometry design of inlet distributors was established through CFD simulation, using the Hydrodynamic-mass transfer model previously described by Plascencia-Jatomea et al. 2015. The characteristics dimensions of the conventional MABR and the liquid flow circuit reported in the mentioned work were retained. A schematic diagram of the liquid flow circuit for the MABR reactor used in the RTD experiments is shown in Fig. 4.1.

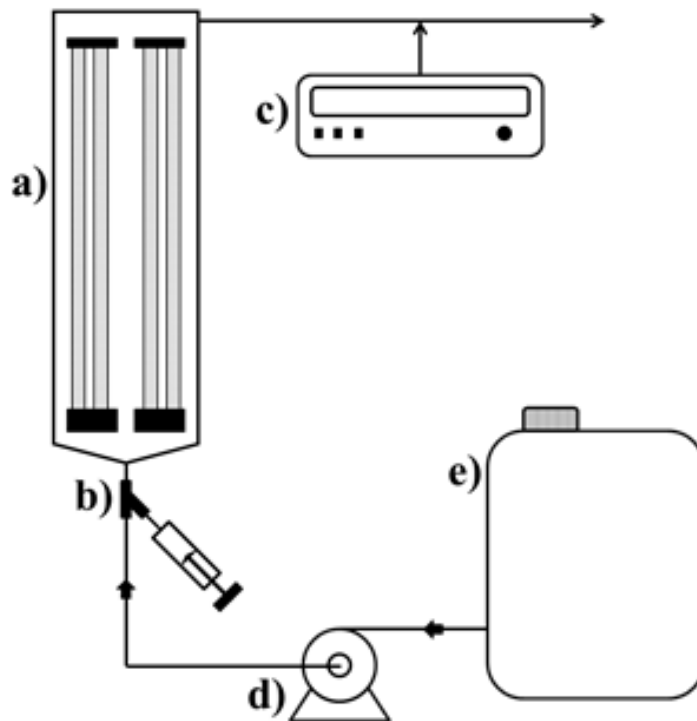


Figure 4.1. Schematic of the membrane aerated biofilm reactor (MABR) and liquid flow circuit used for RTD experiments: a) MABR, b) Type-Y connector, c) UV-Vis spectrophotometer, d) Peristaltic pump and e) Container (Plascencia-Jatomea et al. 2015).

The reactor has an operation volume of 1.95 L and is packed with 24 tubular hollow membranes 32 cm length, 5 mm inner side diameter, 1 mm thickness (superficial membranes area=0.17 m<sup>2</sup>). The membranes are distributed in almost all the cross-sectional area of the reactor whose internal diameter is 8.2 cm and height of 46 cm. The intermembrane pressure was maintained at 2 psi (*molecular oxygen*); the pressure was set to carry out the dissolution of oxygen preventing the formation of a steady stream of bubbles.

Different geometric configurations of inlet flow distributors were design and tested using Comsol Multiphysics 4.3b; plane distributor, concave distributor, coronary distributor, plane-

convex distributor, plane-inverted cone distributor, convex distributor, plane wall distributor, and conical wall distributor. The inlet flow distributors are 1 inch of external diameter and high of 0.25 inches. In Fig. 4.2, the geometric configurations of the inlet flow distributors tasted are presented in cross-section view. The external diameter is represented by  $x$  and the high of the inlet flow distributors is represented by  $y$ .

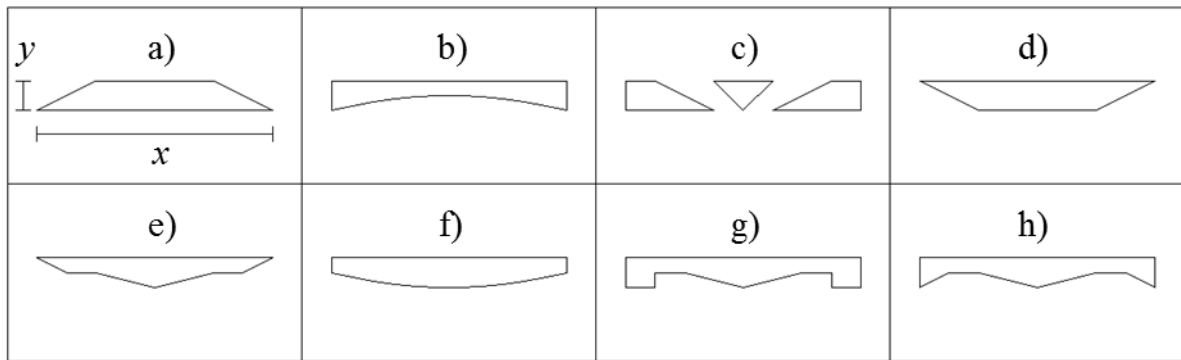


Figure 4.2. Geometric configuration of the inlet flow distributors. a) plane distributor, b) concave distributor, c) coronary distributor, d) plane-convex distributor, e) plane-inverted cone distributor, f) convex distributor, g) plane wall distributor and h) conical wall distributor. The scheme of the flow distributors are presented in cross section view. The external diameter is represented by  $x$  and the high of the inlet flow distributors is represented by  $y$ .

These new geometry distributors met four constrains: a) the same velocity of fluid elements at the beginning of the active zone (membrane zone); b) minimize high and low velocity zones inside the active area; c) achieve a fully developed flow within the active area and d) the flow distributors should be collocated at the central perforation of the airtight distribution chamber of the MABR (see Figure 4.3).

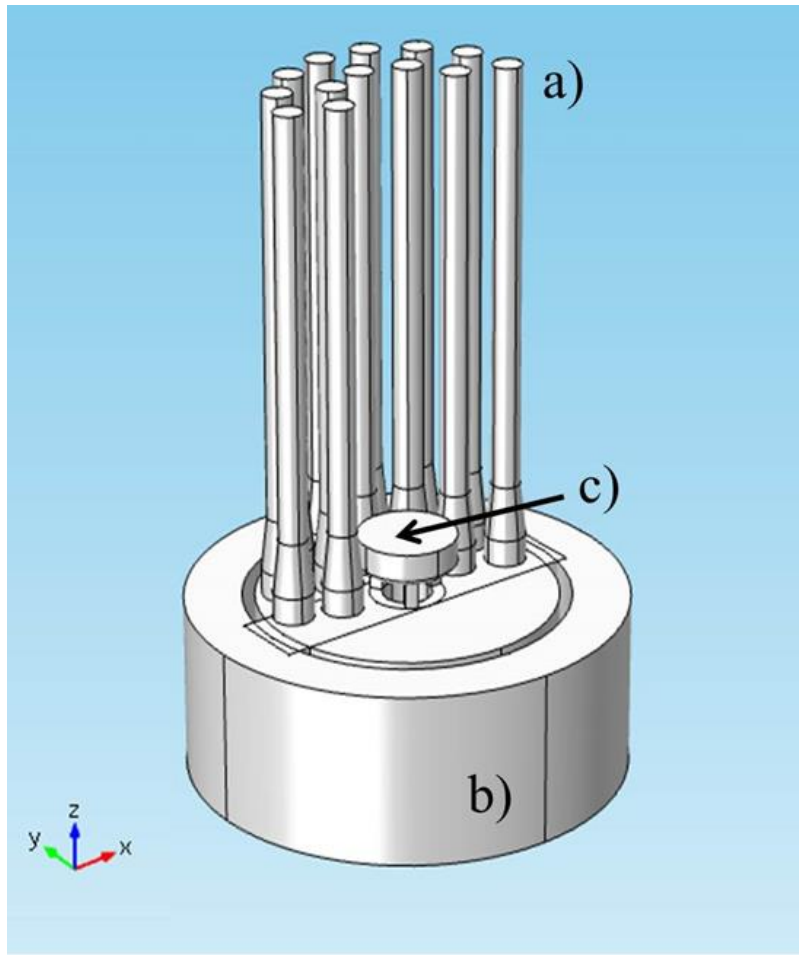


Figure 4.3. Inlet flow distributors position at the MABR. a) tubular membranes, b) airtight distribution chamber and c) flow distributor

#### **4.3.3 Simulation of experimental RTD curve with hydrodynamic-mass transfer model for laminar flow**

The description of RTD experimental curves by “theoretical step-signal method” in CFD was carried out in order to emulate the RTD experimental curves obtained by a “pulse-signal experimental method”. Therefore, to emulate the flow pattern inside the MABR it was necessary to introduce the geometry of the reactor in Comsol Multiphysics 4.3b, then solve the hydrodynamic for laminar flow and mass transport (convection-diffusion equation) models

and transform mass step signal at the reactor outlet to Gaussian curve throughout the derivative of the cumulative function  $[d(F(t))=d(C_i/C_{0,s})]$ , where  $C_{0,s}$  is the concentration at the reactor inlet in steady state. A detailed description of the hydrodynamic-mass transfer model has been presented by Plascencia-Jatomea et al. 2015.

#### 4.3.3.1 Hydrodynamic model

The hydrodynamic of the MABR was simulated by solving the NS equations for laminar flow coupled to continuity equation for incompressible fluid. Assuming that liquid flow is in steady state, the solution of the hydrodynamic is not time dependent.

Assuming negligible variations in viscosity and density, NS model is:

$$\rho(u \cdot \nabla)u = \nabla \cdot \left[ -pI + \mu(\nabla u + (\nabla \mu)^T) \right] + F \quad (1)$$

where  $\rho$  is the density of the fluid (Kg/m<sup>3</sup>),  $u$  is the velocity vector (m/s),  $P$  is the pressure (Pa),  $\mu$  is the dynamic viscosity (Pa•s),  $F$  is the volume force vector (N/m<sup>3</sup>) and  $T$  represent the absolute temperature (K).

The boundary conditions employed to solve NS equations were:

- a) At the inlet (constant velocity entry):

$$u = -U_0 n \quad (2)$$

Where  $U_0$  is the initial average velocity (m/s) at the inlet of the reactor which was calculated, taken into account the transversal area of the tube that fed the reactor and  $n$  is the normal vector that points out the fluid domain.

b) At the walls (no slip conditions):

Since all velocities must disappear on the wall, therefore, the wall boundary conditions adjacent to a solid wall are:

$$u = 0 \quad (3)$$

c) At the outlet of the reactor (no gradient forces):

$$\left[ \mu(\nabla u + (\nabla u)^T) \right] \cdot n = 0 \quad P = 0 \quad (4)$$

#### 4.3.3.2 Mass transport model (convection-diffusion equation)

The mass transport of the tracer inside the MABR was simulated with convection–diffusion equation in transient and laminar regime using a “step-signal” at the inlet of the reactor. In this study we did not use a “pulse-signal” as it was used in RTD experimental curves, because the major difficulty when using a pulse function is to define a mathematical function (Gaussian or Dirac delta functions) that represents an actual tracer pulse injection in precise fashion. For this, it is necessary the use of a little step sizes of analysis requiring long time period of simulations besides the requirements of large storage capacity of the hardware. To overcome this difficulty a step signal ( $-n \cdot N_0 = U_0 C_0$ ) was used at the inlet and the mass step signal at the reactor outlet was transformed to Gaussian curve through the derivative of the cumulative function:

$$\frac{d[F(t)]}{dt} = \frac{d}{dt} \left( \frac{C_i(t)}{C_{0,s}} \right) \quad (5)$$

Therefore, to describe mass transport of the tracer in water (binary mixture) for a dilute solution in transient regimen, the equation convection-diffusion in laminar regimen was used:

$$\frac{\partial C_i}{\partial t} = \nabla \cdot (D_i \nabla C_i) - u \cdot \nabla C_i \quad (6)$$

Where  $u$  is the average velocity field,  $C_i$  is the averaged concentration field and  $D_i$  is the diffusion coefficient.

The boundary and initial conditions employed to solve Eq. 6 were:

a) Initial conditions

$$C_i = 0, \quad t \leq 0 \quad (7)$$

b) At the reactor inlet (step-signal at entry)

$$C_i = 0, \quad t > 0, \quad -n \cdot N_0 = U_0 C_0 \quad (8)$$

c) At the walls (impermeable walls)

$$-n \cdot N_i = 0 \quad (9)$$

d) At the reactor outlet (no more mass flux):

$$-n \cdot D_i \nabla C_i = 0 \quad (10)$$

The equations of hydrodynamics and mass transport (convection–diffusion equation) were solved in 3D using the software Comsol Multiphysics 4.3b, in an Alienware Aurora computer

equipped with a quad-core Intel® Core i7 processor, Windows® 7 HomePremium64-bit, 16GB, 1600MHz RAM and NVIDIA® GeForce® GTX 6904GBvideocard.

In order to obtain a good convergence and minimize the computing time, the geometric construction was elaborated avoiding small elements where the meshing is considerably increased. On the other hand, the simulation meshing was chosen by user: a coarse mesh was used in the domain, but near solid walls the meshing was finer; in this case only three mesh layers were used in the walls. In order to obtain a first convergence, the simulation was initialized with a coarser mesh, later on it was refined till the response curves no longer depended on the size of the mesh. The computational domain meshing consisted of 998,322 cell elements (669,556 tetrahedral elements; 323,894 prismatic elements; 3552 hexahedral elements; 1320 pyramidal elements), the solver used was PARDISO.

#### ***4.3.3.3 RTD curves from step signal response***

Once hydrodynamic and mass transport equations in laminar regimen were solved, the average concentration at the out let tube surface (outlet boundary condition) as a function of time was obtained, which corresponds to response curves of the step-signal introduced at the beginning of the MABR. Fig. 4.4 shows the response curves of the step-signal for the MABR without inlet flow distributor, and with inlet flow distributors; plane wall, conical wall and convex flow distributor at a  $Q$  of 10 mL/min.

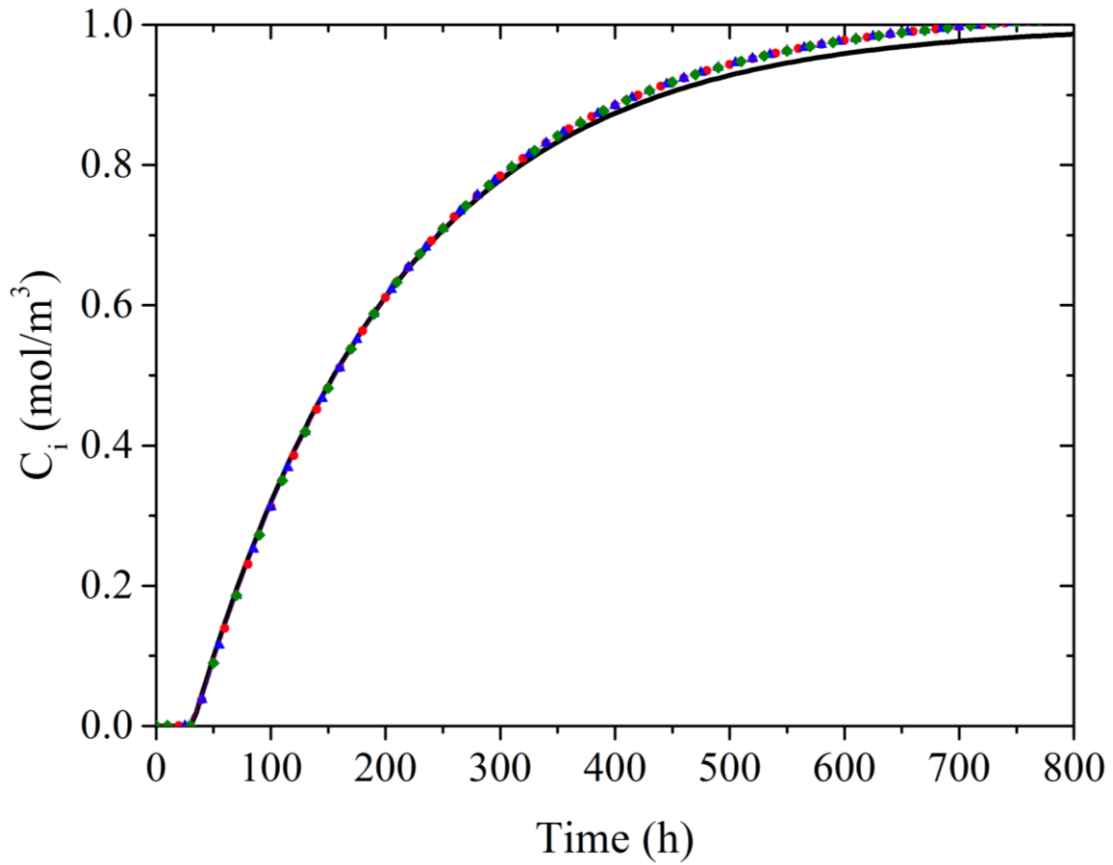


Figure 4.4. Output response curves of the step-signal at the entrance of MABR. Without flow distributor (black line), convex (red circle), conical wall (green diamond) and straight wall flow distributor (blue triangle). Volumetric flow rate ( $Q$ ) of 10 mL/min.

The next step was to find the dimensionless cumulative function of the response curves:

$$F(t) = \frac{C_i(t)}{C_{0,S}} \tag{11}$$

The derivative of Eq. (11) is equivalent to age distribution function  $E(t)$  obtained with a pulse-signal (Levenspiel, 1999):

$$\frac{dF(t)}{dt} = \frac{d}{dt} \left( \frac{C_i(t)}{C_{0,S}} \right) = E(t) \quad (12)$$

Then a dimensionless age distribution curve was obtained from E(t) data by employing the average residence time ( $\tau$  or  $\theta$ ) according to the method of moments:

$$\tau = \frac{\int_0^{\infty} t C dt}{\int_0^{\infty} C dt} = \frac{\sum_{i=0}^n t_i C_i \Delta t_i}{\sum_{i=0}^n C_i \Delta t_i}, \quad \theta_i = \frac{t_i}{\tau}, \quad E(\theta) = \tau E(t) \quad (13)$$

## 4.4 Results and discussion

### 4.4.1 Analysis and selection of the inlet flow distributor; comparison of hydrodynamic behavior

Eight flow distributors with different geometric configuration were tasted using CFD. A quantitative analysis of the fluid velocity profile was done for the selection of the best geometric configuration of the flow distributor. In Figure 4.5, the velocity profiles of the MABR reactor without and the eight flow distributors are shown. The multicolor bar located beside image represents the magnitude of the velocity field, dark blue color represent the lowest velocities and red color represents the highest velocities.

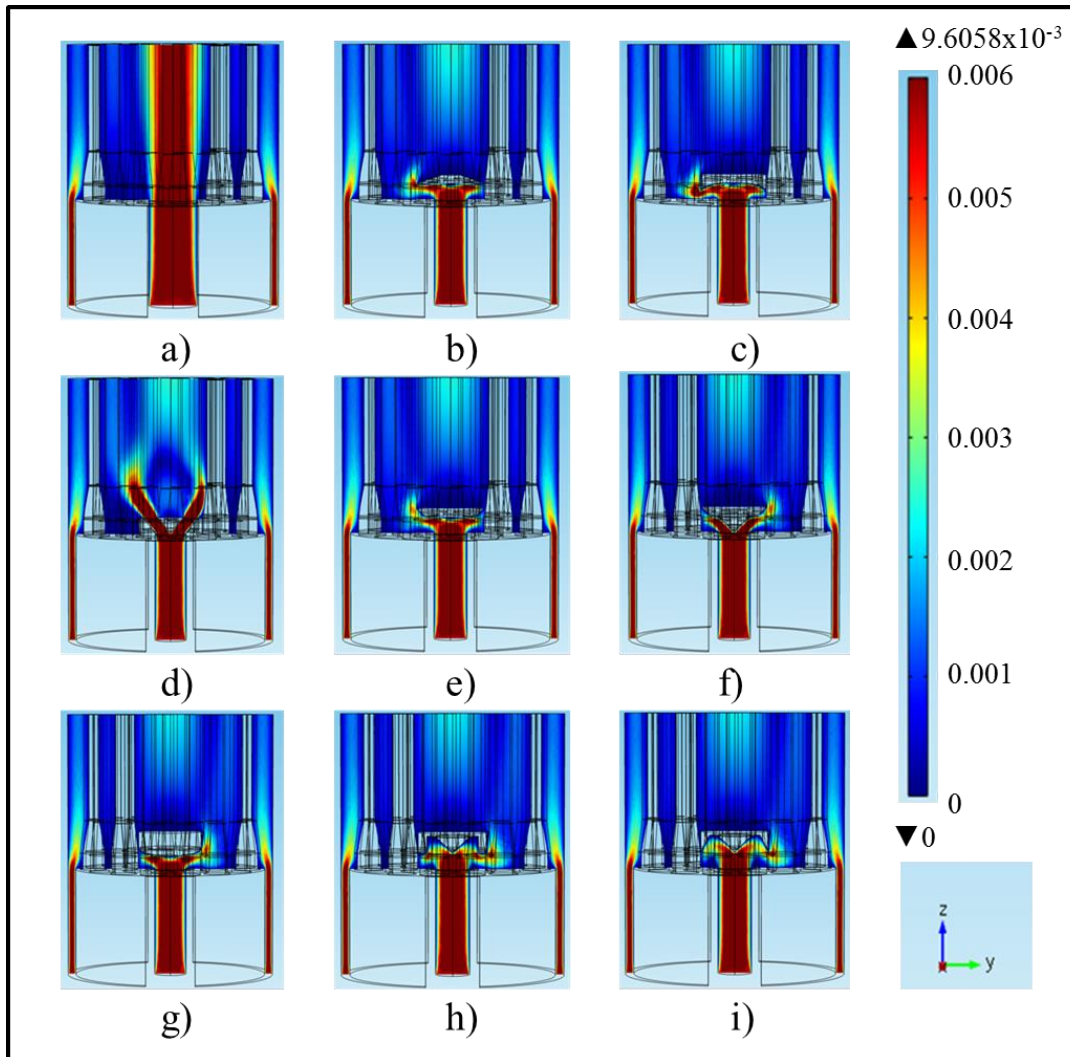


Figure 4.5. Influence of the geometry of flow distributors on fluid velocity profiles (m/s) of the MABR obtained with Comsol Mutiphysics 4.3 b (volumetric flow rate ( $Q$ ) of 10 mL/min). a) without distributor, b) plane distributor, c) concave distributor, d) coronary distributor, e) plane-convex distributor, f) plane-inverted cone distributor, g) convex distributor, h) plane wall distributor and i) conical wall distributor. The images have shown the first 10 cm of the MABR from the inlet to the top.

Figure 4.5-a), represent the normal hydrodynamic profile of the MABR reactor (without design improvement). According to the hydrodynamic profile, two flow velocity zones can be identify: high velocity zone (channeling zone,  $cz$ ) identified by red color and located in the central region beginning from the central perforation of the distributor chamber to the outlet of the reactor, and low velocity zone (stagnant zone,  $sz$ ) identified by dark blue color presented in a high proportion of the reactor volume and it seems to be homogeneous. The hydrodynamic behavior of the common MABR (without distributor), shown in Fig. 4.5-a, was previously reported by our research group in Plascencia-Jatomea et al. 2015.

According to these results, all of the flow distributors shown satisfactory correction of the  $cz$  (center of the reactor) since these new geometry flow distributors were proposed to meeting the following constrains: a) the same velocity of fluid elements at the beginning of the active zone (membrane zone); b) minimize high and low velocity zones inside the active area; c) achieve a fully developed flow within the active area. However, the selection of the flow distributor that works better is difficult to observe, since the color does not allow identifying a real difference between the new inlet flow distributors.

In order to get a better understanding of the velocity profile of the bulk liquid inside the reactor a velocity study was done in a cross-section of the reactor from center to the inner wall of the reactor passing through two membranes (see Fig. 4.6) and at different reactor heights (membranes zone).

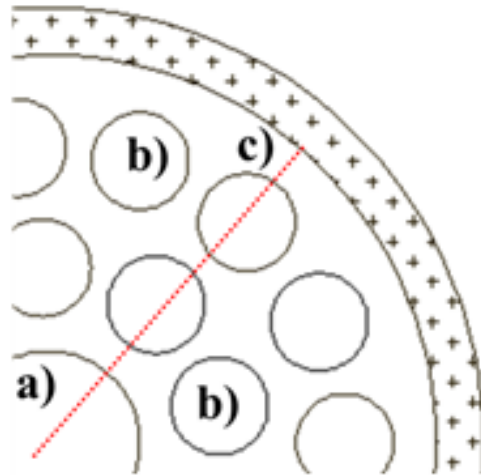


Figure 4.6. Scheme of cross-section of the MABR: a) Central perforation of the distribution chamber, b) Tubular membrane and c) Inner wall of the reactor.

Figure 4.7, shows the normalized velocity field between tubular membranes at specific  $Q$  of 10 mL/min. The velocity profile was analyzed at different heights founding that there was no difference in the membrane zone. The velocity profile is similar at all volumetric flow rates ( $Q$ ) tested for each flow distributors.

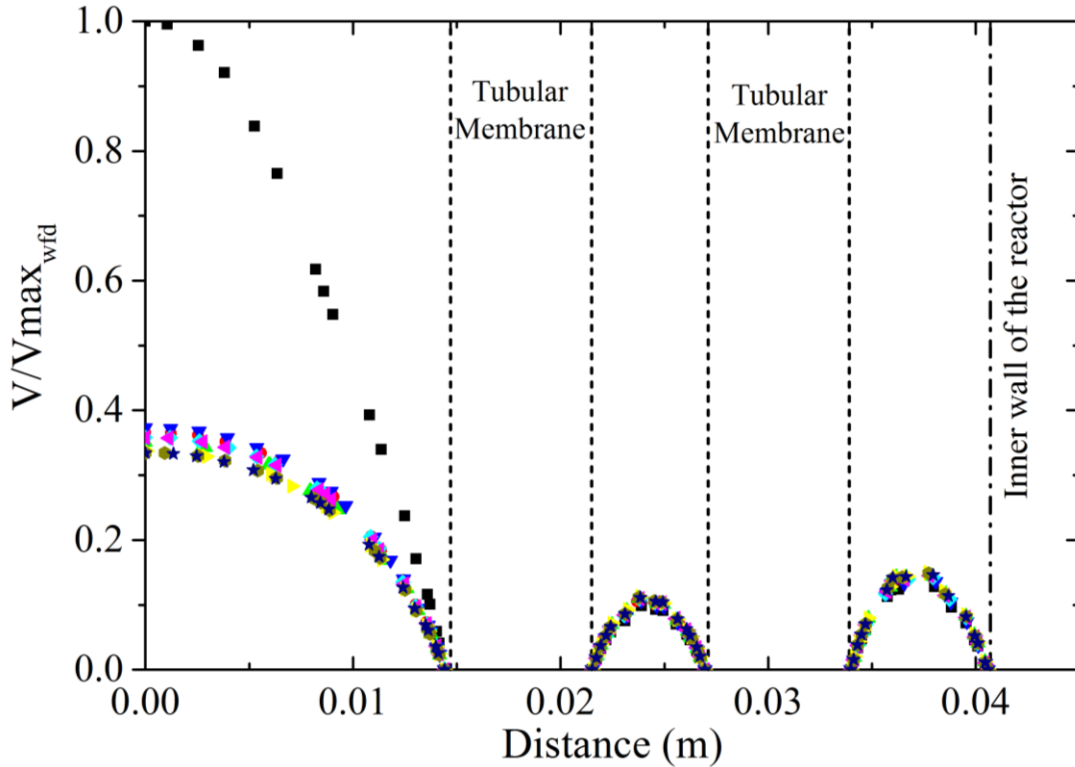


Figure 4.7. Comparison of normalized velocity profile in cross-section obtained with different geometries of inner flow distributors in steady state of the MABR. Without distributor (black square), plane distributor (red circle), concave distributor (green triangle), coronary distributor (blue inverted triangle), plane-convex distributor (ciani diamond), plane-inverted cone distributor (purple left triangle), convex distributor (yellow right triangle), plane wall distributor (olive hexagon) and conical wall distributor (blue star). Volumetric flow rate ( $Q$ ) of 10 mL/min.

The normalized velocity profile is the ratio of the average fluid velocity and the maximum value of the in the  $cz$  without flow distributor ( $V_{max_{wfd}}$ ). The highest normalized velocity value (1) obtained without flow distributor corresponds to the center of the reactor and diminishes almost to zero in the region nearest to the external wall of the membranes and in the inner wall of the reactor due to the shear stress (see Fig.4.7, black square). In the other hand the region between tubular membranes and tubular membrane-inner wall of the reactor maximum velocity is similar.

The use of the new inlet flow distributors can diminished the fluid velocity at the  $cz$  (center of the reactor) in 62-70%, indicating that the use of a inlet flow distributor is a promising alternative to improve the hydrodynamic profile of the MABR. This fact is reinforced by analyzing the velocity ration ( $R_{V_{maxcz}/V_{maxsz}}$ ) of the maximum average fluid velocity in the channeling zone ( $V_{max_{cz}}$ ) and the maximum average fluid velocity in the stagnant zone ( $V_{max_{sz}}$ ).

The MABR without flow distributor presented a ( $R_{V_{maxcz}/V_{maxsz}}$ ) of 8.8, and this profile is maintained at different reactor heights (membranes zone). Table 4.1 shows the velocity ratio ( $R_{V_{maxcz}/V_{maxsz}}$ ) of maximum average fluid velocity in the channeling zone and the maximum average fluid velocity in the stagnant zone.

Table 4.1. Velocity ratio ( $R_{V_{maxcz}/V_{maxsz}}$ ) of maximum average fluid velocity in the channeling zone and the maximum average fluid velocity in the stagnant zone of the MABR, with and without inlet flow distributors.

Distributor	$V_{max_{cz}}$ (m/s)	$V_{max_{sz}}$ (m/s)	$R_{V_{maxcz}/V_{maxsz}}$
a) Without	0.0067	0.00076	8.82
b) Plane	0.0025	0.00083	3.01
c) Concave	0.0023	0.00085	2.71
d) Coronary	0.0025	0.00081	3.09
e) Plane-convex	0.0024	0.00084	2.86
f) Plane-Inverted cone	0.0024	0.00085	2.82
g) Convex	0.0023	0.00088	2.61
h) Straight wall	0.0022	0.00087	2.53
i) Conical wall	0.0022	0.00086	2.56

According to these results (see Table 4.1) it is possible to determine that the geometric of inlet flow distribution which present a better correction of the hydrodynamic profile of the MABR were three; the convex distributor, straight wall distributor and conical wall distributor. These devices presented a velocity ratio ( $R_{V_{maxcz}/V_{maxsz}}$ ) of  $2.56 \pm 0.04$ , which represent a diminution of 70% with respect to the velocity ratio obtained without inlet flow distribution ( $R_{V_{maxcz}/V_{maxsz}}=8.8$ ). Due to this, these inlet flow distributors were selected and constructed to being used in the RTD experimental test.

#### **4.4.2 Comparison of RTD experimental curves and evaluation of the dispersion grade of MABR reactor with COMSOL Multiphysics 4.3b and mixing cell model (MCM)**

The improved hydrodynamic flow pattern inside the MABR due to new inlet geometry (inlet flow distributor) was confirmed by RTD experiments carried out to evaluate the dispersion degree. The RTD curves constructed by the hydrodynamic and mass transport evaluation using Comsol Multiphysics 4.3b, and MCM were compared with RTD experimental data. Fig. 4.8 shows the comparison of RTD experimental curves obtained with common (without flow distributor) and new geometry (convex, straight wall and conical wall flow distributors). In both cases, the RTD curves for 3.6, 6, 8 and 10 mL/min were approximated with MCM. For all  $Q$  the RTD experimental curve showed the same profile.

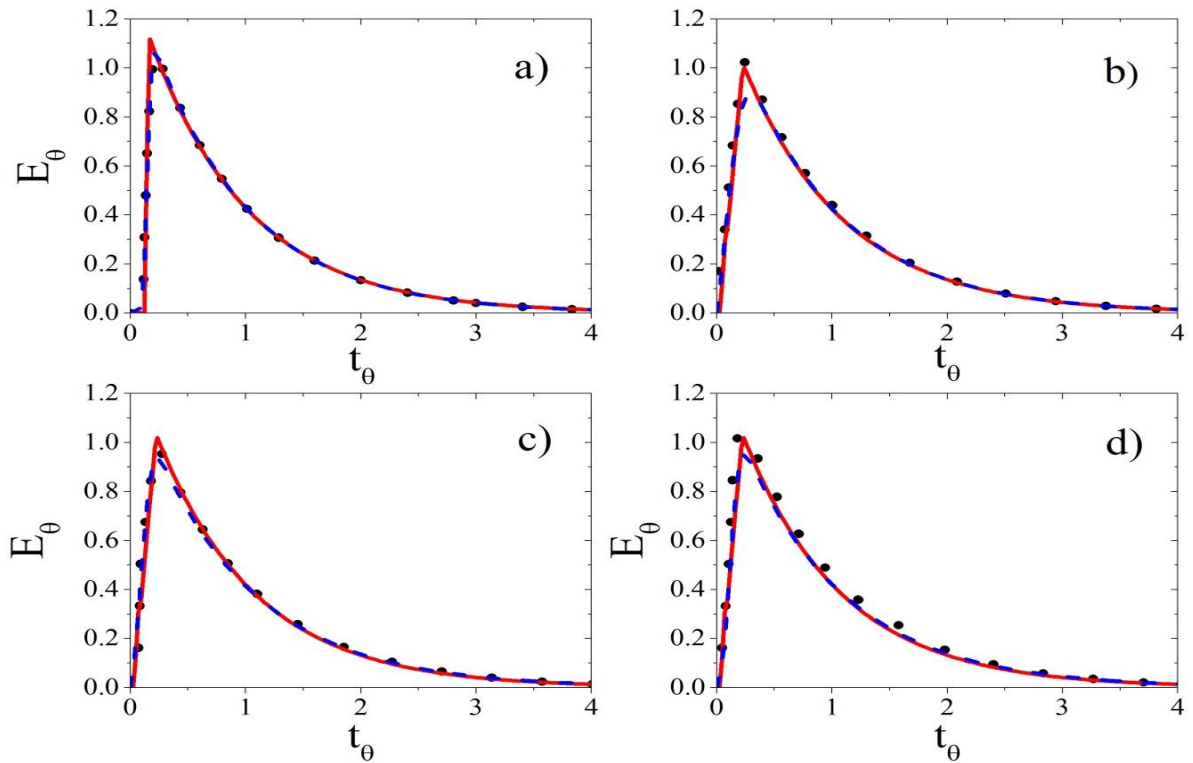


Figure 4.8. RTD curves obtained in the MABR with different geometric arranges of inlet flow distributors at a volumetric flow rate ( $Q$ ) of 10 mL/min. a) without flow distributor (normal operation), b) straight wall flow distributor, c) conical wall flow distributor and d) convex flow distributor. Experimental data (black dots) and constructed RTD curves with different model: COMSOL Multiphysics 4.3b (continuous red line) and MCM (blue dashed line).

The uncertainty of the RTD experiments was  $\pm 1.95\%$ , this value was determined by measuring the response of the tracer concentration three times in each experiment, after which the average of standard deviations was calculated, indicating that all experiments have a good reproducibility.

#### 4.4.2.1 Validation of hydrodynamic and mass transport simulation using RTD experiments

In order to verify if NS for laminar flow and convection–diffusion equations solved with Comsol Multiphysics 4.3b adequately represent the actual hydrodynamic profile and mass transport of the tracer inside the MABR, the RTD experimental curves were compared with those obtained by Comsol Multiphysics 4.3b ( see Figure 4.8). The model was capable to describe de hydrodynamic and mass transfer phenomena inside the MABR for all tasted experimental conditions (see Figure 4.8). In Table 4.2, a comparison between the RTD function ( $t_m$ , mean residence time) obtained from RTD data using Comsol Multiphysics and RTD experimental data is shown.

Table 4.2. RTD experimental conditions and parameter values obtained from experimental data, mixing cell model (MCM) and Comsol Multiphysics 4.3b.

RTD	$t_{m\text{-exp}}$ (min)	$t_{m\text{-COMSOL}}$ (min)	$t_{m\text{-MCM}}$ (min)
without flow distributor	233.4	225.1	228.04
straight wall flow distributor	219.7	211.2	204.9
conical wall flow distributor	221.1	213.1	210.42
convex flow distributor	218.6	211.9	205.7

$t_m$  average residence time of tracer

\*values corresponds to a volumetric flow rate of 10 mL/min

The RTD curves obtained with Comsol Multiphysics 4.3b are in agreement with RTD experimental curves with a percentage of error lower than 4% for all cases (see Figure 4.8 and Table 4.2). This reinforced the validation of the NS for laminar flow and convection–diffusion equations solved with Comsol Multiphysics 4.3b, indicating that the model has good reliability in the simulated data.

#### ***4.4.2.2 Validation of hydrodynamic and mass transport simulation using RTD experiments***

The RTD curves were approximated with the MCM because the presence of channeling zones and tailing phenomena (stagnant zone). This mathematical model has the capacity to describe this phenomenon as it was demonstrated by Plascencia-Jatomea et al. 2015. The model considers that a fraction of the inflow ( $\alpha$ ) passes to  $V_1$  (stagnant zone), where the flow velocity is low, and the rest of the inflow ( $1-\alpha$ ) passes to  $V_2$  (dynamic zone), where the flow velocity is high. Finally, both flows mix and produce an output with concentration  $C_3$ .

The parameter values obtained with the MCM are reported in Table 4.2. According to results, the MCM was capable to describe correctly all experimental RTD curves using only one mixing cell with and without inlet flow distributor. The MCM showed an error of ~6%, indicating that the model has good reliability.

#### **4.4.3 Effect of the inlet flow distributors in the hydrodynamic and mass transfer inside the MABR.**

Once that the NS for laminar flow and convection–diffusion equations solved with Comsol Multiphysics 4.3b and the MCM were validated a complete analysis was done in order to identify the real impact of the new inlet flow distributors. For this, the MCM model was used

to select the inlet flow distributor that best works in the improvement of the hydrodynamic performance of the MABR. In Table 4.3, the parameter values obtained with the MCM without flow distributor (data reported by Plascencia-Jatomea et al 2015) and with the inlet flow distributors are presented.

Table 4.3. Parameter values obtained for the best fit of experimental RTD curves with the mixing cell model (MCM).

Experimental condition	$V_1$ (L)	$V_2$ (L)	$V_1/V_2$	$\alpha$
without flow distributor	1.65	0.3	5.5	0.85
convex flow distributor	1.72	0.13	13.2	0.93
straight wall flow distributor	1.71	0.14	12.2	0.92
conical wall flow distributor	1.74	0.11	15.8	0.94

*\*values corresponds to a volumetric flow rate of 10 mL/min*

The common operation (without flow distributor) of MABR presents a  $V_1$  of 1.65L which correspond to a stagnant zone were the fluid present low velocity with a volume ratio of stagnant and channeling zone of 5.5. The implementation of the inlet flow distributors (convex, straight wall and conical wall) showed an improvement of the hydrodynamic performance of the MABR by augmenting the volume ratio of stagnant and channeling zone around  $240 \pm 34$  %. However, the inlet flow distributor that shown the bests results is the conical wall flow distributor with a volume ratio of stagnant and channeling zone of 15.8. In

addition, this inlet flow distributor presented the lowest error value in the validation of MCM (4.8%). These results proved that the conical wall flow distributor is the best device that can improved the hydrodynamic performance of the MABR.

#### **4.4.4 Hydrodynamic profile and mass transport of the tracer inside MABR with flow distributors obtained with Comsol Multiphysics 4.3b.**

Although the RTD study is an effective technique to determine whether a reactor has an ideal flow pattern behavior (CSTR or plug flow) or shows deviations from an ideal reactor (stagnant or dead zones, channeling, recirculation, by-pass and back mixing), the information obtained with this technique is at macromixing level (global mixing). The local mixing flow pattern (micromixing), however, helps to find zones that cause deviations in the ideal flow pattern inside the reactor. In the present work these data were obtained by solving hydrodynamics in steady state and mass transport of the tracer (step signal) in transient regimen using Comsol Multiphysics 4.3b. The liquid flow rates here presented correspond to 10 mL/min (laminar regimen).

Fig. 4.9 shows the mass transport of the tracer distribution inside the MABR with the conical flow distributor in transient regimen at different times and distances along the reactor; in each figure the multicolor scale bars correspond to tracer concentration ( $\text{mol/m}^3$ ), red color indicates higher concentration and green color corresponding to lower values.

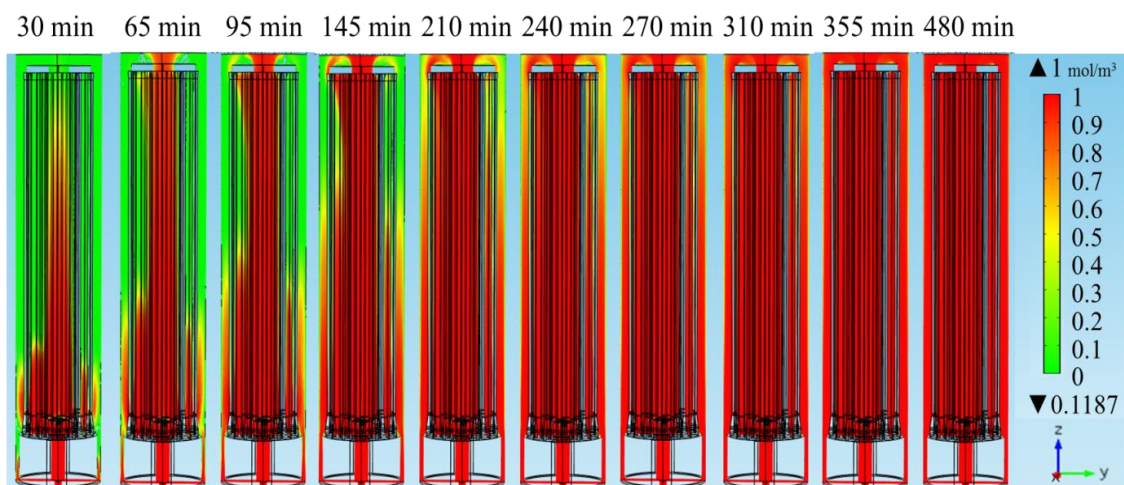


Figure 4.9. Mass transport distribution of tracer inside along the MABR in transient regimen obtained with Comsol Multiphysics 4.3b. Different times passing after the fluid entrance on the reactor are indicated in the figure. The figure corresponds to a volumetric flow rate of 10 mL/min..

After 30 min of the tracer injection (see Fig. 4.9), the tracer is displacing with higher concentration in the center of the reactor with respect to active zone (membranes zone), and this behavior is damped as the tracer moves along the channel (30–65 min), forming two concentration zones with almost the same concentration along the reactor width, but always in the active zone displace a little slower than middle zone (center).

## 4.5 Conclusions

New geometry of the MABR inlet (flow distributors) consisting in the collocation of several flow distributors design in the central perforation of the airtight distribution chamber. These new geometry inlet flow distributors satisfied three constraints: a) the same velocity of fluid elements at the beginning of the active zone (membrane zone); b) minimize high and low velocity zones inside the active area; c) achieve a fully developed flow within the active area and d) the flow distributors should be collocated at the central perforation of the airtight distribution chamber of the MABR. According to CFD results, it was observed that with the new inlet flow distributor the velocity at the center of the reactor in each distributor duct at the beginning showed an important diminution providing a more homogeneous velocity field in entire reaction zone (membrane zone). The RTD experimentals curves were compared with those RTD curves obtained through CFD (Comsol Mutiphysics 4.3b) and MCM. The parameter values of the RTD experimental curves evaluated with MCM, using the inlet flow distributors (conical straight wall) shown a reduction of the channeling zone volume. Therefore, liquid flow pattern with the flow distributor has less deviation from a complete stirred tank reactor (CSTR).

## References

1. Comsol Multiphysics 4.3b. License number: 1038192.
2. F.J. Hurtado, A.S. Kaiser, B. Zamora (2015). Fluid dynamic analysis of a continuous stirred tank reactor for technical optimization of wastewater digestion. *Water Research* 71, 282-293.
3. Lamia Ben Gaida, Christophe Andre, Carine Bideaux, Sandrine Alfenore, Xavier Cameleyre, Carole Molina-Jouve, Luc Fillaudeau (2012). Modeling of hydrodynamic behavior of a two-stage bioreactor with cell recycling dedicated to intensive microbial production. *Chemical Engineering Journal* 183, 222-230.
4. Levenspiel, Octave. *Chemical Reaction Engineering*, 3th edition, Limusa-Wiley, Mexico.
5. M. Brannock, G. Leslie, Y. Wang, S. Buetchorn (2010). Optimising mixing and nutrient removal in membrane bioreactors: CFD modeling and experimental validation. *Desalination* 250, 815-818.
6. R. Plascencia-Jatomea, I. González, J. Gómez, O. Monroy (2015). Operation and dynamic modeling of a novel integrated anaerobic–aerobic–anoxic reactor for sewage treatment. *Chemical Engineering Science* 138, 31-40.
7. R. Plascencia-Jatomea, F. J. Almazán-Ruiz, J. Gómez, E. P. Rivero, O. Monroy, I. González (2015). Hydrodynamic study of a novel membrane aerated biofilm reactor (MABR): Tracer experiments and CFD simulation. *Chemical Engineering Science* 138, 324-332.
8. Pang Haoran, Letisse Valérie, Paul Etienne, Hébrard Gilles (2013). The influence of porous structure and biofilm on the hydrodynamics of two types of trickle filters. *Chemical Engineering Journal* 231, 163-171.

## **CHAPTER 5: Epilog**

## **5.1 General Conclusions**

This work is one of the first studies about the use of integrated biological reactors for municipal wastewater treatment, which is important due to the significant advantages of these systems compared to conventional treatment systems. The results of this study allowed developed knowledge of this type of reactors on carbon and nitrogen compound degradation in the same system and its close relationship with diffusional phenomena (hydrodynamic-mass transfer hydrodynamic-reaction). Finally, everything mentioned above allowed the possibility of design improvements of this kind reactor for large-scale application in the treatment of municipal wastewater.

### **Operation and dynamic modeling of a novel integrated anaerobic-aerobic-anoxic reactor for sewage treatment.**

The uses of the integrated column reactor in the municipal wastewater treatment for the degradation of organic matter allowed obtain COD removal efficiencies of 83%, approximately. This efficiency degradation is similar to that obtained in conventional wastewater systems, demonstrating the feasibility of its application. In case of nitrogen compound's oxidation, the reactor could carry out a stable nitrification process with nitrite accumulation; however, the obtained ammonia/nitrite ratio is still above the required stoichiometric value (1.32).

The operation of the integrated column reactor allowed the acquisition of experimental data under different operational conditions, enabling the appropriate development and validation of an integrated mathematical model (hydrodynamic-mass transfer-reaction). This model could

predict the behavior of the reactor with an error of <5%, demonstrating the feasibility of the use of this model to predict the reactor behavior. According to model simulations, this system can be improved in design aspects and experimental conditions in order to establish a nitrification process with nitrite accumulation to obtain a suitable stoichiometry ratio by manipulating the reaction time, dissolved oxygen and the improvement of hydrodynamic behavior (reduction of the channeling zone).

### **Hydrodynamic study of a novel membrane aerated biofilm reactor (MABR) Tracer experiments and CFD simulation.**

The hydrodynamic study of a reactor is critical, as this directly affects the transport of contaminants and therefore, the reaction of degradation of polluting compounds. For this purpose in the membrane aerated biofilm reactor (MABR) different tests were carried out; the technique of residence time distribution using blue dextran as a model tracer, mathematical models of mass transfer (mixing cell model) and computational fluid dynamics (CFD). According to these results, the MABR presents deviations from the ideal flow pattern; preferential flow (center of the reactor) and stagnant zones where the fluid has a low speed in the membrane area. The hydrodynamic flow pattern of the reactor was described with an error of <5%. Once the flow pattern was described, the hydrodynamic model was used as the base for the formulation of an integrated mathematical model (hydrodynamic mass-transfer reaction).

### **Hydrodynamic improvement of a MABR using CFD and experimental validation with residence time distribution (RTD)**

The importance of formulating mathematical models with a correct validation process for improving the reactor performance relies on simulating the behavior of the system under

different experimental conditions. The use of the integrated models allowed the knowledge that the reactor design improvements can increase the degradation efficiencies of organic matter and nitrogen, giving a guideline to find out possible strategies for the improvement of the mixing flow pattern within the reactor.

Computational fluid dynamics (CFD), allowed designing devices that allowed improving the flow pattern behavior of the MABR by reducing the channeling of the reactor. These devices were analyzed by the technique of the residence time distribution, providing that the use of a flow distributor in the airtight distribution chamber of the MABR decreases the channeling zone by 50%. This computational tool proved to be extremely valuable for the design of biological reactors.

## 5.2 Perspectives

The implementation of integrated reactors is a reliable option for the treatment of municipal wastewater. This would represent an important advance in the implementation of new treatment processes with minimum space requirements and operational cost. However, it is worth to mention that this type of system is still developing, even missing work to be done in terms of operations and design aspects.

According to the results described in this paper, the proposed reactor prototype showed satisfactory results in the degradation of organic matter and nitrogen contained in municipal wastewater. However, some aspects in the design and operation strategies of the reactor should be improved making necessary future investigation.

Some interesting aspects are the implementation of devices that improve the flow pattern of the reactor which according to simulations obtained with integrated carbon-nitrogen removal model (ICNRM) the efficiency of COD degradation can be increased.

The operation of the integrated column reactor under the operational conditions described by the integrated mathematical model (ICNRM) will be critical to give greater certainty to the model. It will allow the proper operation of nitrification with nitrite accumulation.

*“This was just the end of the beginning; there is still work to do...”*

### **5.3 Recommendations**

The integrated column reactor should be operated with the implementation of the new flow distributors (conical wall flow distributor) in order to diminish the channeling zone of the MABR. It is expected that this device increases the pollutant's degradation efficiency.

The analysis about the operational volumes of the system could be determinate by the integrated model (hydrodynamic-mass transfer-reaction). The knowledge of the design equations of the system which are completely described by the integrated model will allow carrying out this procedure as well as known the reactor performance under these operational conditions.

It is recommended to carry out a complete study by using the computational fluid dynamics about the redesign of the airtight distribution chamber. This study will help in the reduction of the channeling zone in a better way.

The study about the physical characteristics of the biofilm (thickness) will make possible to modify the integrated model which could increase its certainty degree in predicting the reactor operation.

## **Conclusiones generales**

Este trabajo se encuentra entre algunos de los primeros estudios sobre el uso de reactores biológicos integrados para el tratamiento de aguas residuales municipales, lo que resulta importante debido a las significativas mejoras que presentan estos sistemas en comparación a los sistemas convencionales de tratamiento. Asimismo, los resultados de este estudio permiten profundizar el conocimiento de este tipo de reactores sobre la degradación de compuestos carbonados y nitrogenados en un mismo sistema y su estrecha relación con los fenómenos disfuncionales (hidrodinámica-transferencia de masa-reacción). Finalmente, todo lo mencionado anteriormente abre la posibilidad de mejorar el diseño de estos reactores para su aplicación a gran escala en el tratamiento de aguas residuales municipales.

## **Operation and dynamic modeling of a novel integrated anaerobic-aerobic-anoxic reactor for sewage treatment**

El uso del reactor integrado en columna en el tratamiento de aguas residuales municipales para la degradación de material orgánica, permitió obtener eficiencias de degradación de DQO de aproximadamente 83%. Esta eficiencia de degradación es comparable a la obtenida en sistemas convencionales, demostrando con esto su viabilidad de aplicación. En cuanto a la oxidación de compuestos nitrogenados, el reactor fue capaz de llevar a cabo el proceso de nitrificación con acumulación de nitrito de una manera estable, sin embargo la relación obtenida de amonio/nitrito se encuentra aún por arriba del valor estequiométrico requerido (1.32).

La operación del reactor integrado en columna permitió obtener información experimental

bajo diferentes condiciones operacionales, permitiendo la formulación y validación adecuada de un modelo matemático integrado (hidrodinámica-transferencia de masa-reacción). Este modelo fue capaz de predecir el comportamiento del reactor con un error menor al 5%, demostrando la viabilidad del uso de este modelo para predecir el comportamiento del reactor bajo diversas condiciones experimentales. De acuerdo a las simulaciones del modelo, este sistema puede ser mejorado en aspectos de diseño y condiciones experimentales que permiten mejorar el proceso de la nitrificación con acumulación de nitrito al obtener una relación estequiometría adecuada, mediante la manipulación de los tiempos de reacción, concentraciones de oxígeno disuelto, así como la mejor hidrodinámica (reducción de zonas canalizadas dentro del reactor).

#### **Hydrodynamic study of a novel membrane aerated biofilm reactor (MABR): Tracer experiments and CFD simulation**

El estudio hidrodinámico de un reactor es de suma importancia, ya que ésta afecta de manera directa el transporte de contaminantes y por ende la reacción de degradación de compuestos contaminantes. De acuerdo a los estudios hidrodinámicos realizados en el reactor de biopelícula de membrana aireada (MABR) mediante la utilización de la técnica de distribución de tiempos de residencia usando un trazador inerte (azul dextran), modelos matemáticos de transferencia de masa (celdas mezcladas) y dinámica computacional de fluidos (CFD). El patrón hidrodinámico del reactor fue descrito con un error menor al 5%, estimando que éste presenta desviaciones de la hidrodinámica ideal, es decir, presenta una zona de flujo preferencial (centro del reactor) y zonas estancadas donde el fluido presenta baja velocidad en la zona de membranas. Una vez descrito el patrón característico de este reactor, se estableció

un modelo hidrodinámico que sirvió de base para la formulación del modelo matemático integrado (hidrodinámica-transferencia de masa reacción) utilizado en la validación y simulación del funcionamiento del reactor integrado en columna.

### **Hydrodynamic improvement of a MABR using CFD and experimental validation with residence time distribution (RTD)**

La importancia de la formulación de modelos matemáticos validados para la mejora en el funcionamiento de un reactor radica en que permiten simular el comportamiento del sistema bajo diversas condiciones experimentales. El uso del modelo integrado permitió el conocimiento de que el mejoramiento en el diseño del reactor permitía incrementar las eficiencias de degradación de materia orgánica y nitrogenada, dando pauta a la búsqueda de estrategias para la mejora del patrón de mezclado dentro del reactor.

La dinámica computacional de fluidos (CFD), permitió diseñar dispositivos que permitían mejorar el patrón de flujo al disminuir la canalización del reactor. Estos dispositivos fueron analizados mediante la técnica de distribución de tiempos de residencia, estableciendo que el uso de un distribuidor de flujo dentro del reactor disminuye la canalización del reactor en un 50%. Esta herramienta demostró ser de suma valía para el diseño de reactores biológicos.

## **Perspectivas**

La implementación de los reactores integrados es una alternativa confiable para el tratamiento de aguas residuales municipales. Esto representaría un importante avance en la implementación de nuevos procesos de tratamiento con requisitos mínimos de espacio y costo operativo. Sin embargo, es importante mencionar que este tipo de sistema aún está en desarrollo, aún falta trabajo por hacer en términos de estrategias operacionales y de diseño.

De acuerdo con los resultados descritos en este documento, el prototipo utilizado mostró resultados satisfactorios en la degradación de la materia orgánica contenida en las aguas residuales municipales. Sin embargo, algunos aspectos en el diseño y su operación deben ser investigados más afondo, haciendo necesario la continuación de esta investigación científica.

Algunos aspectos interesantes son la implementación de dispositivos que mejoran el patrón de flujo del reactor, que de acuerdo con las simulaciones obtenidas con el modelo de eliminación de nitrógeno de carbono integrado (ICNRM); la eficiencia de la degradación de DQO se puede aumentar.

El funcionamiento del reactor de columna integrada en las condiciones operativas descritas por el modelo matemático integrado (ICNRM) será fundamental para dar mayor certeza a la modelo. Esto permitirá el funcionamiento correcto de la nitrificación con la acumulación de nitrito.

*“Esto solo nos acerca al final del principio; aún queda trabajo por hacer”*

## **Recomendaciones**

El reactor integrado en columna debe ser operado con los distribuidores de flujo (distribuidor de flujo de pared cónica) para permitir disminuir la zona canalizada del reactor. Se espera que este dispositivo permita aumentar la eficiencia de degradación de contaminantes.

El análisis sobre la distribución de volúmenes del sistema puede ser determinado mediante el uso del modelo integrado (hidrodinámica-transferencia de masa-reacción). El conocimiento de las ecuaciones de diseño del reactor; las cuales están descritas en el modelo integrado permitirán realizar este paso, así como conocer su comportamiento bajo estas nuevas condiciones.

Se recomienda realizar un estudio haciendo uso de la dinámica computacional de fluidos para el rediseño total de la cámara de distribución de oxígeno. Este estudio permitiría reducir la zona de canalización del reactor de mejor manera.

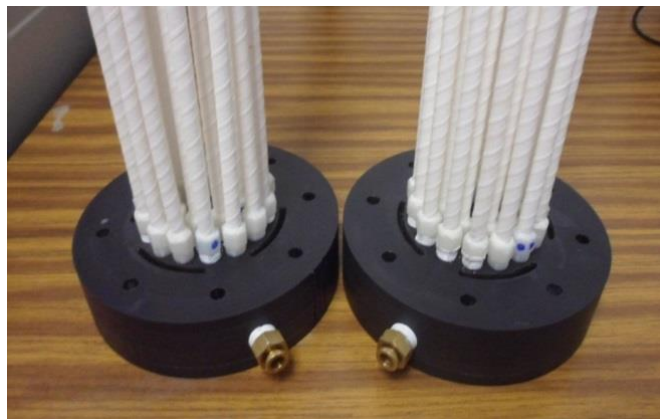
El estudio de las características físicas de la biopelícula en cuanto a su espesor, permitirá hacer modificaciones al modelo integrado que podrían aumentar su grado de certidumbre en la predicción del funcionamiento del reactor.

## ATTACHMENTS

### A1. Tubular hollow membranes (PCI Membranes)



### A2. Airtight distribution Chamber and support for the tubular membranes.



### A3. Integrated Column Reactor (ICR)





**A4. Residence Time Distribution.**



## A5. Works derivate from this thesis

### *CONGRESS PARTICIPATION*

- *INTERNATIONAL*

1. **R. Plascencia-Jatomea**, Jorge Gómez, Ignacio González and Oscar Monroy. “Operation, model validation and simulation of an integrated reactor for sewage treatment”. XI Simposio Latinoamericano de Digestión Anaerobia. La Habana, Cuba, del 24 al 27 de noviembre de 2014.
2. **R. Plascencia-Jatomea**, Jorge Gómez and Oscar Monroy. “Operational study of an integrated anaerobic-aerobic-anoxic reactor for wastewater treatment”. 13<sup>th</sup> World Congress on Anaerobic Digestion: Recovery (bio) Resources for the World. Santiago de Compostela, España, del 25 al 28 de junio de 2013.

- *NATIONAL*

1. **R. Plascencia-Jatomea**, Jorge Gómez and Oscar Monroy. “Star-up and operation of an integrated anaerobic-aerobic-anoxic reactor for wastewater treatment”. XV Congreso Nacional de Biotecnología y Bioingeniería. Cancún, Quintana Roo, México, del 23 al 28 de Junio de 2013.